Effect of Water Saturation on Air Permeability in Unconsolidated Sands of Oyster, Virginia

By:

Robert Graf Taylor

Submitted in Partial Fulfillment of the Requirements
for the Degree of Master of Science in Hydrology

New Mexico Institute of Mining and Technology
Department of Earth and Environmental Sciences
Socorro, New Mexico

April, 1997

Abstract

Outcrop studies are used to investigate the spatial variability of aquifer properties, especially permeability as measured with an air minipermeameter. In the arid Western United States, water content is usually low enough that an air permeability reading can be used as an approximation for the intrinsic permeability of a sample. In more humid areas, higher water content reduces the air permeability and biases the measurements. Most humid zone outcrop studies are conducted in "sand pits" where some percentage water saturation is required to help maintain slope stability. We conducted an air minipermeameter study of the spatial variability of permeability in an outcrop, located on the Eastern Shore of Virginia, of unconsolidated prograding spit deposits composed of fine to coarse grained sands. The measurements were biased by the naturally humid conditions at this site.

Laboratory measurements of saturation dependent gas permeability have historically been made in cores and columns, but not in the diverging flow geometry of an air minipermeameter. A dry gas flow can evaporate water, and at higher percentage water saturation can actually displace the water. We performed laboratory calibration experiments in repacked samples of fine to coarse sands. Below residual water saturation, about 10% in our study, the change in permeability due to the percentage of water saturation present is less than 5%. Above this threshold the bias depends on the water saturation and the grain-size distribution of the sample. Correctable measurements can be made up to 50% water saturation.

During the field study, we kept track of the water saturation of the different facies. We studied the importance of this correction on a 2 m x 1 m outcrop section, dominated by a Cross-Stratified sand facies. Geostatistical measures of spatial variability were prepared for corrected (intrinsic permeability) and uncorrected (effective air

permeability) data sets, which were compared to determine the significance of the corrections given conditions at the Oyster, Virginia study site.

We found that the presence of water in the outcrop affected the different facies types in different ways. In the Cross-Stratified facies, the presence of water lowered the mean permeability value and raised the variance, skewness, and kurtosis of the data set. The water also caused the correlation length in the direction parallel to the primary bedding to increase by 20% with the effective air permeability data compared to the correlation length found with the approximated intrinsic permeability data set. Though an increase in correlation length was observed, there was no significant geostatistical difference between the two calculated variograms. There was also no significant difference normal to the principal bedding plane. In the Horizontally Stratified facies, the water acted to reduce the mean permeability slightly, but affected the rest of the distribution little. The near homogeneous nature of this facies led to a small correction factor and little difference between the measured effective permeability and the approximated intrinsic permeability. There was also no significant change in the spatial variability of the data set when comparing the corrected and uncorrected data sets.

For percentages of water saturation between 10% and 25%, there was no statistical difference in the spatial variability of the measured natural log effective permeability data set compared to the estimated natural log intrinsic permeability data set. Our results indicate that there could be a more significant difference in the spatial variability of permeability for water saturation values greater than 25% in unconsolidated sediments.

Acknowledgments

This research was supported by the U.S. Department of Energy, Subsurface Science Program, Bacterial Transport Subprogram directly (Grant # 29D9GA021) as well through the University of Virginia (# 29P9BB200). The support of Dr. Frank J. Wobber (DOE), and Aaron Mills and George Hornberger (UVA) is gratefully acknowledged.

Thanks to Dr. John L. Wilson, Dr. Fred M. Philips, and Dr. Peter Mozley for being my committee members on this project. A special thanks to Dr. John L. Wilson for providing me with a Research Assistantship and being my primary advisor.

This research provided in this thesis is just a small portion of a larger collaborative effort of researchers from Idaho National Enigineering Lab (INEL), Pacific Northwest National Lab (PNNL), Old Dominion University (ODU), and Golder Associates. Some of the data used herein was collected by researchers from these institutions. Travis McLing and Bob Smith (INEL) collected cores in the field and distributed water saturation data. Cathy McConaugha and D.J.P. Swift (ODU) conducted the grain size distribution tests on the transect cores. Andrew Muller (ODU), Brian Parsons (ODU), and Robert Holt (NMT) conducted the geologic characterization of the site.

Thanks to; The Nature Conservancy, Tim Griffen (Golder Associates), Chris Murray (PNNL) for permitting and/or assisting with the field studies. Thanks to Glen LeSiege (NMT), and Mohammad Suboor (NMT) for their efforts on the new air minipermeameter.

Thanks to Dr. Allan Gutjahr for his review of the geostatistical section.

A special thanks (and love) to my wife, Jennifer, for editing this thesis and supporting me through my work.

TABLE OF CONTENTS

LIST OF FIGURES

LIST OF TABLES

CHAPTER 1 - INTRODUCTION

1.1 Rationale

Hydrogeologists and petroleum geologists commonly use field outcrop studies to characterize the geologic variability that influences various subsurface hydrologic processes. Outcrop studies provide a "window" into the subsurface environment by showing the spatial relationships and composition of geologic depositional packages. The geometry of the packages can be mapped and various properties measured. In the arid western United States, outcrops are abundant and accessible. A suite of field air mini-permeameters have been developed to take large numbers of permeability measurements in this environment (Goggin et al., 1988; Kittridge et al., 1989; Dreyer et al., 1990; Davis et al., 1994; and others). Since the outcrops are dry the measured air permeability gives a good approximation of the intrinsic permeability of the geologic material. However, in the more humid eastern United States, outcrops are poorly exposed and must often be exposed with backhoes and shovels in borrow pits. The outcrop material has a naturally high residual water saturation that can bias air minipermeameter measurements. Hydrologic based outcrop studies are often focused on unconsolidated sediments, mainly sands. Here the capillary tension of the residual water saturation that remains in the pore spaces may help hold unconsolidated sands together. If the cementation is sufficient, then sandy outcrops remain stable when they are allowed to dry out. Otherwise, they may become friable and unstable. In the east sandy outcrops must be characterized under humid or even wet conditions. With a second fluid (i.e., water) present in the system, the assumption that measured or effective air permeability can approximate the intrinsic permeability is questionable.

An important physical parameter, in this (and other) hydrologic studies, is the hydraulic conductivity, K, of the porous media. K is related to the intrinsic permeability, k, by the formula $K = \frac{k\rho g}{\mu}$, where ρ, μ, and g are the density of the fluid, viscosity of

the fluid, and gravitational acceleration, respectively. The intrinsic permeability is related to the structure of the porous media and is independent of the fluid in the system provided the porous media is saturated with a single fluid. For the two-fluid phase case, the intrinsic permeability of an aquifer is related to the effective fluid permeability, k_f, by $k = \frac{k_f}{k_{rf}}$, where k_{rf} is the relative permeability of the fluid, varying from 0 to 1.0. As the amount of water saturation in an outcrop decreases, the air relative permeability, k_{ra}, approaches a value of 1.0 and the measured air permeability approaches the intrinsic permeability. This is often the case in the arid West. As the percentage of water saturation increases, as in the humid East, k_{ra} decreases until the air permeameter becomes ineffectual. We are concerned with the influence of resident water saturation on outcrop measured air permeability and how it affects the assumption that measured air permeability is a good approximation for intrinsic permeability.

In 1994, the Department of Energy Subsurface Science Program (SSP) funded a study of aquifer characterization and bacterial transport near the town of Oyster on the Eastern Shore of Virginia. Prior to beginning the bacterial transport experiments in the saturated zone, numerous characterization experiments were conducted on the physical, chemical, and biological characteristics of the aquifer material (Mixon, 1985; Golder, 1995; Parsons and Swift, 1995). Coring, ground-penetrating radar, and preliminary tracer injection studies were conducted by other investigators. We participated in a field outcrop study at a nearby sand pit, which has been shown to be from the same depositional environment as the aquifer material found in the bacterial transport experimental zone (Muller et al., 1996). Sampling the outcrop allowed us to correlate the spatial variability of permeability to the geology. This spatial information was then coupled with chemical data, core data, and ground-penetrating radar data to build a conceptual model of the three dimensional layout of the subsurface geology. This information is currently being employed in a mathematical model to predict aquifer transport of different bacterial organisms and to interpret the bacteria transport experiments (Scheibe et al., 1996).

Three major facies types in the depositional environment of the Chesapeake Bay Mouth Shoal have been identified on the basis of "examination of faces excavated into the sides of the Oyster pit and on the basis of laboratory grain size analysis of the samples" (Muller et al., 1996). A facies refers to a "stratigraphic unit distinguishable by lithologic, structural, and organic characteristics detectable in the field" (Boggs, 1987). The coarsest facies type was named the Gravelly Shelly sand facies and was presumably formed when gravel was swept off the sea floor and up onto the shoreline during extremely intense storm events. This first facies type is characterized as having particles greater than 2 mm in diameter (gravel) for greater than 10% of its weight. The two other facies types have a gravel content of less than 10% of their weights. The second facies type consists of a Cross-Stratified sand facies that is thought to have been deposited on the upper shore face by migrating sand waves during storm amplification of tidal currents. This facies type is characterized by a mean grain-size diameter less than 2.00 phi, where phi=$-\log_2$*(grain size). The third facies type is a Horizontally Stratified sand facies that was most likely deposited from suspension during the same storm events. This facies type has a mean grain-size diameter greater than 2.00 phi (see Figure 1.1). The Horizontally Stratified facies has better sorting than the Cross-Stratified facies. It is now believed that the Gravelly Shelly facies may simply be gravelly based lag layers of the Cross-Stratified facies (Andrew Muller, personal communication, 1996). However, for the present discussion, the Gravelly Shelly class is still considered a distinct facies.

During the geologic characterization of the outcrop, we conducted thousands of air permeability measurements to characterize the spatial variability of permeability in this system. Virginia is very humid. The unconsolidated sand in the outcrop contained some water that began to evaporate as soon as we exposed the outcrop face. What effect did the residual water saturation have on our readings? After a few days the evaporation of the water made the outcrop surface friable, and contact with the surface caused the sand to fall, especially in the Gravelly Shelly facies. The second fluid phase, water, held

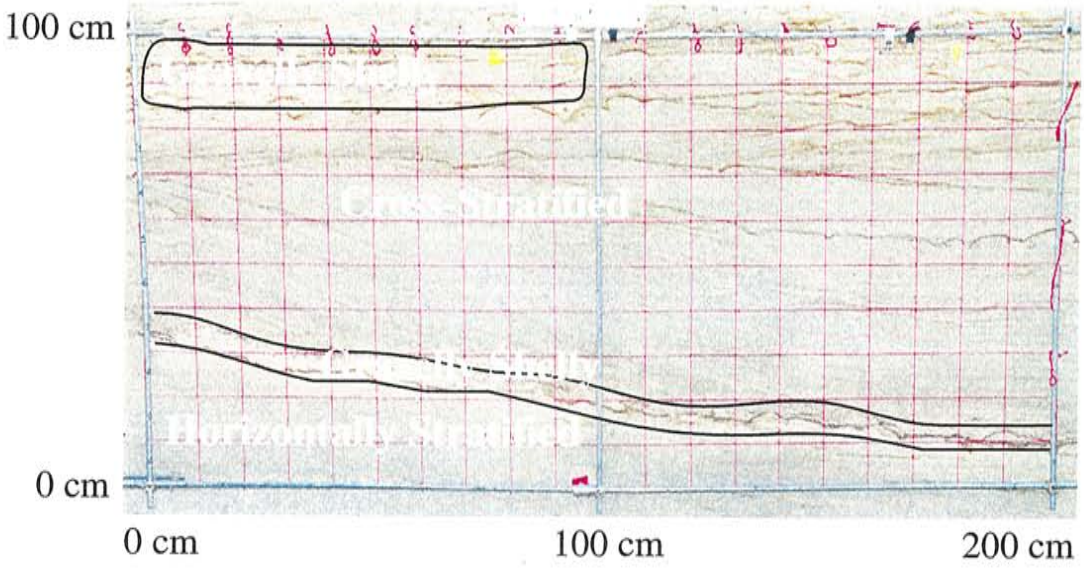

Figure 1.1 — Tier 2. Central Panel (5). Three distinct facies types and their extent within a 2 m x 1 m gridded section. This panel is also shown in Figure 2.1, lower center part of that photograph.

the sand together through capillary tension. Were our effective air permeability readings adequate approximations of the intrinsic permeability of the system? How much of an effect did the remaining water saturation within the outcrop have on our readings? If the effect was significant, could we correct the measurements for the bias due to the *in -situ* water saturation?

1.2 Objectives

The presence of water in the unconsolidated sands of Oyster, Virginia, presents a number of interesting questions. For each of the three facies encountered in the aquifer and the outcrop we asked these questions: (1) for water saturations found in the field, is it possible to define a non-wetting phase relative permeability curve (correction factor) that will remove the bias from the effective air permeability and thus yield an estimate for the intrinsic permeability?; (2) is there a water saturation below which the measured effective air permeability approximates the intrinsic permeability?; (3) is the bias introduced by uncorrected data significant in the geostatistical sense?; and (4) what lessons can we learn about conducting outcrop experiments in humid environments? Though our experiments were site specific, answers to these questions are important when conducting air permeameter outcrop studies in any situation where some amount of water saturation is present, and especially when dealing with unconsolidated sands in humid environments.

1.3 Scope

Since these experiments were conducted for a very specific site, Chapter 2 presents a discussion of site geology, with an emphasis on depositional environment, followed by a review of the April, 1996, field sampling program. Chapter 2 also contains a discussion of measurement devices used for field water saturation measurement. Chapter 3 is concerned with air permeameter use and contains a discussion of our newest

prototype air mini-permeameter. The laboratory methods employed to answer questions 1 and 2 above are briefly explained in Chapter 4, with the details documented in Appendix A. Chapter 4 also includes a discussion of the geostatistical analysis method for one section of the outcrop study used to answer the third question. Chapter 5 discusses results from both the laboratory and the field studies, with references to data, charts, and graphs found in Appendices B and C. Appendix D details an analysis of the Brooks and Corey (1964) and Mualem (1976) models as applied to our laboratory results. Finally, a summary of our answers to the four questions posed earlier is addressed, including recommendations as to how to best address the major issues of using air minipermeameters to determine permeability in unconsolidated sand outcrops in humid regions.

CHAPTER 2 - FIELD OUTCROP STUDY SITE

2.1 Introduction

When conducting controlled experiments to determine the fundamental mechanisms governing flow and transport in heterogeneous porous media, it is necessary to characterize the spatial variability of hydraulic properties, such as permeability. Outcrop studies are widely used since they provide a cross sectional view of the geology in associated aquifers. By studying the spatial variability of permeability in these outcrops, one can find the geostatistical properties of the sedimentary structures and then apply those statistics to aquifer models. Previous outcrop studies have used air mini-permeameters on well-lithified rocks (Eijpe and Weber, 1971; Goggin et al., 1988; Heller, 1991; Suboor et al., 1995) where the samples contained negligible water. In these studies, the measured air permeability was assumed to be identical to the intrinsic permeability of the samples. In other words, these studies assumed a relative permeability to air of unity, $k_{ra}=1.0$. Unlike these studies, however, we wanted to study the spatial variability of permeability on outcrops of unconsolidated sediments where the presence of some water was vital to their cohesion and the stability of the outcrop and where $k_{ra}<1.0$.

2.2 Geology of Study Site

The SSP bacterial injection transport study was conducted along the lagoonal shoreline of Virginia's Eastern Shore peninsula on land owned by the Nature Conservancy. The experimental zone was chosen within the Butler's Bluff Member of the Nassawadox Formation (Mixon, 1985) because it met certain criteria which provided a maximum likelihood of interpretable results, namely: (1) adequate permeability and porosity and well characterized recharge and discharge conditions, (2) small hydraulic gradients, (3) simple mineral chemistry, (4) coated and uncoated minerals, and (5)

minimal chemical heterogeneity of the groundwater (SSP, 1994). Our portion of the study focused on the permeability characterization of aquifer materials.

Parsons et al. (1996) suggest that the geologic unit was deposited as a barrier spit which prograded southward during the sea level highstand of 125,000 years before present. Like most beach and barrier island systems, the Butler's Bluff Member is a shore deposit formed primarily by wave action along the shore face. The well-sorted, medium- to coarse-grained sand was deposited in the oceanic side of the spit, in the tidal shoal, and in the spit tip environments (Parsons et al., 1995). The majority of the deposition is assumed to have occurred during storm amplification, and these events caused the formation of the three aforementioned facies types. Although the majority of the sand had undergone little change and was uncoated, zones of buried pelecypod valves allowed precipitation of ferric iron on some of the grains. The iron oxides in solution were the result of oxidizing conditions which caused ferrous iron minerals interacting with soil water to release ferric iron into solution. The ferric iron solution migrated downward through the sand and was neutralized by the calcium carbonate that made up the pelecypod shells (Bob Smith, personal communication, 1997). These coatings formed within lag layers and play an important role in determining the physical and chemical aspects of the aquifer characterization.

2.3 April 1996 Field Outcrop Program

In April, 1996, a team of 20 investigators from Golder Associates, Dartmouth College (DC), Idaho National Engineering Lab (INEL), Pacific Northwest National Lab (PNNL), Old Dominion University (ODU), the University of Virginia (UVA), and the New Mexico Institute of Mining and Technology (NMT), traveled to Oyster, Virginia, to conduct an outcrop study in anticipation of the bacterial injection tests performed later that summer. A previous field outcrop program, conducted in 1994, had studied 3 m x 3 m sections that were 10 m and 30 m apart, respectively. The 1994 field program resolved

"mesoscale heterogeneity such as geometry of cross-strata sets," but failed to resolve "larger scale features such as master bedding planes, stratal continuity, and offlapping bed sets" (Parsons and Swift, 1995). To resolve the larger scale features it was decided to cut a 20 m wide section into three tiers approximately 2 m in height and set back by steps about 2 m wide.

Photographs of the three tiers, taken near the end of the study, are shown in **Figures 2.1 and 2.2**; a close-up of the central panel of the second tier (Panel 5) is shown in **Figure 1.1**. On each tier a variety of characterization methods were used on the outcrop. Surveyors shot stations at one meter spacings along the top of each tier. Stratigraphic sections were prepared at each of these stations (ODU). IR (infra-red) imaging was recorded along the outcrop in 2 m long sections to be used later for assessing the relationship between the water saturation controlled surface temperature and the measured air permeability variations (PNNL). The outcrop facies were mapped at the set and co-set level (NMT). Sample grids were set up for air mini-permeameter measurements (NMT) at roughly 1000 points, for 50 cc core samples (INEL) at about 250 of the same points, for 10 cc syringe samples (UVA; DC) at other of the points (for water hydraulic conductivity measurements), and for a series of larger core and box samples (DC; ODU) for various analyses. **Figures 2.1 and 2.2** show evidence of this sampling. The 50 cc cores were split and examined for extractable iron and aluminum (INEL), porosity, bulk density, and water saturation (INEL), grain size distribution (ODU), and a variety of other measurements (UVA; Univ. of Arizona). The analysis and interpretation of the large data set is a continuing activity of other investigators and is not part of this thesis.

A heavy rain the night before excavation of the first and upper tier kept the surface of the sediment quite wet and prevented excavation until the afternoon of April 16, 1996. Once the back hoe had cleared the majority of the sand away, project personnel planed the outcrop face with shovels and trowels. Surveyors shot the 1 m stations along

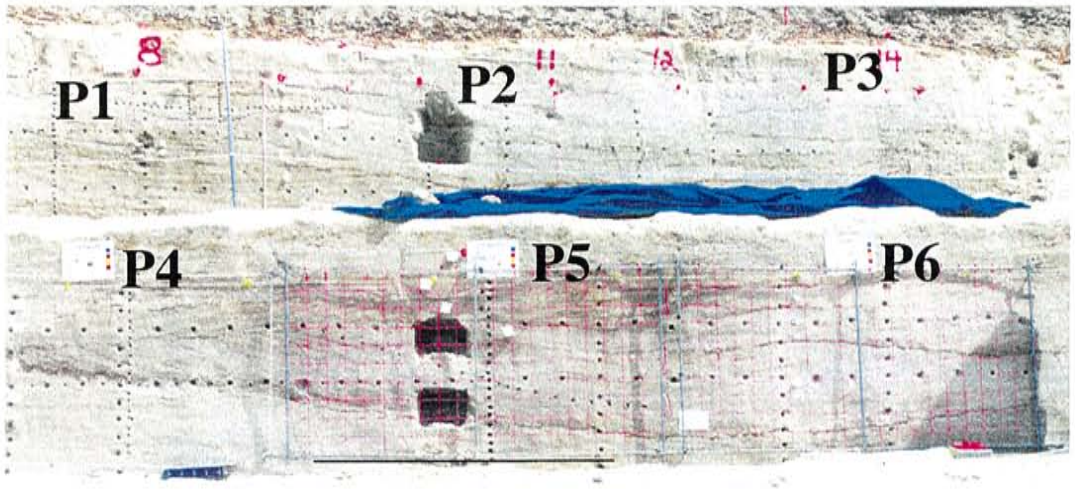

Figure 2.1 — Center of Tiers 1 & 2 showing Panels 1-6 after core samples were taken; stratigraphic sections measured each meter

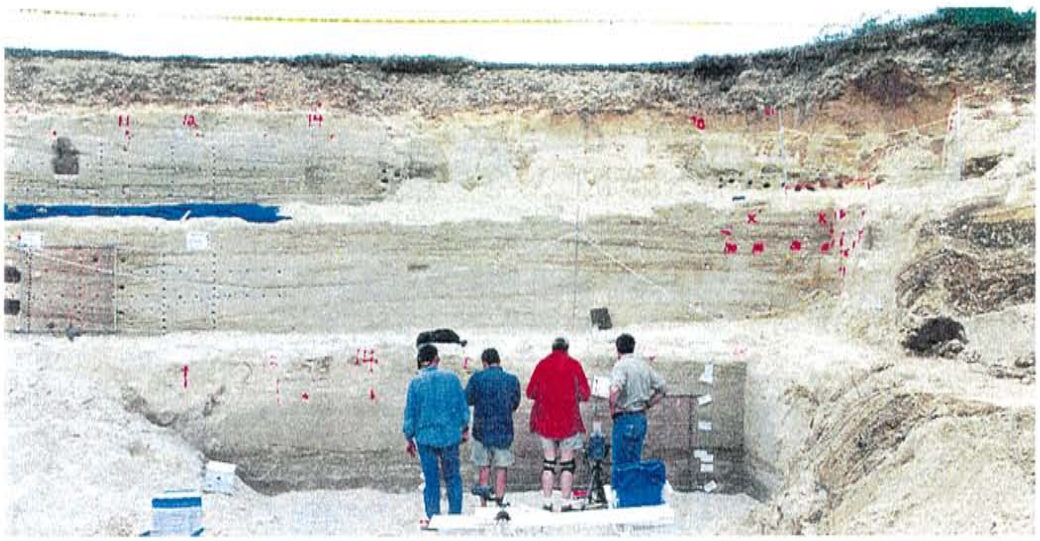

Figure 2.2 — Right side of three tiers showing vertical extent of outcrop.

the top of the tier, and characterization began with detailed photographs and stratigraphic section sketches. Due to recent rain, which caused high water saturations within the tier, we decided to allow the tier to dry overnight before beginning our air permeability measurements. From April 17 to April 20, 1996, the group worked to collect multiple readings over each of the three tiers. The second tier was cut beneath the first on the afternoon of April 17, 1996, while the third and bottom tier was cut on April 19, 1996. A time line of excavations and outcrop face preparation and the times at which air mini-permeameter measurements were made is shown below (Figure 2.3).

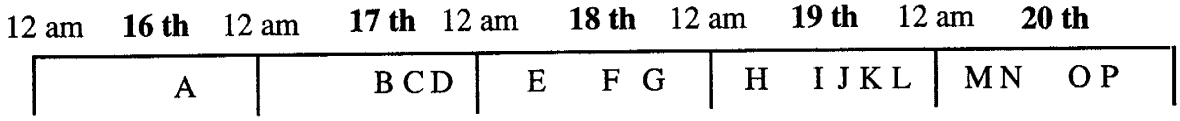

A: 2 pm - Tier 1 excavation
B: 1 pm - Panel 1 transects
C: 4 pm - Panel 2 transects
D: 8 pm - Panel 3 transects
E: 9 am - Tier 2 excavated
F: 12 pm - 4 pm - Biased studies of T1
G: 5 pm - 100 samples on Panel 3
H: 10 - 11 am - Panel 4 and 5 transects
I: 12 - 2 pm - Biased studies of T2
J: 2:30 pm - Panel 6 transects
K: 3 pm - Panel 5 left side (100)
L: 4 pm - Tier 3 excavation
M: 9 am - Biased studies of T2
N: 10 am - Panel 5 right side (100)
O: 1 - 4 pm - Biased studies of T2
P: 4:30 pm - Panel 7 transects

Figure 2.3 - Time line of excavations and air permeameter readings

Due to time constraints, the group could not extensively sample the entire 20 m x 6 m outcrop for all the physical and chemical characterization studies. To best relate the spatial variability of the different measurements (permeability, extractable iron and aluminum, and water saturation) to the measured geology (grain size distribution and facies type) in an unbiased fashion we first chose to sample a number of vertical and horizontal transects in the central area of the outcrop. This sampling scheme provided the best structure to test for spatial correlation and cross-correlation because the sample points were on a uniform grid, lined up horizontally and vertically. To address issues not accessible by sampling along transects, the group decided to conduct a number of biased studies elsewhere on the outcrop. For example, one biased study was designed to examine an iron oxide stained and cemented basal lag boundary layer.

For each of the various transect and biased studies, we first sampled air permeability at each of the measurement points, as illustrated in **Figure 2.4**, followed by coring and/or syringe samples. 2 m by 1 m gridded panels were used to control sample spacing across the center 6 m of the top two tiers (Figure 2.1). Panels 1 to 3 were used on the upper tier; Panels 4 to 6 were used on the second tier. We also chose to more heavily sample the central panel (5) of the second tier for air permeability in an unbiased, gridded fashion (see Figure 2.5). The lower tier was only sampled along transects within a single 1 m x 2 m gridded panel. For each of the air permeability readings taken, we recorded the location within the grid, the time of day, the temperature, the force applied to the outcrop face by the air mini-permeameter tip (see Chapter 3), and the time, in seconds, it took for the air volume to be injected out of the air mini-permeameter and into the outcrop face (see Chapter 3), along with any special notes concerning the type of facies being sampled. During the campaign, we collected air permeability measurements at over 1000 locations.

The changing water saturation, air and soil temperature, and time of day, were sporadically recorded throughout the week to determine the effects of the length of exposure to the atmosphere, and, more importantly, to the sun on each of the outcrops. As each face was opened to the air, the sand was very stable and damp to the touch. Water in the outcrop provided the capillary tension that holds the sand together. During most days, outcrops collected solar radiation. On the afternoon of April 19, 1996, there was a light rain shower that caused an addition of water to most of the field site, though the central panels were covered with tarps. Each night there was the chance for redistribution of water from deeper in the sand back towards the surface of the outcrop as diurnal temperature fluctuations would also have affected the rate of water loss from the surface of the outcrop (Hillel, 1980). We conducted no water saturation experiments at night so the effects of redistribution of water could only be estimated by comparing the end of the previous day's readings with early readings from the following morning. The water

Figure 2.4 — Air permeability measurement taken within a sampling grid on Tier 1.

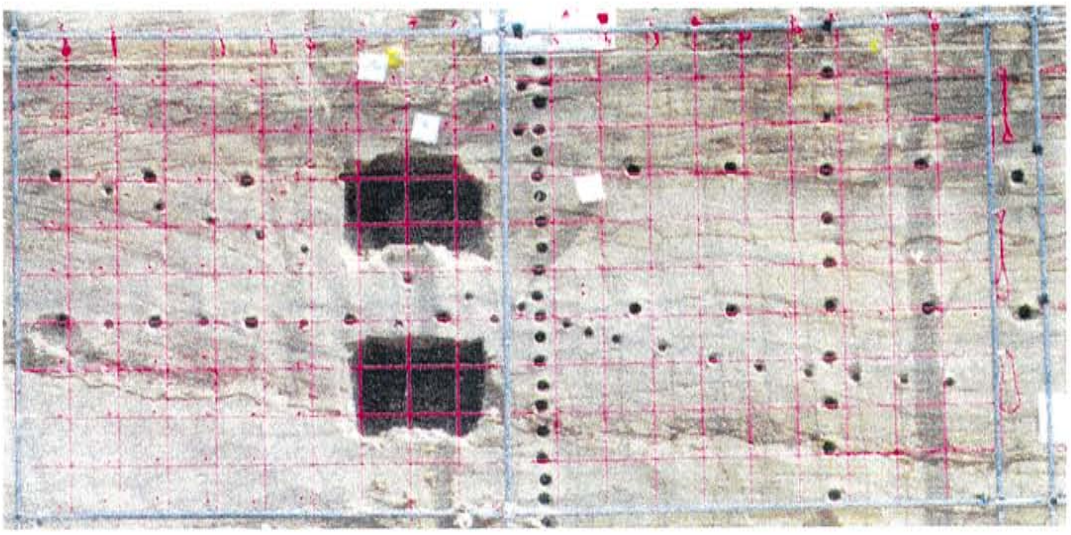

Figure 2.5 — Panel 5 showing 2 m x 1 m grid, transect cores, and box cores; Air permeability was sampled on a uniform 10 cm grid on this panel (210 unifomly spaced samples). Also evident are cores taken from a biased study along a dipping bed of a cross-stratified set.

saturation within the different facies types was bound to be variable in the field since each of the facies types had different grain size distributions.

Among the many studies being conducted, ours was potentially the most strongly affected by changes in water saturation close to the surface of the outcrop, and how it changed through time. The air minipermeameter employed measured the permeability of the outer 1 to 2 cm the outcrop. Throughout each day in the field we collected a representative volume of sand from the top 5 cm of the face using 100 cc sampling rings in a control section on the right side of each of the tiers. We recorded the facies type and geologic coset where each reading was taken. These samples were analyzed for average water content by gravimetric analysis (see Appendix D). The transect cores were collected within each of the sampled panels using 2.5 cm diameter tubes that were pushed into the outcrop face. These samples measured the average water saturation of the outer 10 cm of the outcrop face. These data values provide the basis for the air permeameter corrections from effective air permeability to intrinsic permeability. Since the air minipermeameter measures the outer 1 to 2 cc of the outcrop face, our corrections are conservative and probably overemphasize the degree of correction needed. To address the question of defining non-wetting phase relative permeability curves (correction factors), a number of laboratory experiments were run to try to estimate the effects of the water saturation for the different grain size distributions found within the Oyster Site sand.

CHAPTER 3 - THEORETICAL DISCUSSION OF AIR PERMEAMETERS

3.1 Introduction

Probe, or mini-, permeameters were first described by Dystra and Parsons (1950). Mini-permeameters are simple, gas-flow devices designed to obtain a large number of non-destructive permeability measurements quickly and rapidly in the field. Their use has enabled a number of scientists to inexpensively characterize the spatial variability of permeability upon outcrops. Goggin (1993) surmised that probe permeametry provided one of the best ways of "determining the vertical and lateral controls on fluid flow." Past studies assume that the measured air permeability is an approximation of the intrinsic permeability, and when studying only dry, consolidated sediments this approximation was probably appropriate. However, little work has been done in unconsolidated sands and in humid environments. This discussion begins with a review of previous, theoretical and field work using a variety of air permeameters on dry, consolidated sediments. We then compare the prototype Lightweight Syringe Air Mini-Permeameter (LSAMP) created by Davis et al. (1994) for dry poorly consolidated sediments, with the new prototype LSAMP II constructed for the dry unconsolidated sediments of the Oyster Site.

3.2 Air Permeameters

There are a number of important issues in using air permeameters correctly in the field. First, one must define the flow geometry present for the permeameter used. The permeability of the rock governs whether there will be a Klinkenberg (gas slippage) effect (low permeability samples) or a high-velocity non-linear effect (high permeability samples). Pressure losses within the permeameter must be accounted for through calibration. Finally, the user must make sure that the tip seal is applied to the outcrop face

with a sufficient force that the injected air will travel through the outcrop and not bypass the outcrop by escaping between the tip seal and the outcrop face.

Goggin et al. (1988) may have been the first to mathematically model "the response of the mini-permeameter in flow patterns consistent with its applications." Permeameters measure the steady-state gas rate and the injection pressure at the point where a gas is injected. The primary factors that affect these two readings are the permeability of the sample, the viscosity of the gas, the gas slippage effect for low permeability samples, the high velocity non-linear effect for high permeability samples, the sealing quality of the tip seal upon the outcrop face, and the gas flow geometry. Goggin et al. (1988) focused their study on the specific gas flow geometry used in these devices. To apply Darcy's Law, they determined a geometric factor, $G(b_D)$, based on the dimensions of the tip seal and the dimensions of the sample. They assumed that the media was homogeneous, so that application to a heterogeneous media introduces an unquantifiable error in the estimates of permeability. Their findings showed that the volume of the rock being sampled by the gas was strongly related to tip seal size, being roughly a hemisphere with a radius four times the internal tip seal radius. Provided that the tip seal radius was small enough, or the sample media was locally homogeneous, the measured volume could be considered to be approximately homogeneous and the error due to heterogeneity could be reduced. Goggin et al. (1988) further found that the gas-slippage effect caused higher than accurate readings when the mean free path of the air was comparable to the pore size, and the non-linear effect of high velocity gas flow (turbulence) caused additional pressure losses within the outcrop system resulting in an underestimation of permeability. As the mean free path of air at atmospheric pressure is on the order of 10^{-8} m (Adamson, 1979) and the pore sizes of our outcrop system are on the order of 10^{-4} m, gas slippage was considered negligible. In our unconsolidated sediments, the permeability ranged from about 10 to upwards of 100 darcys, which gives

values for the Reynold's number of less than 0.5. Therefore, our samples should not be affected by high-velocity flow effects.

A number of compressed gas source probe permeameter studies have focused on the permeability of highly consolidated reservoir rocks (e.g. Chandler et al., 1989; Dreyer et al., 1990; Hartkamp et al., 1993). Chandler et al. (1989) used a compressed gas source that could make between 200 to 500 measurements in the field before having to replace the gas source. The device had a range of 0.05 to 10 darcys and was used on consolidated reservoir rocks. Dreyer et al. (1990) used a compressed gas permeameter to study the spatial variability of consolidated channel sand bodies along the Yorkshire Coast of England because the sand bodies formed an analog for the main reservoir elements of the North Sea fields. They studied sandstone with a range of 0.1 to 7.5 darcys, with the majority of measurements being between 1 and 2 darcys. To prevent leakage, they used a silicone rubber tip seal, but they did not discuss the tip seal force they applied to the rock face. Hartkamp et al. (1993) used a compressed nitrogen gas permeameter to study lightly consolidated cross-bedded reservoir sandstone in Tertiary fluvial deposits of central Spain. The sandstone ranged from 0.9 to 12 darcys. They removed the first few centimeters of friable sandstone to avoid the problem of displacing the sand with the compressed gas and used a controlled tip seal force to avoid varying the inlet pressure while measurements were being taken. Tidwell and Wilson (1997) studied the effect of tip seal size on permeability measurements of Berea sandstone. As tip seal size increased, they found a reduction of permeability variance, and an increase in permeability mean and correlation length. All of these studies worked with compressed gas, but in our case such a gas source would easily displace and blow out our sand since the main force holding the sand grains together is water saturation capillary tension.

Suboor and Heller (1995) designed and tested an automatic, computerized laboratory air permeameter that used the ambient air and a falling piston to determine the characteristics of permeametry critical to the use of these devices. They worked with

Berea sandstone. Unlike Goggin, who focused on the flow geometry, Suboor and Heller (1995) focused their study on the issue of the amount of tip seal force applied to the rock sample and the permeability readings obtained. They also looked at the question of the volume of the region that the permeameter was sampling. They further looked at the assumption of rock homogeneity and found that, although most natural porous media were truly heterogeneous, the "computed streamlines and iso-pressure surfaces (could) be taken to be quite correct *on the average*." Having established that Goggin's work was valid for their case, they proceeded to test how much tip seal force was required to get a good seal between the tip of the permeameter and the Berea sandstone rock face. They found that, at very low tip seal force, the gas might find a way to short circuit the sample by flowing beneath the tip seal instead of through the rock, giving higher permeability readings. However, as the pressure on the sample increased they saw that a steady value of permeability was reached. They noted that increased force could deform the tip seal radius and change the geometric factor in an unmeasurable way. To account for the change of tip seal deformation, they recommended that the ratio of the outer to inner tip seal radius (b_D) be greater than 1.5, because for $b_D < 1.2$, the geometric factor, $G(b_D)$, is too sensitive to changes in radius (Figure 3.1). For higher values of b_D, the sensitivity flattens and minor deformations caused by the applied force compacting the tip seal against the surface do not change $G(b_D)$ significantly. These studies show the importance of applying a constant, steady force to obtain a good seal between the tip and the outcrop face. Though Suboor and Heller (1995) showed that, in the absence of tip seal deformation, increased tip seal force would lead to a better assessment of air permeability, at Oyster we had to be careful not to apply so much force that we would compact our unconsolidated sands during measurement.

3.3 LSAMP I and II

Davis et al. (1994) developed a lightweight syringe air mini-permeameter (LSAMP I) for collecting numerous spatially distributed permeability measurements on weakly lithified sediment outcrops in the field. The device consisted of a glass syringe with falling piston that displaced a set volume of ambient air into the outcrop, a timing device to measure the elapsed time for the set volume of air (giving a flow rate), and a tip seal that was applied to the face of the outcrop. The device was portable but required the operator to lift the syringe piston with one hand while holding the tip seal away from the

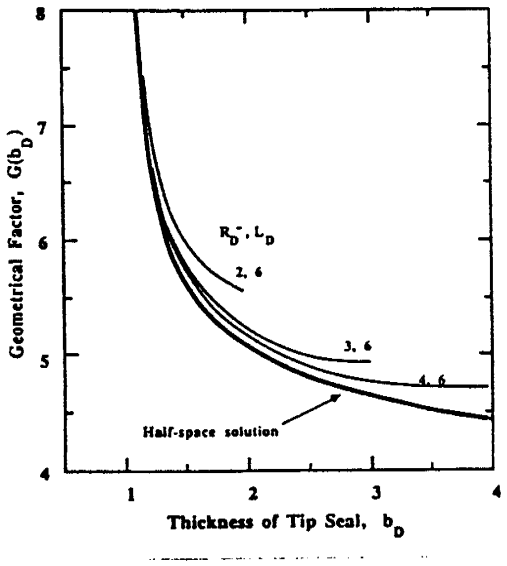

Figure 3.1 - Plot of Geometric Curves showing the effect of core sample radius (from Goggin et al. (1988))

outcrop with the other hand, allowing intake of air but not sand. Once the piston was raised the tip seal was replaced on the outcrop and the released piston fell by the force of gravity. The tip seal was applied to the outcrop by hand and it was up to the operator to maintain a steady and similar force upon the tip seal for each measurement. Each measurement of piston fall time was repeated at least three consecutive times, but the removal and replacement of the tip seal upon the outcrop sometimes caused the sediment

to fall away when the sample was friable and prevented the exact replacement of the tip seal to its original position. This device solved the problem caused by a compressed gas source that would easily displace and blow out unconsolidated sediments, but it suffered from two limitations. First, it did not control tip seal force throughout a reading or from sample to sample. Second, it required that the tip seal be removed from the face between readings, potentially causing variable results.

Following a test of this first-generation device at the Oyster outcrop in 1994, John L. Wilson, Glenn Lesarge, and Mohammad Suboor designed a number of improvements into a second generation device (LSAMP II) that uses the same falling piston principle. The LSAMP II (patent pending) was modified from LSAMP I by adding more robust electronics and a mechanical pumping device that fills the syringe with ambient air without lifting the tip seal, so that the operator can concentrate on maintaining a constant tip seal force against the outcrop. Ambient air enters the syringe through a solenoid three-way valve, allowing the tip seal to remain in the same location upon the outcrop. A tip seal pistol grip and linear spring force gauge were also added to the LSAMP II. Similar to a handgun handle, the operator holds the tip seal against the outcrop and applies a prescribed force. Then the operator activates the pump and solenoid three-way valve by pressing a trigger on the pistol grip. As the piston falls, the operator is able to observe the applied force on the tip seal and can make sure that it remains steady for each measurement. The time to displace the volume of air into the outcrop is recorded and then the trigger can be pressed again to make a second and then a third measurement, all within seconds. These improvements solved the problem of variable applied tip seal force and eliminated the need to lift the tip seal from the outcrop face between readings. Finally, the tip seal itself was designed with a special soft rubber compound inserted into a machined brass holder to ensure a good seal and undeformable inner and outer radius. The LSAMP II provided less variability in readings than Davis et al's (1994) earlier version.

Since the basic design of the LSAMP II followed the same principle as the earlier model, we were again able to calculate the permeability for the tip seal geometry by using Goggin et al.'s (1988) and Davis et al.'s (1994) equations for air permeability;

$$k = \frac{2\mu q P_1}{a[G_0(b_d)](P_1^2 - P_0^2)} \qquad (3.1)$$

$$P_1 = P_0 + P_n = P_0 + [\frac{mg}{A} - \frac{\beta v^2}{A} - \alpha q + b] \qquad (3.2)$$

where
k = effective permeability [m^2];
μ = viscosity of air [Pa s];
q = volumetric flow rate [m^3/s];
P_1 = air pressure applied at tip seal/outcrop interface [Pa];
P_0 = atmospheric air pressure [Pa];
a = radius of tip seal orifice [m];
$G_0(b_d)$ = Goggin (1988a) geometric factor [dimensionless];
b_d = dimensionless tip seal radius (outer/inner);
β = coefficient of mechanical friction acting on syringe piston [N s^2/m^2];
α = coefficient of resistance in the permeameter plumbing [Pa s/m^3];
b = pressure parameter found during linear regression calibration [Pa];
v = q/A = piston velocity [m/s];
A = area of the piston [m^2];
m = mass of the piston [kg];
g = gravitational acceleration [m/s^2].

This model assumes that the measured samples are both homogeneous and isotropic, that the flow is steady and laminar through the sample, and that the gas slippage effect is minimal. As reported earlier, gas slippage and non-linear flow effects are negligible in our samples. We have yet to calibrate for the frictional losses associated with the design of the LSAMP II.

Finally, although not used in the field on this project, several of the design improvements were also incorporated into the original device, LSAMP I. The tip seal air supply tube was replaced with the new tip seal, along with a pistol grip with linear spring force gauge. The air supply tubing for the remainder of the LSAMP I was replaced with larger diameter tubing to reduce the frictional losses within the system.

CHAPTER 4 - LABORATORY METHODS AND GEOSTATISTICAL ANALYSIS

4.1 Introduction

The LSAMP I and II were calibrated, accounting for the internal frictional losses within the devices. Once calibrated, we determined non-wetting phase relative permeability curves (correction factors) for effective air permeabilities at known water saturations for the different Oyster facies types. With these laboratory corrections, we examined the spatial variability of permeability in each of the facies types found at the Oyster, Virginia field site. The methods for these three steps are summarized below.

4.2 Calibration of the LSAMP II

To apply the equations of Goggin et al. (1988) and Davis et al.'(1994) to solve for the air permeability of a reading we needed to account for the frictional losses within the two different LSAMP versions. LSAMP I was previously calibrated by Davis et al. (1994), but in the intervening time it had been used in the field extensively and had undergone much wear and tear that significantly changed the various instrument coefficients. The original LSAMP I, our improved version it, and the new LSAMP II were all calibrated to account for these frictional losses. Multiple methods were used to determine the various frictional coefficients in each of the devices to ensure accuracy. We will explain procedures by focusing on LSAMP II calibration.

The syringe piston was weighed to find its mass, m. The injected volume of air, V, was measured by filling the syringe with de-ionized water and measuring the amount of water displaced between the starting and stopping times of the clock, controlled by two photosensors. The test was repeated two additional times for accuracy. The volume was also estimated by measuring the area of the piston and the distance between the two photosensors. These measurement techniques yielded readings within 5% of each other.

To determine the α and β coefficient in Equation 3.2, a Dwyer Slant Manometer (Pat. 1917637, Model No. 424) was used to measure the pressure differences over different parts of the system for various samples. The Dwyer slant manometer used red gauge oil of 0.826 specific gravity and measured a range from 0 to 200 mm of H_2O, which was an adequate range of pressures for these conditions. To determine β for the syringe and the three-way valve, a T-connector was placed downstream of the valve (port 1), with its third branch connected to the manometer. (see Figure 4.1)

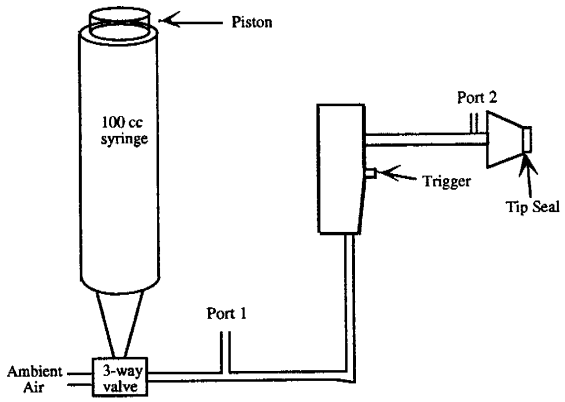

Figure 4.1 - Schematic of locations of ports used to determine coefficients of friction for the LSAMP

Various consolidated sand standards were used to obtain a range of velocities. The fastest velocity was obtained with no resistance and the slowest velocity was obtained by placing the tip seal on an impermeable material, such as a glass plate. For each step, the syringe was raised by the pump (by hand on LSAMP I), the tip seal was placed on the appropriate standard with the appropriate tip seal force, and the syringe was dropped (automatically in LSAMP II). The manometer recorded the air pressure in the system for different standards. Care was taken to ensure that a steady state flow condition was reached before the pressure differences were recorded. After converting mm H_2O to frictional force [Pa] and time to velocity, we plotted the frictional force versus the velocity and fit a quadratic function to the data (Appendix A). β is the absolute value of the coefficient of the square term in equation 3.2. After determining a value for β, the T-connector was attached to the end of the tubing line just before the tip seal (port 2). The same method as above was

used to determine the pressure drop through the entire LSAMP II system. Plotting these results as a quadratic function also yielded a good fit. We converted the frictional force to pressure and subtracted the effect of the piston from the total line calibration. This gave us a change in pressure versus velocity, which we converted to volumetric flow rate, q. We then plotted ΔP versus q and fit a straight line to determine the α coefficient and b parameter by applying $\Delta P = \alpha q - b$ to the resultant data. Head losses due to the tip seal could not be corrected for with this method, but they were approximated (see below). **Table 4.1** presents the coefficients that we determined during the calibrations of each of the devices. Appendix A contains the data and graphs used in these determinations.

	Description of parameter	LSAMP II	LSAMP I new	LSAMP I old
β =	Coeff.of friction [-]	39	105	280
α =	Coeff. of resistance [-]	6.39E+05	3.18E+06	5.60E+06
b_D =	Dimensionless tip seal radius (b/a) [-]	3.83	3.83	3.83
$Go(b_D)$ =	Geometric factor (Goggin et al. 1988)	4.5	4.5	4.5
a =	Radius of tip seal orifice [m]	0.003315	0.003315	0.003315
m =	Mass of piston [kg]	0.14	0.18	0.18
V =	Volume of air diplaced [m^3]	6.45E-05	5.50E-05	5.50E-05
A =	Area of plunger [m^2]	9.62E-04	1.01E-03	1.01E-03
b =	Pressure parameter regression intercept	3.01	9.94	-24.5

Table 4.1 - Numerical parameters for LSAMP II and LSAMP with new and old plumbing

With multiple versions of the LSAMP, independently determined permeabilities for the standards allowed a cross-comparison. Davis et. al. (1994) used a CFAMP to determine the air permeability of a number of standards. Using these standards, each device should have given the same value of air permeability once the proper calibrations were computed; that they did not give the same air permeability value implied that there was a difference in head loss across the uncalibrated tip seals. The tip seals in LSAMP II and the new version of LSAMP I were of the same design. The tip seal on the old version of LSAMP I had deteriorated and appeared worn. The LSAMP II tip seal design also had less resistance than the original version. We determined a multiplicative correction factor

of 0.74 between the older version of LSAMP I tip seal and the new LSAMP II tip seal (Table 4.2). A factor of 1.11 was determined between LSAMP II and the new version of LSAMP I, probably due to the differences in plumbing between the two versions, such that effective air permeability = 1.11*(reading given by new LSAMP I).

Std. #	LSAMP I old (A)	LSAMP I new (B)	LSAMP II (C)	Relationships	r^2
1	60 [darcys]	46.7 [darcys]	52.4 [darcys]	B = 0.67*A	0.991
2	111.8	77.7	91	C = 0.74*A	0.984
3	228.9	148.5	163.2	C = 1.11*B	0.998
4	19.6	17.2	18.9		

Table 4.2 - Comparison of air permeabilities [darcys] given for each of the LSAMP versions. Linear relationships given between versions.

4.3 Laboratory Methods

Metal or lucite sampling rings of approximately 100 cc volume (5 cm diameter x 5 cm length) were used to hold the repacked sand samples. The mass of the sand, the porosity of the sand, and the grain-size distribution of the sand were characterized using standard practices of gravimetric oven drying and sieving (see Appendix B for full details). The volume and porosity of the sands were used to determine the water retention relationships for the different samples.

Once the LSAMP II was calibrated, it was used in laboratory tests to determine the effects of water saturation on air permeability in the unconsolidated sands of Oyster, Virginia. To perform these laboratory tests, standard hanging columns attached to Buchner funnels were used to produce a uniform water saturation in each sample (Figure 4.2). Klute (1986) documents the standard method for running hanging column experiments and concludes that for repacked cores 2.5 cm high, the experimenter should allow a "minimum of two and preferably three days for equilibrium" to be reached for each step. Klute (1986) also found that "the time for reaching equilibrium (was) proportional to the square of the height of the sample." Our samples were 5 cm high and required more time to reach an approximate equilibrium. Jucá (1993) found that for 2 cm

samples of sands, silts, and clays, full equilibration was not reached in 2 weeks. From the above review, and with time constraints, we used between 3 and 7 days for our equilibration time between steps.

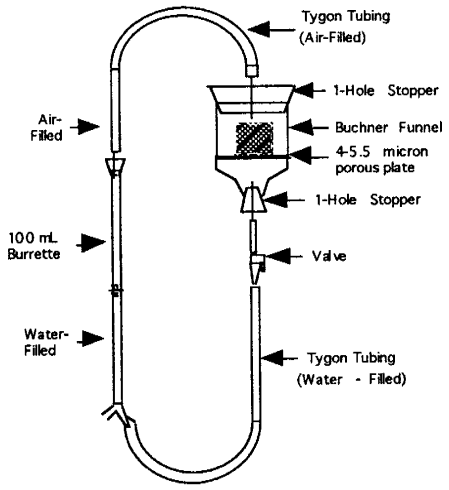

Figure 4.2 - Hanging Column schematic

Disturbed samples of sand for the Oyster Pit were collected in the field by Brian Parsons of ODU in the fall of 1995. These samples were bagged and sent to NMT where they were repacked in the 100 cc rings, 5 cm tall and 5 cm in diameter. The bottom of each ring was fitted with a paper filter to prevent sample loss and to improve the seal with the porous plate in the Buchner funnel. Samples were packed by pouring the sand into the 100 cc sample rings while continuously vibrating the samples to induce settling of the sand, to promote homogeneity of the sand pack, and to prevent layering. We then placed the repacked Oyster sand samples onto the porous plate in the Buchner funnels and wetted them from below to limit the amount of trapped gas. We measured the percentage of water saturation versus the suction (-cm) applied, to get standard moisture retention curves.

The first eight repacked samples (R3-R10) constituted our trial runs in the hanging column method, but for these samples we only waited about a day for each equilibrium state. We set up blanks to track the changes in water saturation for each step and to help us determine whether we had reached an approximate equilibrium state. Our

blanks consisted of a hanging column containing an unpacked ring sample. Eleven repacked samples (R11-R20 and R24), and two undisturbed samples (R25-R26) taken from the field in April of 1996, were successfully completed. The retention curves that these experiments generated were modeled with the Brooks and Corey (1964) and the Mualem (1976) models (Appendix D).

The hanging column set-up method allowed the repacked sand samples to equilibrate to specific water saturations. For water saturations of 50% and lower, air permeability of the samples were measured using the LSAMP II. Wyckoff and Botset (1936) found that, for repacked fine sand of 70 to 120 standard sieve mesh size (phi = 3.0 to 2.25) at liquid saturations less than 40%, the samples had a high enough gas to liquid flow ratio that the movement of the air through the sample would not affect the water present in the sample. For saturations higher than 40%, they found that the effect of pushing air through a sand column would be to push water out of the surrounding pores thus creating a flow path for the air out of the sample. Wyckoff and Botset (1936) also found that, at 50% liquid saturation, the effective permeability due to air was only about 1/3rd of the intrinsic value for their sands. Below residual water saturation, found to be about 10% by Wyckoff and Botset (1936), their samples retained the same air permeability. In our early experiments (R3-R10) LSAMP II measurements were made in sand samples with water saturations above 50%. Water was displaced by the injected air. These experiments confirmed that below about 50% water saturation, water was no longer being displaced out of the hanging columns by the injected air volume. The hanging columns allowed measurements on the samples down to the residual water saturation value, where further suction resulted in negligible removal of water. Though Wyckoff and Botset (1936) advocated using evaporation to remove the remaining water, we concluded that evaporation would cause a drying front to move through the sample, which would prevent a uniform water saturation to be reached. A Vapor Equilibrium

System, or VEQ (Mark Ankeny, personal communication, 1996), was used to uniformly dry the samples below the residual water saturation.

The VEQ is a closed system that flows air through the sample to remove water in the vapor phase, allowing the entire sample to reach a uniform water saturation. The system uses a closed loop to circulate air through the sample and a downstream container holding a desiccant. The air flow direction is reversed every minute to reduce nonuniform drying and the pressure at each end of the sample is measured using a differential pressure transducer to monitor changes in air permeability. The switching of flow direction also allows water trapped in dead end pores to be better accessed. Upon reaching apparent residual water saturation in the hanging columns, the samples were removed to the VEQ and dried in steps. The samples were weighed at each step to determine the amount of water removed and air permeability readings were taken at each step using the LSAMP II. The *in situ* air permeability of the VEQ was not measured. When the water saturation reached between 5% and 10% (depending on the sample), the sand became very friable, allowing the flow of air from the LSAMP II to compress and displace the sand, causing inaccurate readings and degrading the samples. The value of water saturation at which the sample became so friable that it fell apart was recorded as the lower limit of use for the LSAMP II. Below this lower limit of water saturation, the samples were oven dried to determine the final water saturation, the grain size distribution, and the porosity.

4.4 Geostatistical Analysis

One purpose of collecting numerous measurements of permeability from outcrops in the field is to model the spatial variability of the permeability for the aquifer geology. Ideally, we would measure the hydrologic parameter directly at each point in the entire aquifer, but this is neither cost effective nor plausible. Instead, we must use the limited information we can gather, and then conduct geostatistical surveys of that information so

that we can infer the relationships for the rest of the aquifer. A brief synopsis of certain aspects of geostatistics is given below. Those interested in a more specialized description of the different aspects of geostatistics should refer to various texts on the subject (e.g., Isaaks and Srivastava, 1989; Deutsch and Journel, 1992).

In geostatistics, the spatial variability of permeability can be described empirically by using semivariograms, which are equal to half the average squared difference between paired data values. The variogram gives a measure of the correlation between pairs of data points based on the distance separating the data points. Variograms are characterized by their range, sill, and nugget. The range is the separation distance between data points such that further separation does not cause the variogram value to change. The range occurs when the variogram reaches a plateau, or sill, which typically is quantified by the variance of the data set. The nugget is the variogram value at zero separation distance and accounts for the sampling error and short scale variability (Isaaks and Srivastava, 1989). Numerous studies (e.g., Johnson, 1995; Ritzi et al., 1995; Koltermann and Gorelick, 1995) have focused on variography as a way to describe the spatial variability and correlation length for permeability and hydraulic conductivity.

For my study, two geostatistical surveys were conducted on the central area of Tier 2, called Panel 5, during the April 1996 field season (Figure 4.3, see also Figure 1.1). Air permeability measurements were taken in the lower right corner of each of the 200 grid squares of Panel 5. The geostatistical studies were similar in method, but the first study was conducted on the measured effective air permeability collected in the field and the second geostatistical study was conducted on the approximate values of intrinsic permeability that we determined based on our laboratory non-wetting phase relative permeability curves (correction factors) for water saturation.

Isaaks and Srivastava (1989) suggested that a geostatistical analysis begin with summary statistics, histograms, cumulative distributions, and checks for normality of the

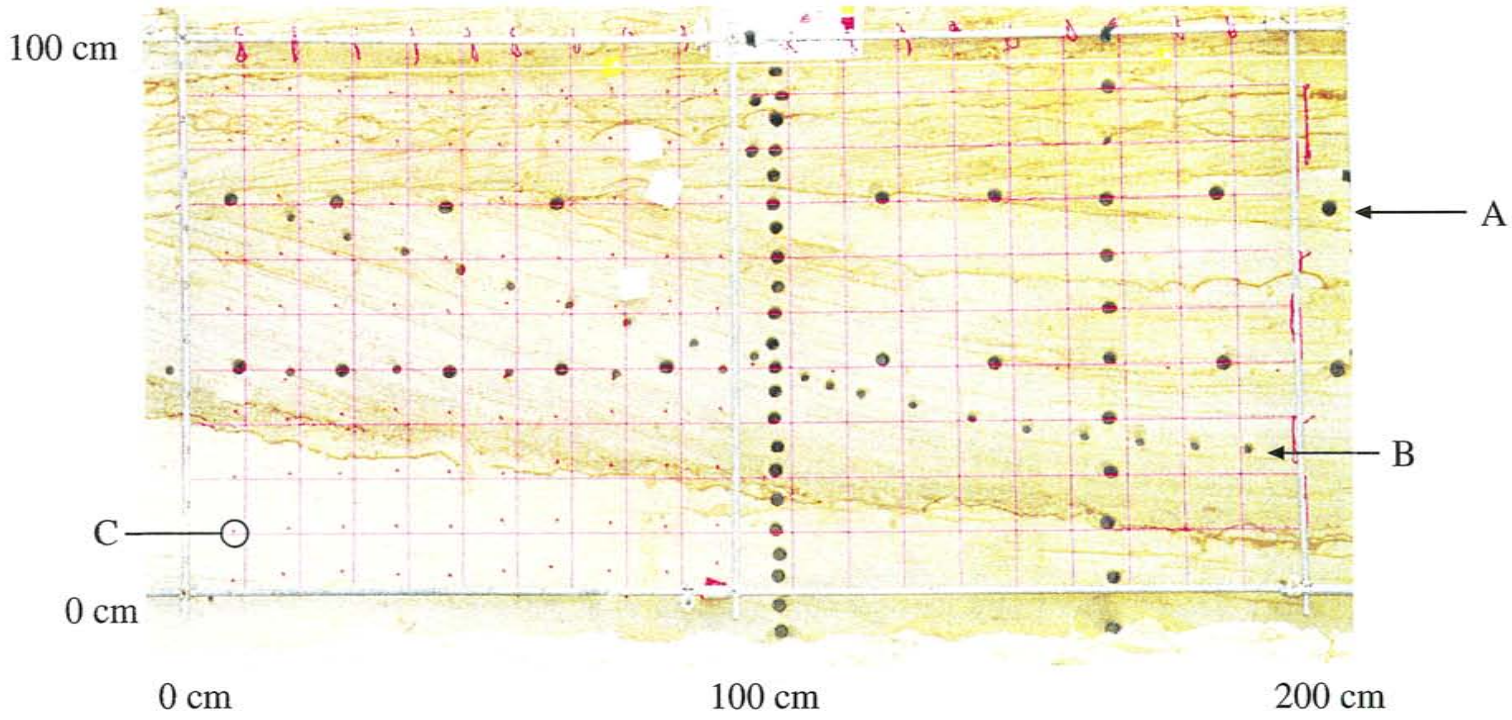

A: 10 cm long, 50 cc cores (INEL) — transects

B: 10 cc grain size only samples (ODU) — along dip

C: Pins denoting location of LSAMP II measurement

Figure 4.3 — Panel 5 with transect holes and pins denoting placement of LSAMP II measurements. Measurements along dip (10 cc cores) are not considered in the statistical determination.

data set. We used SYSTAT 5.2.1 (SYSTAT, Inc., 1990-1992) to conduct these tests as well as check for outliers in the data set. The two outliers found occurred in a sand of the Gravelly Shelly facies type which cut across the panel section (see Figure 1.1 labels). This band of gravel separated the Cross-Stratified sand facies from the Horizontally Stratified sand facies. The data set was studied as a whole and also as two separate facies types. The statistical normality of the data sets was tested using the Kolmogorov-Smirnov equation. Isaaks and Srivastava (1989) have suggested that variography should be used to find the spatial correlation within the data set. We used VARIOWIN (Pannatier, 1994) to perform a variogram analysis on the data sets to check for the range, sill, and nugget. Separate analyses were conducted for the large block of cross-stratified sand facies, for a lower block of horizontally bedded sand facies, and for both together. Directional variograms were computed parallel to the depositional packets and normal to the depositional packets. VARIOWIN allows the user to fit different models to the variograms by choosing a nugget, range, and sill. Through trial and error, the user can find a best fit curve that minimizes the residuals in a way similar to linear regression's best fit straight line to a number of points, although the statistical validity of the resulting variogram fit is not well established.

Once we had performed these statistical analyses on the previously described data sets, we compared the different data sets. Our focus was the difference between the measured effective air permeability and the approximations for the intrinsic permeability that we calculated using our non-wetting phase relative permeability curves (correction factors). We examined the differences for the Cross-Stratified sand facies, the Horizontally Stratified sand facies, and for both facies together. We also examined the influence of water saturation across the outcrop face on the geostatistics of air permeability.

CHAPTER 5 - RESULTS AND DISCUSSION

5.1 Introduction

Earlier we posed these questions: (1) for the water saturations found in the different facies types in the field, could we determine an air permeability correction factor to remove the bias?; (2) is there a water saturation that is low enough for the measured effective air permeability to approximate the intrinsic permeability?; (3) is the bias introduced by the water saturation of geostatistical importance; and (4) what lessons can we learn about conducting experiments in humid environments? The first two questions require that we analyze the water saturation values found in the field in terms of the air permeability saturation dependence found in laboratory samples for the different facies types. To answer the third question, we looked at our geostatistical survey results for Panel 5. Though the majority of our data, graphs, and charts are located in Appendices B through D, the compiled data and results are presented here. The answer to the fourth question will summarize our experience.

This chapter begins by looking at the water saturation and grain-size distributions that were collected in the field from Panel 5 (Figure 5.1), along with the effective air permeabilities collected with LSAMP II. This data is summarized in **Figures 5.2** through **5.4**. The laboratory sand characterizations, water saturation-capillary tension curves, the effective air permeability versus percentage water saturation figures, and the change in the relative permeability at different water saturations for the different laboratory samples are presented next. Discussion focuses on the Cross-Stratified sand facies because the majority of the laboratory samples were from this facies type. A brief discussion of the Horizontally Stratified facies type is included because that facies type is contained in the lower section of Panel 5. The discussion continues with our geostatistical surveys of Panel 5 for the cases of effective air permeability and intrinsic air permeability. The

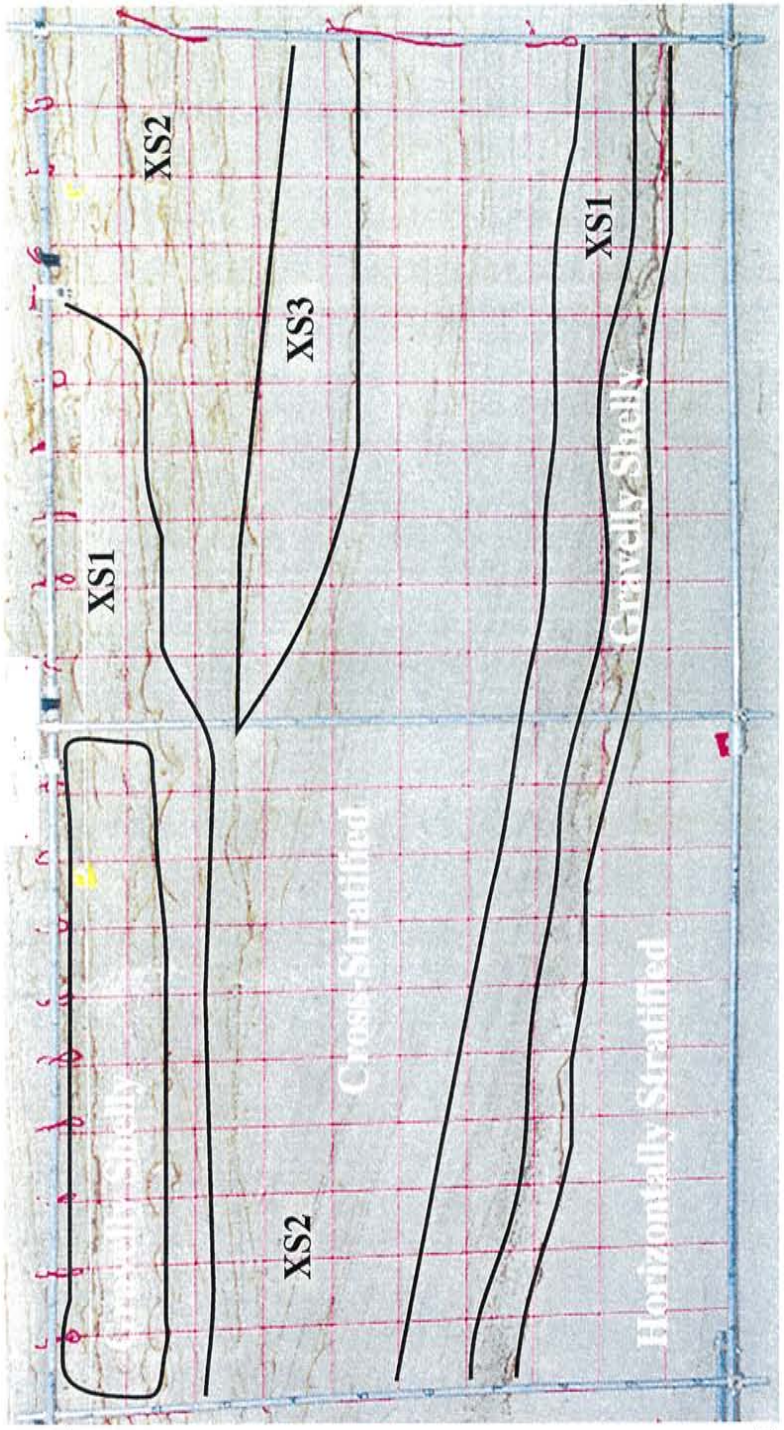

Figure 5.1 — Tier 2. Panel 5. Three distinct facies types and their extent within a 2 m x 1 m gridded section. Cross-Stratified subsets delineated by geologic coset. Directions refer to variography found later in Chapter 5.

discussion ends with some recommendations for the collection of percentage of water saturation readings in the field for future projects.

5.2 Grain size, air permeabilities, and water saturation in the field

Figure 5.2 shows the distribution of mean phi size for the grain size distributions of the transect data. A sharp change is seen on the central vertical transect at a height of about 20 cm. The change in mean phi size is seen again at just above 10 cm height on the right vertical transect. These phi differences, between about 1.50 and 2.50, reflect the change in facies type, from the Cross-Stratified sand facies, above, to the Horizontally Stratified sand facies below. The transects do not sample any of the Gravelly Shelly sand facies that exist as narrow lag layers or bands between the two other facies types (see Figure 5.1). The three subsets in the Cross-Stratified facies were designated based on mean phi size and geologic bedding.

Figure 5.3 shows the location and values of measured air permeability throughout the Panel 5 grid. Each of the two hundred sections of the grid were sampled, plus extra points along the central vertical transect and some additional points in the Horizontally Stratified sand below the bottom of the sampling grid. The two horizontal and two vertical transects were sampled on April 19, 1996 (Figure 2.3). Also sampled on that date were the points located from 0 to 100 cm in the horizontal direction and 50 to 100 cm in the vertical direction. The lower half of the left side and the entire right side was sampled between 10:30 a.m. and 1:00 p.m. on April 20, 1996. The Gravelly Shelly sand facies was sampled only twice at approximate locations (20 cm, 30 cm) and (100 cm, 20 cm). Using these two points as a guide for looking along the boundary between the Cross-Stratified sand facies and the Horizontally Stratified sand facies, it can be seen that effective air permeability drops off significantly from a range of about 30 to 80 darcys in the Cross-Stratified facies, down to values between 10 and 20 darcys in the Horizontally Stratified facies.

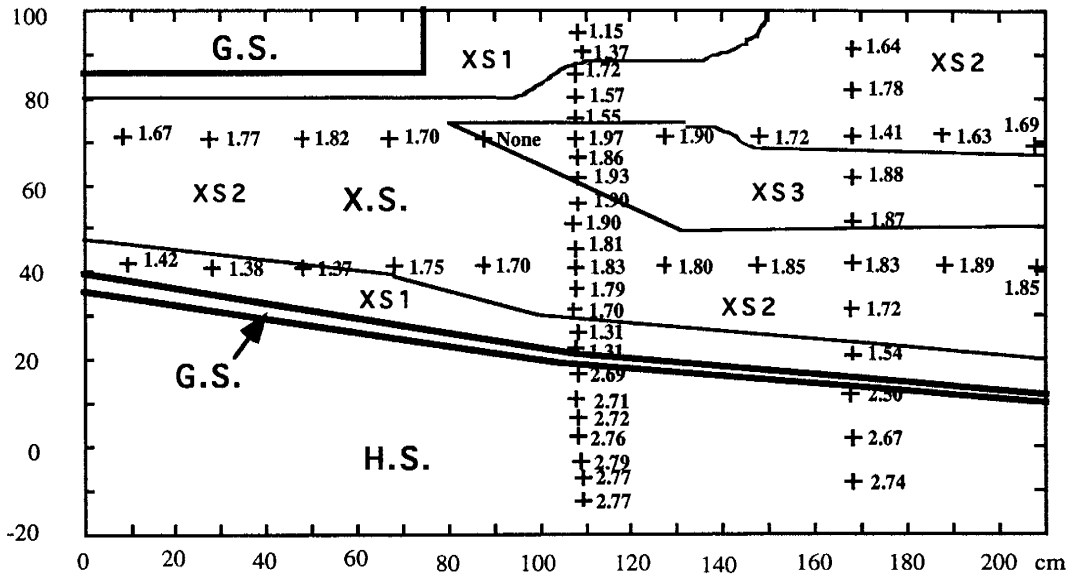

Figure 5.2 - Mean phi size for Panel 5 transects (ODU).
Facies designated based on grain size and geologic bedding.

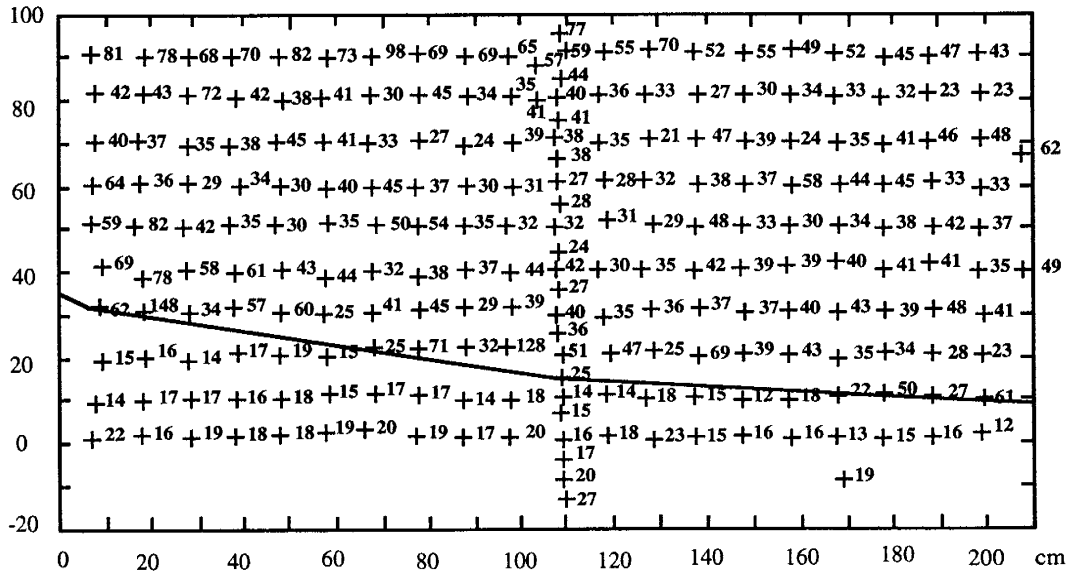

Figure 5.3 - Effective air permeability locations and values (darcys)
for Panel 5 (NMT). Line represents separation of HSF from XSF.

Figure 4.3 shows a photograph of Panel 5 with the vertical and horizontal transect core holes. These 10 cm long cores were taken at approximately noon on April 19th. They were analyzed by INEL for percentage water saturation (Figure 5.4). The field data shows that there was little difference in percentage water saturation regardless of the facies type from which the data came. Panel 5 was located on the second Tier and was less influenced by the recent rain or the capillary fringe above the water table. After separating the Cross-Stratified sands of Panel 5 into the three different geologic cosets (XS1, XS2, and XS3), linear interpolation of the INEL percentage water saturation transect values within each of the cosets was used to estimate the percentage water saturation at each of the air permeability locations (Figure 5.5). These values are also given in Appendix C. The contouring gives a general picture of the water saturation averaged over the 10 cm closest to the face of the outcrop. These values overestimate the water saturation at the surface of the outcrop, which experienced evaporation from the time it was opened, especially during daylight hours when it was exposed to the sun.

We also collected water saturation values for the top 5 cm closest to the surface of the outcrop. We felt that the data from the top 5 cm closest to the face of the outcrop was more accurate since LSAMP II measures the permeability in the top 1 to 2 cm below the tip seal. There were fewer of these samples, they were taken both before and after the air permeability readings were measured. These data are given below (Table 5.1). The nearby readings from the Horizontally Stratified facies, taken around 12:30 p.m. on April 19, 1996, ranged from 17.8% to 18.7%. These values are similar to the INEL core data for this facies. This suggests that our readings from the nearby Horizontally Stratified facies provide a reasonable approximation of the moisture conditions found in the Panel 5 Horizontally Stratified facies. Our 5 cm data from Rows 2, 5, and 8 of Panel 5 (Table 5.1), taken after we finished the LSAMP II sampling of Panel 5, are similar to the INEL Cross-Stratified core data. Therefore, we decided to use the linearly interpolated contoured INEL water saturation values for the Cross-Stratified facies and the NMT

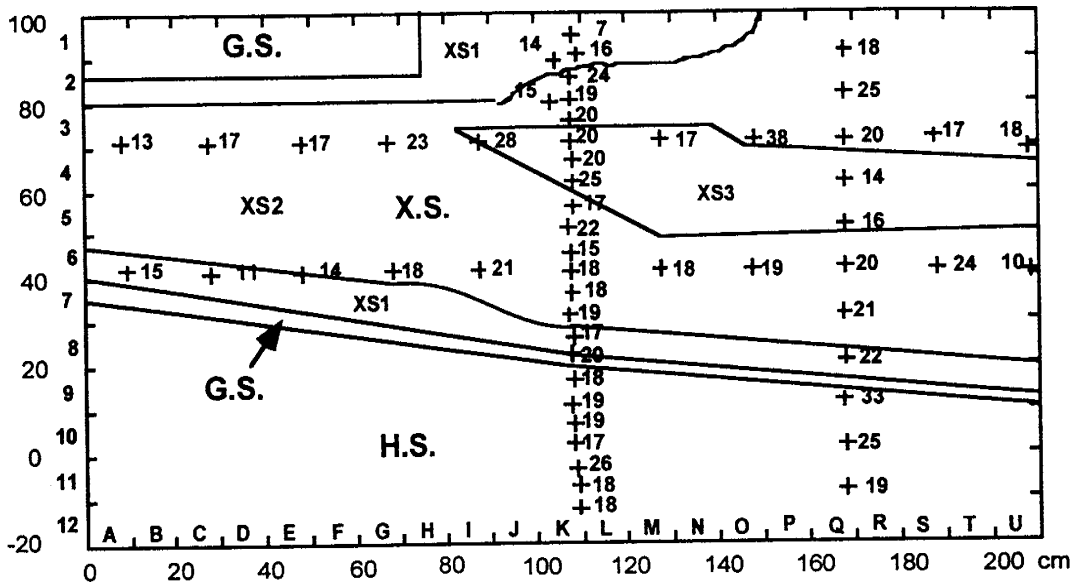

Figure 5.4 - Percentage Water Saturation values for Panel 5 transects (INEL). Axes lettering and numbering corresponds to Field row and column designators.

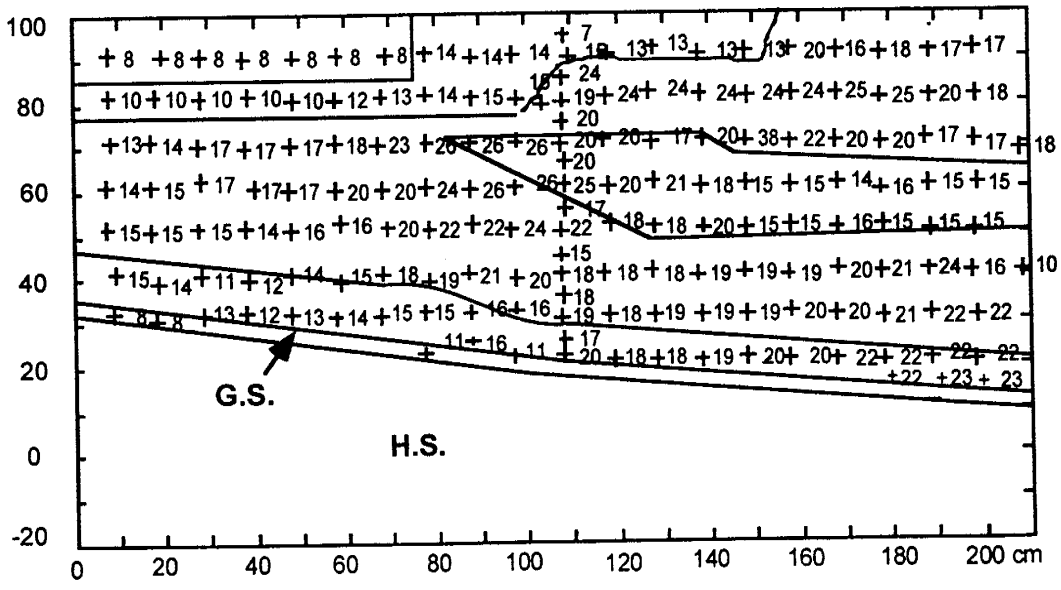

Figure 5.5 - Linear interpolation of percentage water saturation values for each subset of the Cross-Stratified sand facies.

Date	Time	Facies	Saturation %	Mean phi	Notes
4/19/96	9:30	HS	23.5	2.93	Same bed as Panel 5 HS
4/19/96	9:30	HS	23.6	2.93	Same bed as Panel 5 HS
4/19/96	12:30	HS	17.8	2.87	Same bed as Panel 5 HS
4/19/96	12:30	HS	18.7	2.87	Same bed as Panel 5 HS
4/20/96	8:45	HS	15.3	2.89	Same bed as Panel 5 HS
4/20/96	8:45	XS1	18.8	1.66	Similar bed as Panel 5 XS1
4/20/96	11:30	HS	12.8	2.96	Same bed as Panel 5 HS
4/20/96	11:30	XS1	11.2	1.61	Similar bed as Panel 5 XS1
4/20/96	14:30	XS2	26.5	1.76	Panel 5, Row 2
4/20/96	14:30	XS3	17.8	2.02	Panel 5, Row 5
4/20/96	14:30	XS2	22.1	1.70	Panel 5, Row 8

Table 5.1 - Percentage water saturations for Cross-Stratified and Horizontally Stratified facies of Tier 2

measured values from the upper 5 cm of the face for the Horizontally Stratified facies. Since we had no water saturation data from the Gravelly Shelly facies and only 2 air permeability data points from the Gravelly Shelly facies type, and since this was the coarsest fraction of sand and would need the least correction, we did not make a correction on those data points.

5.3 Grain Size Distribution of Laboratory Samples

The Gravelly Shelly facies (GSF) is characterized as containing more than 10% by weight of gravel sized particles. Unfortunately for this study, none of the laboratory samples were from this facies type. The second facies is the Cross-Stratified sand facies (XSF) that is characterized by a mean grain diameter that is less than 2.00 phi units, which is equal to greater than about 250 microns. The majority of the laboratory tested samples fall into this category. The Horizontally Stratified sand facies (HSF) is characterized by a mean grain diameter greater than 2.00 phi units. Only sample number R26 was from the HSF, so it will be discussed separately. Regardless of each of the samples facies types, there were certain characteristics of the grain size distribution shared by all the samples. The majority of the sand in all the samples came from a relatively narrow range of 300 to 417 microns, or 1.75 to 1.25 phi units, U.S. Standard sieve mesh 50 to 40, and a Wentworth size class of medium sand (Boggs, 1987). The

individual results and histograms of grain size distribution are located in Appendix B of this volume, while a compilation of the results for the XSF are shown in **Table 5.2** and **Figure 5.6** below.

Within the 12 XSF samples tested in the lab there appear to be three different grain size distributions that characterize the different samples. We calculated the mean ($\bar{x} = \frac{1}{n}\sum_{i=1}^{n} x_i$) and standard deviation ($s.d. = \sqrt{\frac{\sum_{i=1}^{n}(x_i - \bar{x})^2}{n-1}}$) for each distribution. The first, XS1, is found in samples R3 through R6, R11, and R14. The average of their mean phi size is 1.54 with a standard deviation of 0.06. These samples have a nearly guassian distribution with an average of 41% of the sand falling in the 300 to 417 micron size range. The second group, XS2, consists of samples R8, R10, R12, R13, R16, R17, R20, and R24. The average of their mean phi size is 1.76 with a standard deviation of 0.04. About 36 ± 5% of the sand is in the 300 to 417 micron range, with higher percentages of finer sand than in XS1. Finally, the third group, XS3, consists of samples R7, R9, R15, R18, R19, and R25. The average of their mean phi size is 1.92 with a standard deviation of 0.03. A double peak exists in XS3 with 26 ± 5% of these samples is in the 300 to 417 micron range and 25 ± 5% in the 75 to 212 micron range. Even though each of these samples is from the Cross-Stratified sand facies, the different characteristics of the grain size distribution has led us to separate the samples into these categories when testing for the relationships between water saturation and air permeability.

Though there was only one sample from the Horizontally Stratified sand facies (R26), it had a very homogeneous grain size distribution for the sample (Figure 5.7). Nearly 70% of the weight was from the range of 150 to 210 microns, with 21% from the range 106 to 150 microns. R26 was taken from the Horizontally Stratified section of Panel 5 (see figure 1.1), and has a similar mean phi to the values taken from the transect cores (2.81 compared to a range of 2.50 to 2.80). The standard deviation of the core samples taken from Panel 5 was 0.045 implying homogeneity of the Horizontally

Descriptor/Sample	XS1		XS2		XS3	
Size (microns)	Mean %	Std. Dev. %	Mean %	Std. Dev. %	Mean %	Std. Dev. %
>2000	2.2	2.8	0.2	0.2	0.3	0.4
1000-2000	3.9	2.7	1.3	1.2	1.5	1.2
500-1000	8.6	3.1	8.3	2.7	8.2	3.9
417-500	6.2	2.1	5.5	0.7	3.6	2.8
300-417	41	20	36	5.2	26	12
250-300	17	15	20	1.3	20	5.0
212-250	9.6	4.3	13	1.0	15	3.2
75-212	11	3.5	16	2.0	25	5.9
<75	0.4	6.3	0.1	0.1	0.1	13

Table 5.2 - The repacked laboratory Cross-Stratified facies samples are grouped into three subsets (XS1, 2, and 3)

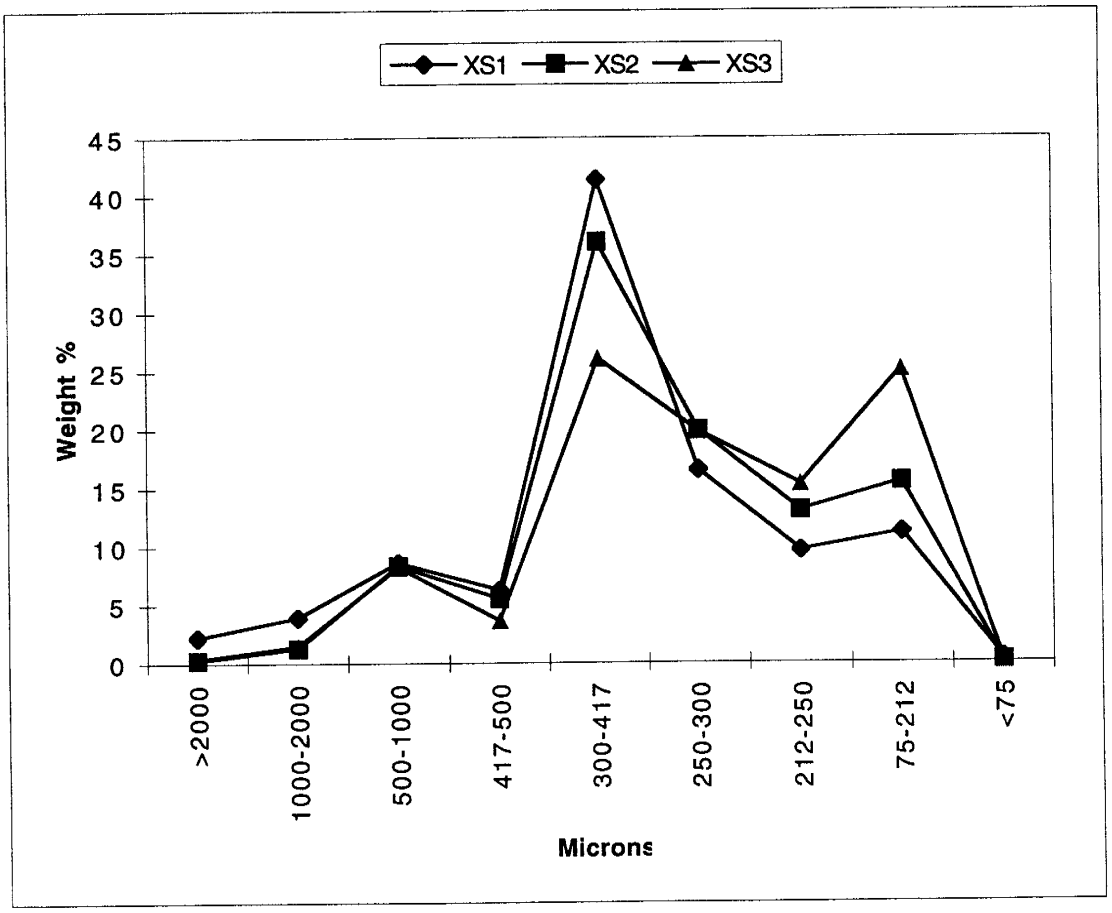

Figure 5.6 - The mean weight percentages of each grain size class for each of the three XSF subsets are plotted as a distribution.

Stratified facies. Though we had saturation data for the measurements in the Horizontally Stratified facies, we had only one sample (R26) on which to conduct laboratory tests to determine a non-wetting phase relative permeability curve (correction factor) for the Horizontally Stratified facies. Though testing just one sample is not statistically significant, we chose to use the results from the R26 water saturation correction laboratory test to correct for the water saturation located in the Horizontally Stratified sand facies of Panel 5.

5.4 Soil Moisture Retention Curves and Air Permeability vs. Percent Water Saturation Relationships

As the majority of the samples, R11-R19, R20, R24, R25, were part of the Cross-Stratified sand facies, this discussion focuses on the relationships between air permeability and water saturation in the Cross-Stratified sand facies. The following plots are compilations of the data collected on each sample (see Appendix C). Use of the hanging columns allowed us to calculate the soil moisture retention functions for each of the sand samples. Each of the curves is calculated using standard methods (see Appendix A) and the compilation is shown in **Figure 5.8**. None of them reached complete saturation during initial saturation of the samples with water. Since we were most concerned with the unsaturated region (<35% water saturation) that we encountered in the field we did not worry about the gas initially trapped within the sample. Since the sands were all composed of the same range of grain sizes and the repacking gave similar sorting characteristics, it was not surprising that each of the samples reached its bubbling pressure at about -30 cm of suction. The hanging column set-ups for R11 through R14, did not allow as much suction as the others, but these samples each seemed to reach their residual moisture saturation at about -60 cm of suction. The value of residual saturation

for the different samples ranged from 6.6% to 12.8% with a mean of 9.9%. Though these values of residual saturation may seem below average, Wyckoff and Botset (1936) found residual water saturations of approximately 10% for a heterogeneous mix of fine to

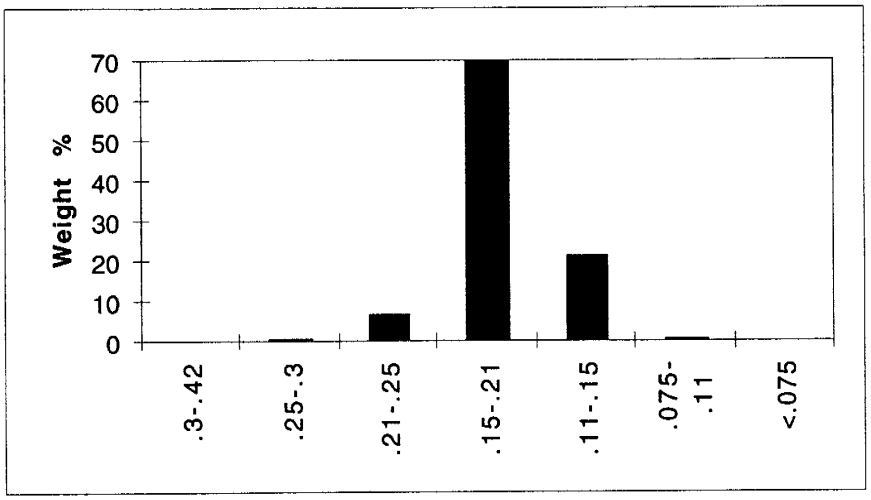

Figure 5.7 - Grain size distribution of HSF sample; x axis in 1000's of microns

coarse grained sand. Likewise, Jucá (1993) found residual water saturations of about 13% for a clayey sand. Finally, Dullien (1992) reported residual water saturations as low as 2.5% for 5.0 mm glass beads. We apply the Brooks and Corey (1964) and the Mualem (1976) models to our moisture retention curves in Appendix D.

The second set of plots (Figure 5.9) has the measured effective air permeability [darcys] plotted against the percentage water saturation of the sample. The water saturation ranges from about 50% to the value where the sand became so friable that it lost its structure during the permeability measurement (about 3-5%). The vertical lines denote the vicinity of residual water saturation where the samples were taken from the hanging columns and placed into the VEQ. The vertical lines differ in location since the different Cross-Stratified subsets showed slightly different residual saturation values. Plotting the values in semilog space in **Figure 5.10**, from 50% water saturation to the residual water saturation value, shows an apparent log-linear relationship of natural log effective air permeability versus percentage water saturation. A compilation of the log-linear regression relationships for all the data, for XS1, for XS2, and for XS3, for the

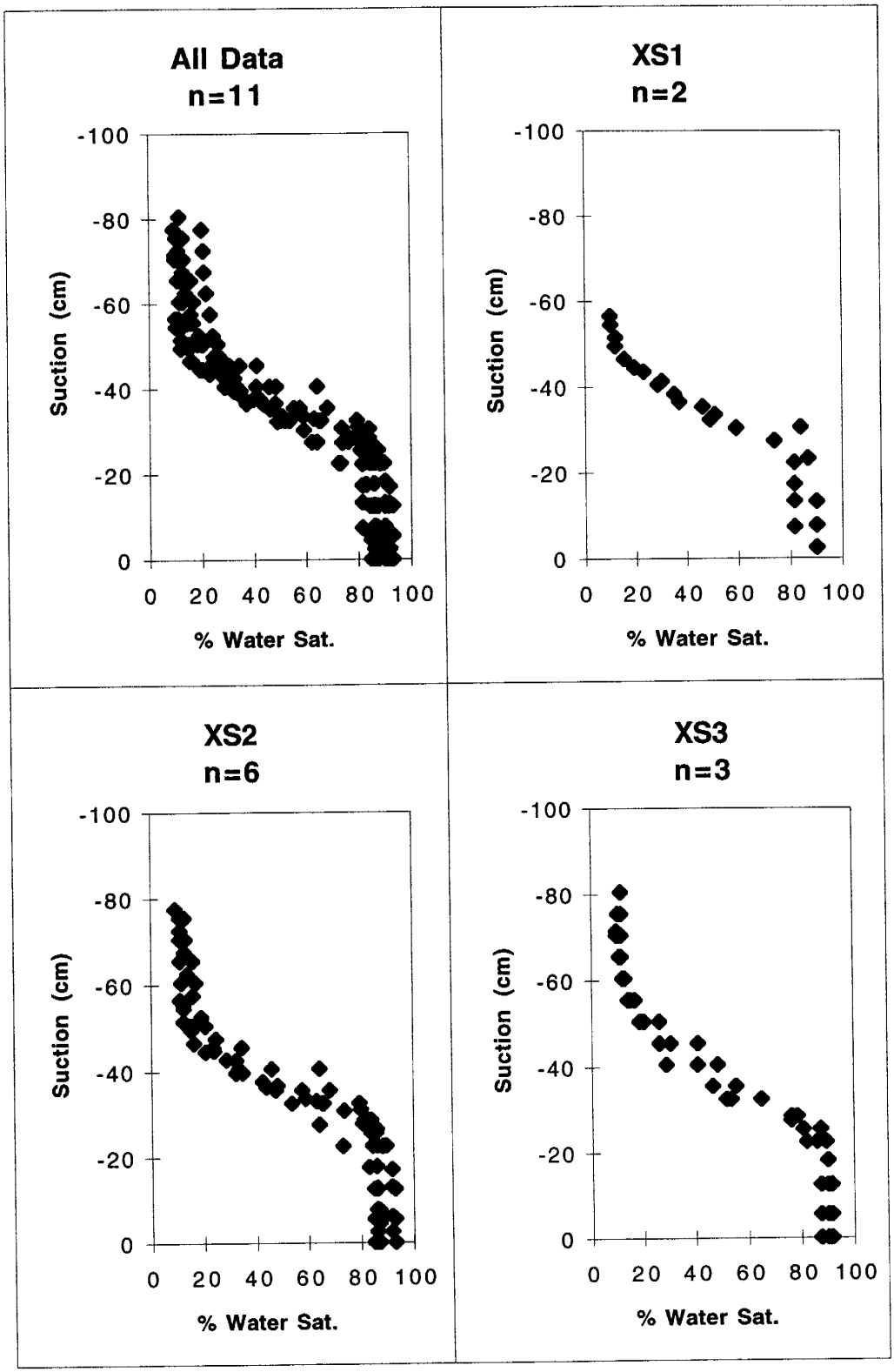

Figure 5.8 - Moisture retention functions for repacked laboratory samples for 3 Cross-Stratified Facies sand subsets

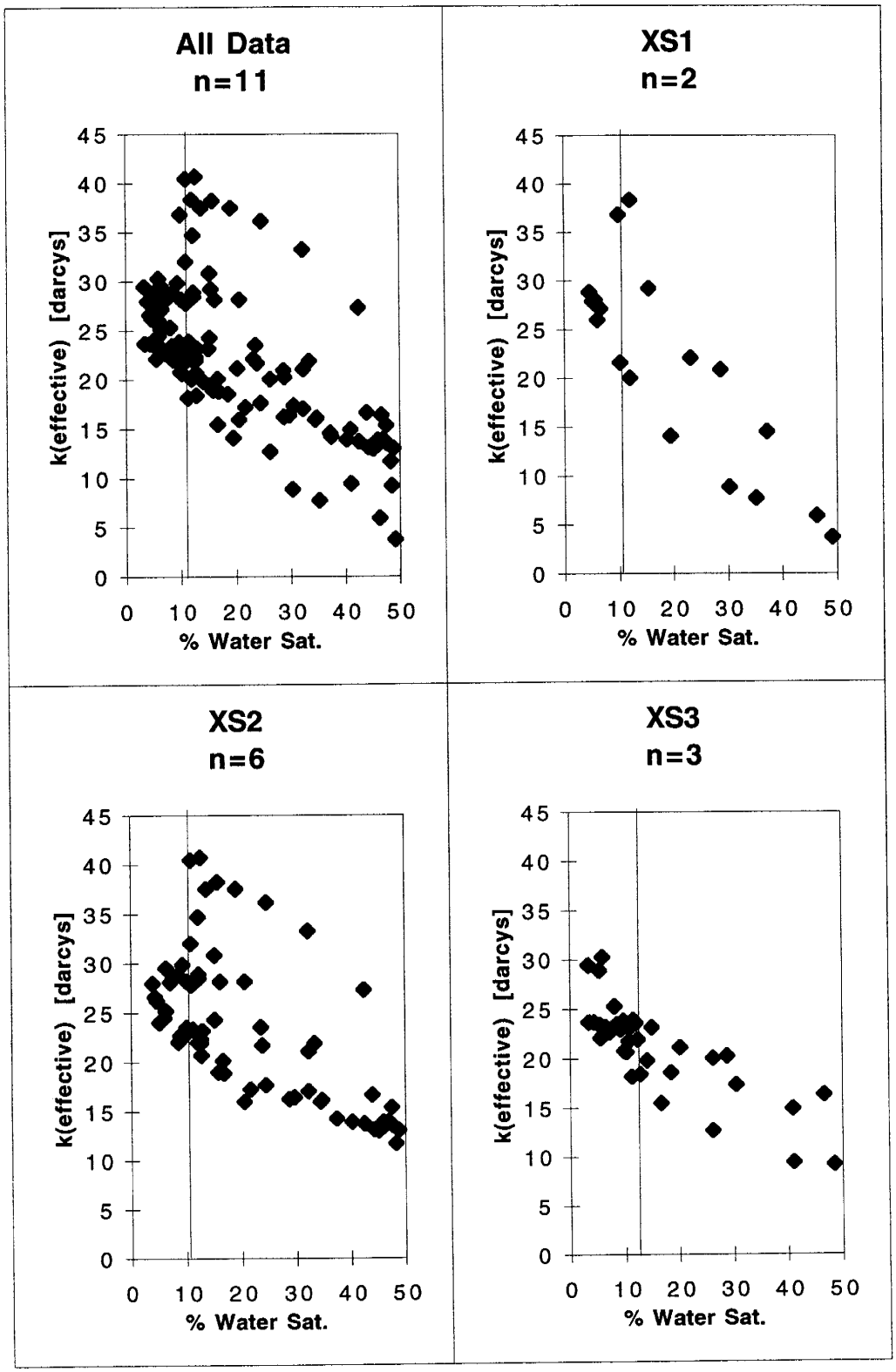

Figure 5.9 - kair(effective) [darcys] versus % water saturation for all repacked laboratory samples for XSF subsets. Vertical lines denote residual water saturation when samples were removed from the hanging columns.

range of water saturation from residual to 50% is contained in **Table 5.3**. By separating the samples into the different grain size distribution classes, the correlation coefficients rise and the slopes change, but the intercept remains fairly constant. Below the residual water saturation, the degree of change in air permeability is negligible for a given percentage of change in water saturation. Below the residual water saturation, the samples show a distinct flattening of the curve in log-space, implying that the effective air permeability approximates the intrinsic air permeability. By extending the flattened curve to the axis, an estimate of the intrinsic permeability for each of the samples was derived (Table 5.4). Using this value for the intrinsic permeability, approximations for the relative permeability versus percent water saturation were obtained for each of the Cross-Stratified sand samples.

Facies	Log Linear Relationship	r^2
All (n=11)	Ln k(eff) = -0.0192*(% Water Sat.) + 3.4359	0.467
XS1 (n=2)	Ln k(eff) = -0.0293*(% Water Sat.) + 3.5662	0.638
XS2 (n=6)	Ln k(eff) = -0.0177*(% Water Sat.) + 3.5049	0.556
XS3 (n=3)	Ln k(eff) = -0.0261*(% Water Sat.) + 3.3219	0.71

Table 5.3 - Log-linear relationships between effective air permeability and percentage water saturation

Only one sample R26 was representative of the Horizontally Stratified sand facies (Figure 5.7). Since the sand came from a much finer grain size distribution with smaller pore sizes, more suction was required (about 152 cm) to reach the residual water saturation. Also due to the finer grain size distribution, the residual water saturation within the sample was larger (about 13%). **Figure 5.11b** shows our measured k_{air}(effective) versus percentage water saturation. Our measurements began at just under 50% water saturation and continued down to our residual water saturation (13%) in the hanging column. We used the VEQ to reduce the water saturation further to the limit of structural stability within the sample (about 9%). **Figure 5.11c** shows the apparent log-linear relationship between the natural log k_{air}(effective) versus percentage water saturation. The Horizontally Stratified sand sample was very homogeneous and well sorted; the effect of the water saturation was reduced within these samples compared to

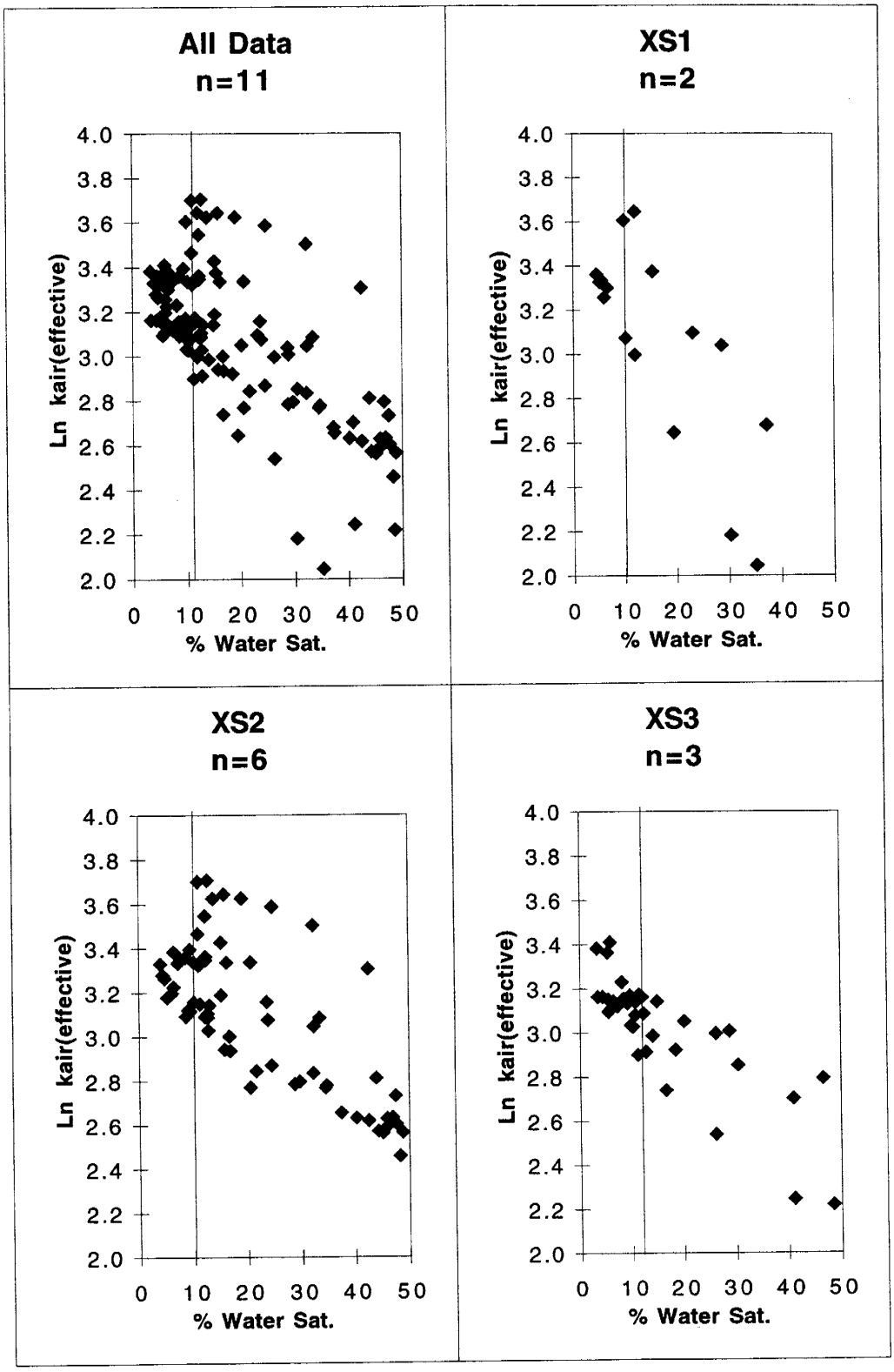

Figure 5.10 - Ln kair(effective) [darcys] versus % water saturation for all repacked laboratory samples for XSF subsets. Vertical lines denote residual water saturation when samples were removed from the hanging columns.

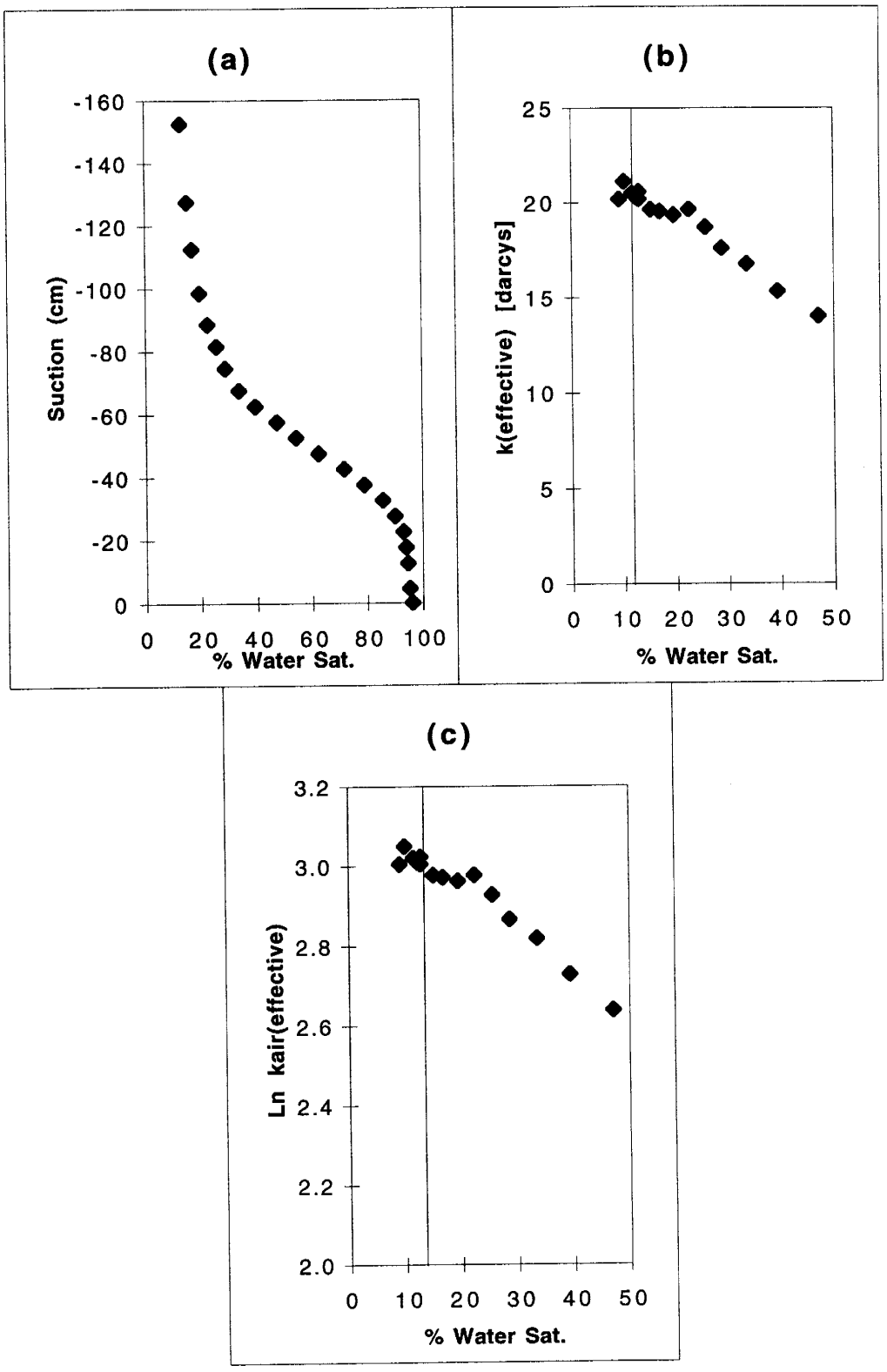

Figure 5.11: HSF Sand Sample (R26); a) Moisture retention function; b) kair(effective) [darcys] versus % water saturation; c) Ln kair(effective) versus % water saturation. Line represents residual water saturation.

Sample #	Subset	Ln k(intrinsic) estimate
R11	XS1	3.61
R12	XS2	3.47
R13	XS2	3.43
R14	XS1	3.34
R15	XS3	3.12
R16	XS2	3.36
R17	XS2	3.20
R18	XS3	3.38
R19	XS3	3.16
R20	XS2	3.33
R24	XS2	3.71
R26	HS	3.02

Table 5.4 - Estimated intrinsic permeability (darcys) from laboratory samples

the more heterogeneous Cross-Stratified sand samples. At a 50% water saturation we measured a k_{air}(effective) of about 14 darcys and the estimated intrinsic permeability was only about 20.5 darcys.

5.5 Air Permeability Corrections

Once the intrinsic permeability of each sample was estimated, the natural log of relative permeability for each of the samples was plotted versus the percentage water saturation (individual graphs in Appendix C). Below the residual water saturation (estimated at roughly 10% water saturation) for each of the samples, the natural log of the relative permeability was close to zero. Above about 10% water saturation the different XSF groups had different log-linear relationships (Figures 5.12 a-c). XS1 was the coarsest of the Cross-Stratified sands and showed the largest non-wetting phase relative permeability reduction and, therefore, the largest correction for a given water saturation. XS2 and XS3 show similar non-wetting phase relative permeability reductions and, therefore, have similar correction factors for a given water saturation.

Similar to the Cross-Stratified sand samples, the grain size distribution of the Horizontally Stratified sand sample controlled the extent of the non-wetting phase relative permeability curve (correction factor) (Figure 5.12d). Though we only had one sample from the Horizontally Stratified sand facies, we performed a similar analysis on

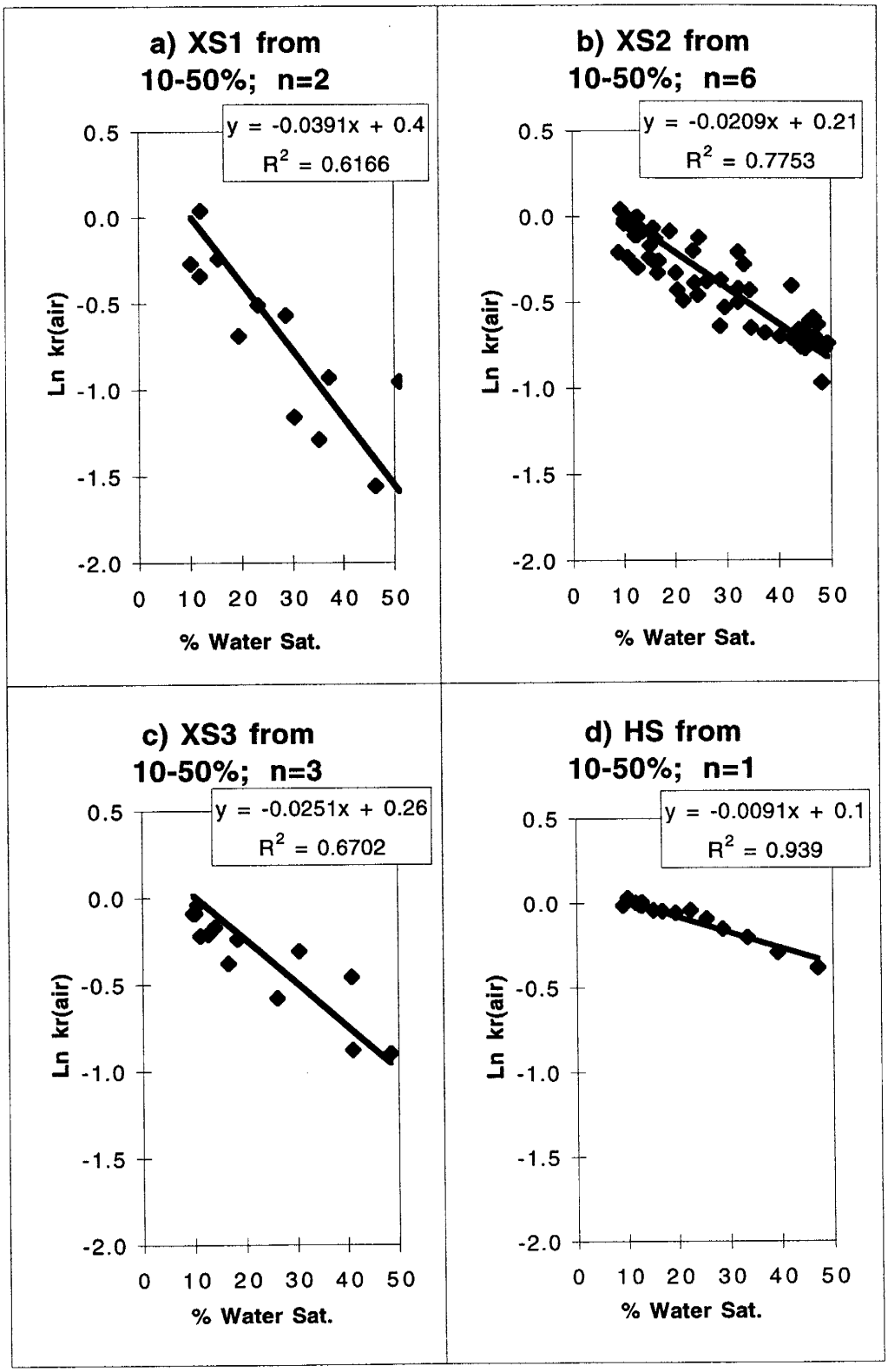

Figure 5.12 - Linear correction relationships for repacked laboratory samples for XSF subsets and HSF sand samples

that sample and found a log-linear fit with an r^2 value of 0.939 (Figure 5.12d). This facies had the smallest correction factor and the finest grain size distribution. This small correction factor coupled with the fact that the water saturations found in the field did not vary greatly within the Horizontally Stratified sand facies implies that there would be only a minor effect of the water saturation on the spatial statistics of the Horizontally Stratified sand facies. **Table 5.5** contains the log-linear relationships for each of the facies groups.

Facies	Log Linear Relationship	r^2
XS1 (n=2)	Ln kr(air) = -0.0391*(% Water Sat.) + 0.40	0.6166
XS2 (n=6)	Ln kr(air) = -0.0209*(% Water Sat.) + 0.21	0.7753
XS3 (n=3)	Ln kr(air) = -0.0251*(% Water Sat.) + 0.26	0.6702
HS (n=1)	Ln kr(air) = -0.0091*(% Water Sat.) + 0.10	0.939

Table 5.5 - Log-linear correction relationships for Cross-Stratified and Horizontally Stratified sand facies

5.6 Pre- and Post-Air Permeability Correction Geostatistics of Panel 5

Using the above correction relationships, we corrected the measured effective air permeabilities to their apparent relative permeabilities using logarithmic rules as follows:

$$\text{Ln } k_{intrinsic} = \text{Ln } k_{air} - \text{Ln } k_{r(air)} \quad (5.1)$$

$$k_{intrinsic} = \exp(\text{Ln } k_{air} - \text{Ln } k_{r(air)}) \quad (5.2)$$

We measured k_{air} values in the field and can determine $k_{r(air)}$ values if we know the grain size distribution and the water saturation value. **Figure 5.1** separates the different measurements into different grain size distribution subsets and can be used to determine which non-wetting phase relative permeability curve (correction relationship) to use. **Figure 5.4** has the estimated values of percentage water saturation for each measurement point which is used in the appropriate correction equation to determineln $k_{r(air)}$ for that measurement point. These values are then plugged into equation 5.1 to determine the estimate of the intrinsic permeability. The measured air permeability and estimated intrinsic air permeability values are found in Appendix C of this volume. Since the

majority of the Panel 5 measurements were XSF, and in particular from the XS2 subset of XSF, we felt that we could reasonably correct the majority of the measured air permeability values to their apparent intrinsic permeability.

5.6.1 Geostatistical Comparison of All Permeability Data

Using our laboratory derived non-wetting phase relative permeability curves (correction factors) for the Cross-Stratified and the Horizontally Stratified facies along with the measured effective air permeability, k_{air}, (Figure 5.3), the mean grain size of the field samples (Figure 5.2), and the measured and interpolated percentage water saturation values (Figures 5.4 and 5.5, Table 5.1), we estimated the intrinsic permeability, k, for Panel 5. We performed a statistical analysis on the ln k_{air} data set and on the ln k data set. **Table 5.6** contains a summary of the basic statistics for the two data sets. We found that the non-wetting phase relative permeability curves (correction factors) caused the ln k data set to have a higher mean value, a slightly (though insignificant) higher variance, a higher skewness, and a higher kurtosis. Two samples from the Gravelly Shelly facies, with k_{air} greater than 120 darcys, influenced the data analysis but are not considered outliers since we were looking at the entire data set. The fact that the data comes from three different populations (different facies types) is one reason why the entire data set does not have a normal distribution according to the Kolmogorov-Smirnov test (shown in Figure 5.13).

Statistic	Ln kair(eff)	Ln k(intrinsic)
N of cases	226	226
Mean	3.551	3.697
Variance	0.222	0.261
Skewness	-0.143	-0.536
Kurtosis	-0.268	-0.440

Table 5.6 - Summary statistics for all the permeability data

We made the assumption that we had five different populations of data; (1) the Gravelly Shelly facies, (2) the Horizontally Stratified facies, (3,4,5) the three subsets of

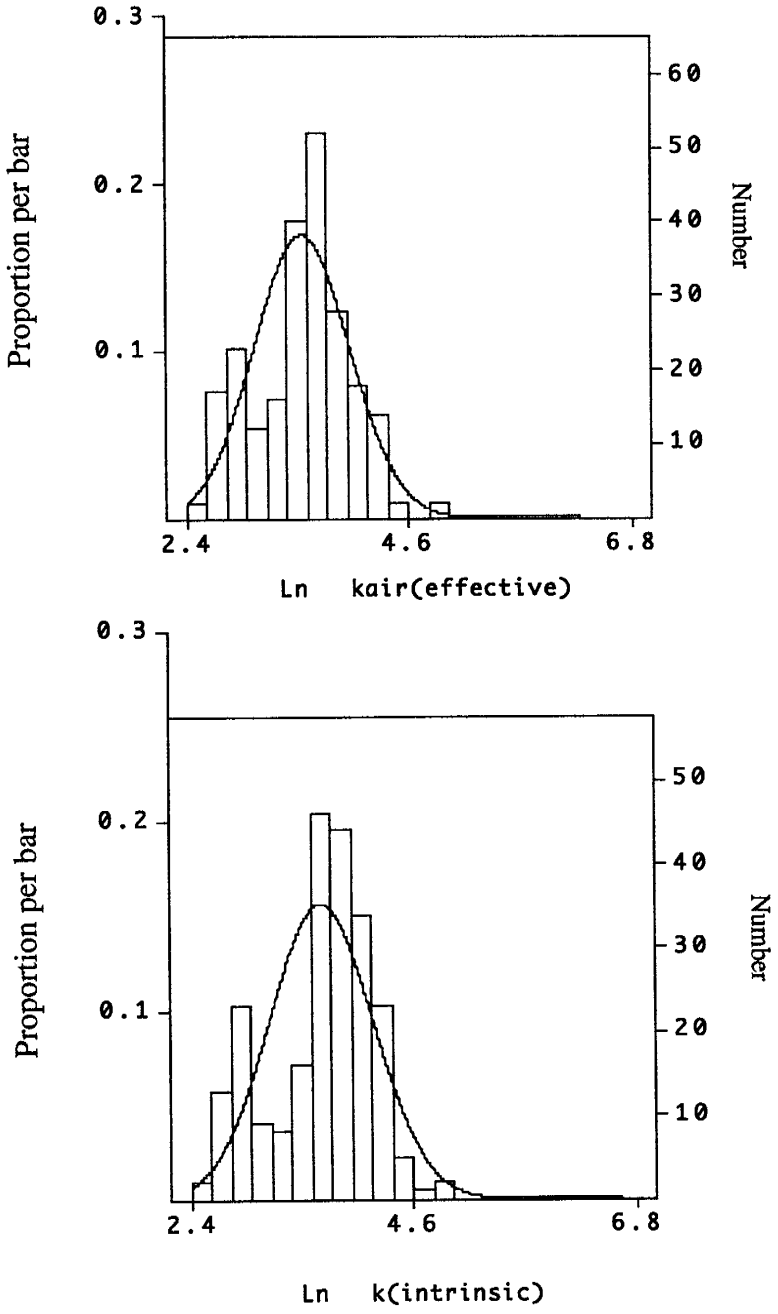

Figure 5.13 - Histograms for all permeability data.
The normal distribution is shown for comparison.

the Cross-Stratified facies. We conducted an Analysis of Variance (ANOVA) to test whether the means of these different populations were different from each other. When we compared all five populations together, we rejected the hypothesis that the means of the ln k_{air} and the ln k data sets were similar. We then performed a Tukey multiple comparison analysis to see how similar each of the populations was to each other. **Table 5.7** shows that the Gravelly Shelly facies and the Horizontally Stratified facies were different from all the other groups. Within the Cross-Stratified facies, we saw that the XS2 subset and the XS3 subset could not be told apart in either the ln k_{air} or the ln k data sets. The XS1 subset showed a significant difference (0 correlation) when compared to the XS2 and the XS3 subset in both the ln k_{air} and the ln k data set. These results are shown graphically in notched box plots (Figure 5.14). The bar at the intersection of the notch is the median value, the ends of the box are the 25th and 75th quartile, and the lines split the remaining data set in half again. "Outside values" (SYSTAT, 1992) are marked by asterisks. Outliers are marked by open circles. The n value is the number of samples from that subset. The extensions of the notches represent the 95% confidence interval about the median value.

We used variography to find the spatial correlation within the data set. The exponential fits used here are in the form $\gamma(h) = \text{nugget} + \text{sill} * [1 - \exp(|-h| / \text{range})]$, where the nugget takes into account the measurement and other undefinable errors, the sill is approximated as the variance of the data set, the range is the spatial correlation length, and h is the distance between measurement locations. When we looked at the entire gridded data set, we had to contend with the fact that the multiple facies types tended to mask out individual characteristics. The variograms for the ln k_{air} and the ln k data sets both indicated a correlation length (range) of between 100 and 95 cm, respectively, when looking in the 0° (x-) direction (Figure 5.15). Perpendicular to this direction, we found that the range for the ln k_{air} and the ln k data sets were both 32 cm (Figure 5.16). The numbers represent the number of pairs associated with that lag

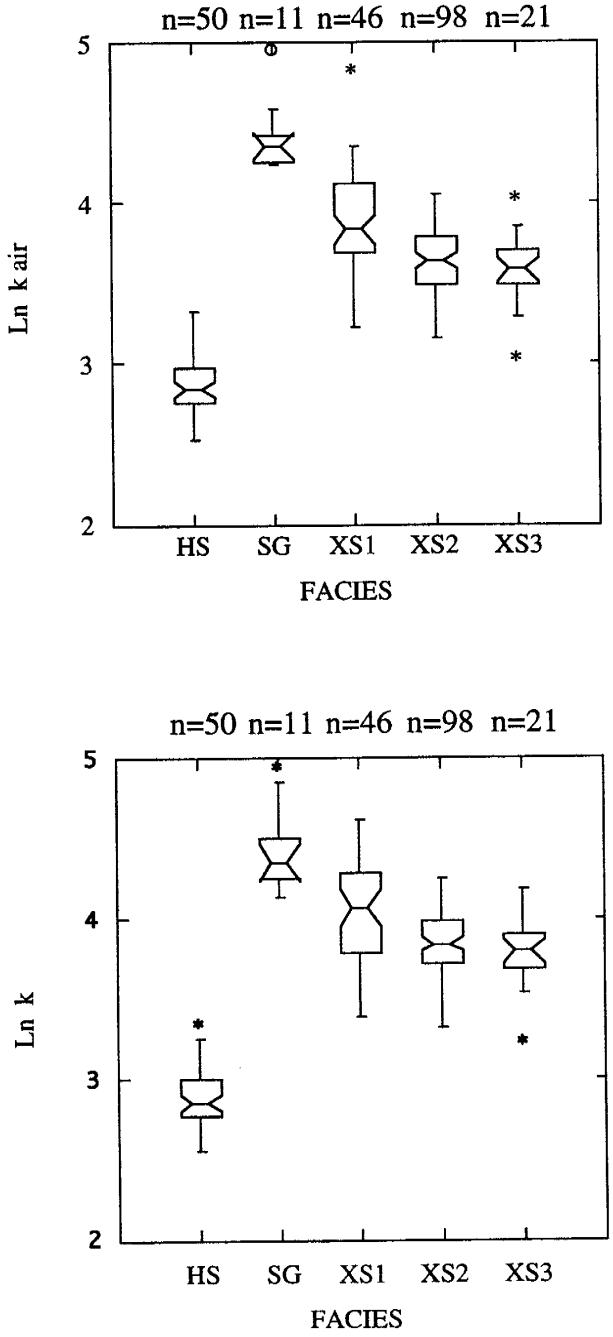

Figure 5.14 - Notched box plots for all permeability data.
Notches are 95% confidence interval about median value.
Inner fence = 25th (75th) quartile - (+) [1.5*interquartile range]
Outer fence = 25th (75th) quartile - (+) [3*interquartile range]
Asterisks mark values beyond the inner fences.
Open circles mark values beyond the outer fences.

	Ln kair(eff)						Ln k(intrinsic)				
	HSF	GSF	XS1	XS2	XS3		HSF	GSF	XS1	XS2	XS3
HSF	1					HSF	1				
GSF	0	1				GSF	0	1			
XS1	0	0	1			XS1	0	0	1		
XS2	0	0	0	1		XS2	0	0	0	1	
XS3	0	0	0	0.696	1	XS3	0	0	0.001	1	1

Table 5.7 - Tukey multiple comparison test for Ln k_{air} and Ln k for all data.
Numbers represent percentage of similarity between groups.

distance. The horizontal line represents the sill, or variance, of the data set. These results lead to the conclusion that the presence of the water saturation has no effect on the geostatistics. This assumes, however, that there are no distinctions between facies types. It is reasonable to assume that different facies types have different spatial characteristics due to the differences in sorting and grain size distribution. To test this hypothesis, we split the data set into the individual facies types and reran the statistical tests.

5.6.2 Geostatistical Comparison of the Cross-Stratified Sand Facies

The majority of the data from Panel 5 was from the Cross-Stratified facies type (Figures 1.1, 4.3, 5.1). **Table 5.8** contains the basic statistical properties of the XSF for the ln k_{air} data set and for the ln k data set. In the XSF, we found that the mean ln k was greater than the mean ln k_{air}, the variance and skewness of the ln k data and the ln k_{air} data were nearly the same, and the kurtosis of the ln k was less than the kurtosis of ln k_{air}. Though the correction for the water saturation caused the distribution of ln k to be more normal, the Kolmogorov-Smirnov test showed that neither ln k_{air} nor ln k had a statistically normal distribution. Figure 5.17 shows the histograms of the XSF data with a normal distribution overlay.

Statistic	Ln kair(eff)	Ln k(intrinsic)
N of cases	165	165
Mean	3.701	3.894
Variance	0.072	0.067
Skewness	0.182	0.190
Kurtosis	-0.19	-0.04

Table 5.8 - Summary statistics for the Cross-Stratified facies permeability data

$\gamma(h) = 0.007 + 0.197*[1-\exp(|h|/100)]$
For Ln k_{air}(effective)

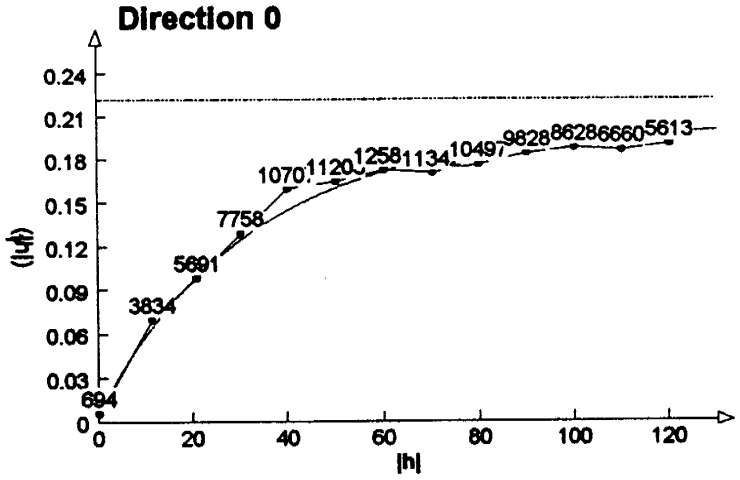

$\gamma(h) = 0.008 + 0.22*[1-\exp(|h|/95)]$
For Ln k(intrinsic)

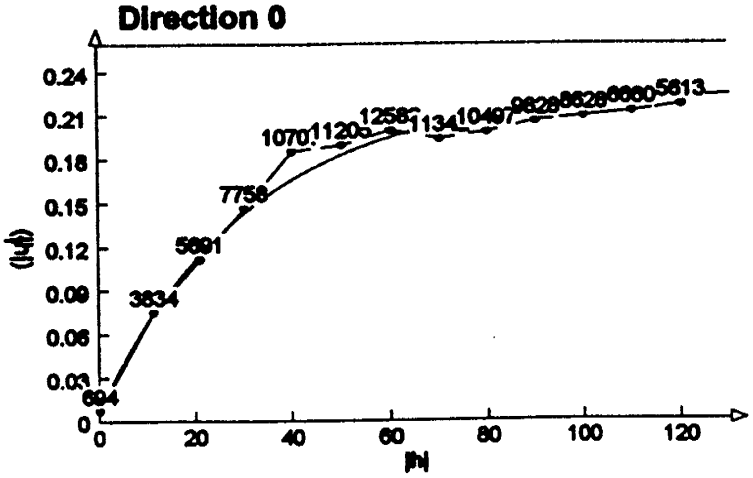

Figure 5.15 - Variograms for entire permeability data set
0° direction; 45° tolerance; 45 cm bandwidth
Numbers represent # of pairs for each lag distance
Lag distance |h| in cm; Horizontal line is sill; Curve is defined by function above the variogram.
Top: Ln k_{air} ; Bottom: Ln k

$\gamma(h) = 0.01 + 0.21*[1-\exp(|h|/32)]$
For Ln k_{air}(effective)

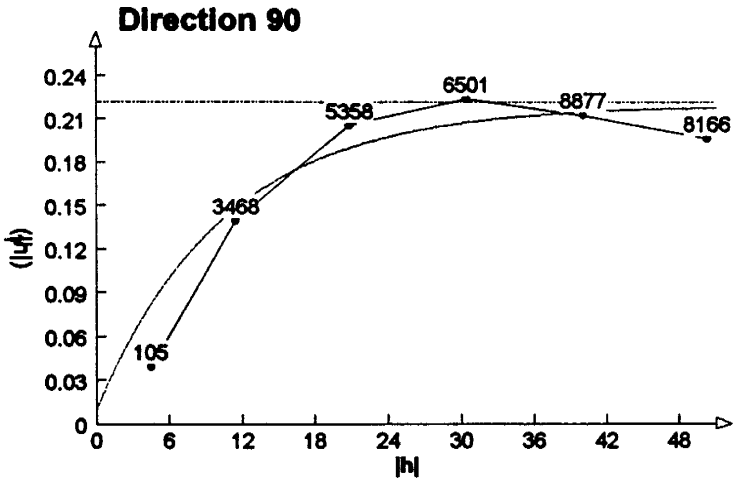

$\gamma(h) = 0.01 + 0.25*[1-\exp(|h|/32)]$
For Ln k(intrinsic)

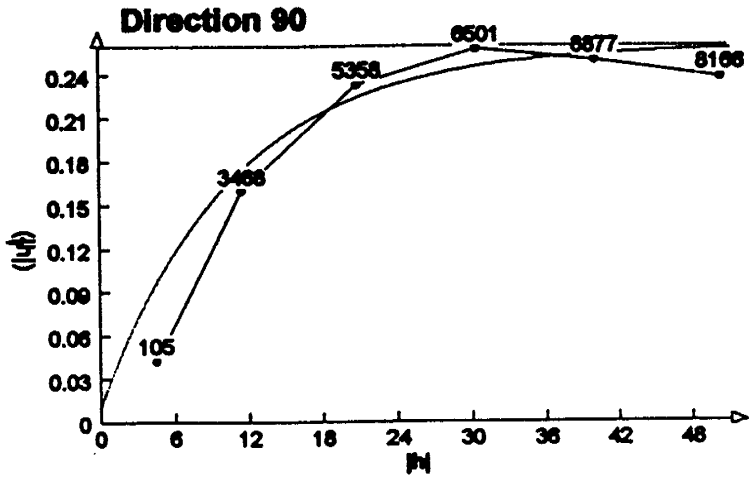

Figure 5.16 - Variograms for entire permeability data set
90° direction; 45° tolerance; 45 cm bandwidth
Numbers represent # of pairs for each lag distance
Lag distance |h| in cm; Horizontal line is sill; Curve is defined by function above the variogram.
Top: Ln k_{air} ; Bottom: Ln k

Similar to our mean comparisons across the entire data set, we tested our assumption that there were three distinct subsets within the XSF data. We conducted an ANOVA test to examine the hypothesis that the means of each of the XSF subsets were the same. The F-ratio of the ANOVA test gave a zero probability for rejecting our hypothesis for both ln k_{air} and ln k. When we compared the individual subsets by using a Tukey Multiple Comparison test, we found some differences when we looked at ln k_{air} and ln k (Table 5.9). When we looked at the ln k_{air} data, we found that the mean of XS1

Ln kair(eff)				Ln k(intrinsic)			
	XS1	XS2	XS3		XS1	XS2	XS3
XS1	1			XS1	1		
XS2	0	1		XS2	0	1	
XS3	0	0.442	1	XS3	0	0.708	1

Table 5.9 - Tukey multiple comparison test for Cross-Stratified subsets.
Numbers represent percentage of similarity between groups.

was statistically different than XS2 and XS3. However, we could not be statistically confident that XS2 and XS3 were different. The results of the Tukey Comparison test changed after we made our corrections and examined the ln k data. For the ln k data, there was no probability that the mean of XS1 was similar to XS2 or XS3. We could not distinguish a difference between the XS2 and XS3 subsets, however there was not a significant sampling of the XS3 subset (21 points) compared to the XS2 subset (98 points). From the geologic characterization, it seems that XS3 is a separate subset of the Cross-Stratified sand, but the limited sampling of the XS3 subset might not be giving us an accurate geostatistical description of this subset. **Figure 5.18** shows these results visually in the form of notched box plots. The ln k data shows that the notches for XS2 and XS3 overlap significantly, whereas the notches for XS1 do not overlap with either XS2 or XS3. The amount of overlap is related to the confidence that the medians of the data sets are similar to each other. These results question the validity of using three subsets in our data. In turn we must consider whether having three non-wetting phase relative permeability curves (correction factors) is appropriate or whether we should

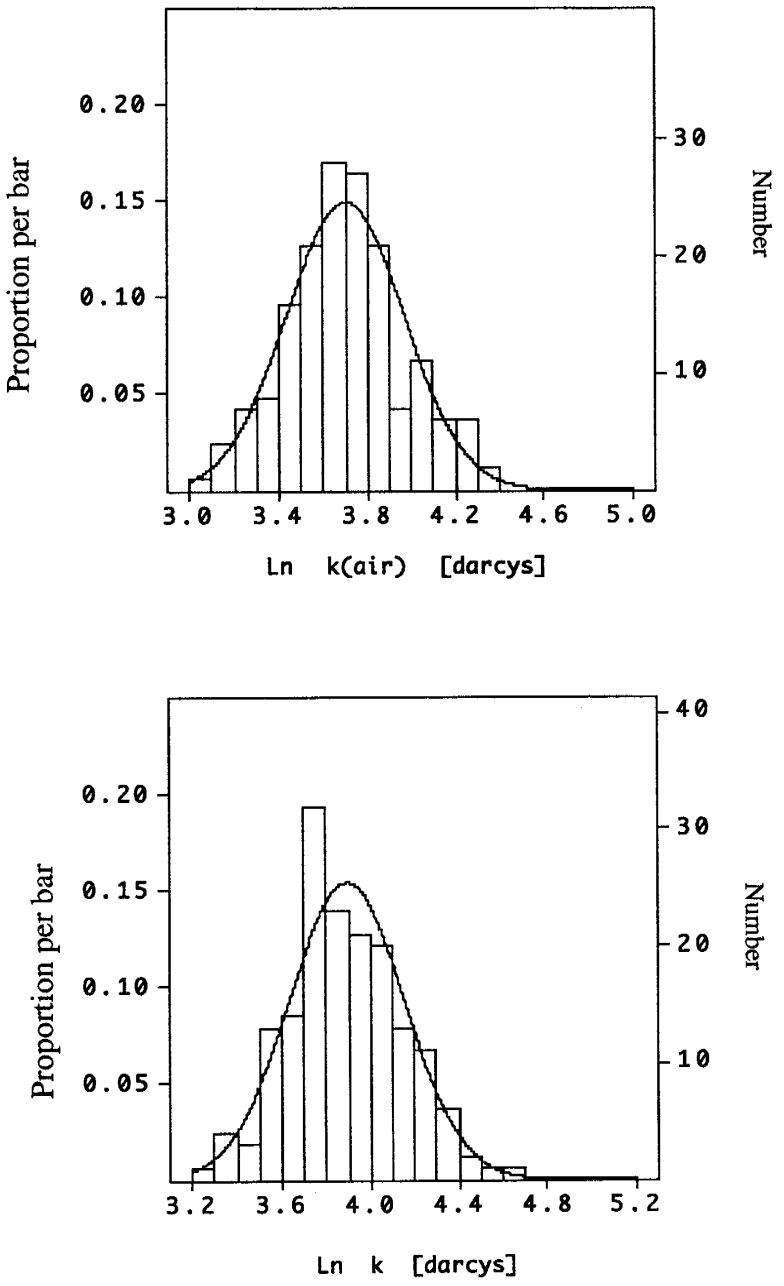

Figure 5.17 - Histograms for Cross-Stratified data.
The normal distribution is shown for comparison.

group the data into two subsets and recompute the non-wetting phase relative permeability curves (correction factors).

Having looked at the individual basic statistics for the XSF data, we proceeded to look at the spatial variability of the data set through the use of variography. Assuming that the greatest correlation would be parallel to the principal bedding, the model uses an angle of 345° relative to the x-axis as the direction of the longest correlation (Figure 5.1). **Figure 5.19 and 5.20** shows the variograms for the principal direction, 345°, and normal to the principal direction, 75°, respectively. The formulas describing the fitted functions are included. Along the direction of principal bedding, the correlation length (range) for ln k_{air} was about 50 cm. Normal to the principal bedding, the range for ln k_{air} was about 17 cm. The range for ln k along the principal bedding was reduced to about 40 cm and the range normal to the principal bedding stayed nearly the same as ln k_{air} at 15 cm.

These tests showed that the presence of the water saturation in the outcrop could be geostatistically important. To test whether the variograms in **Figure 5.19** are statistically different, the "jackknife" technique (Quenouille, 1956) was applied to the data. Using a modified version of the technique (Shafer and Varljen, 1990), we produced variograms for the 345° direction for the Cross-Stratified facies (Figure 5.21) with 95% confidence intervals about each lag distance. Comparing the variograms for the ln k_{air} data and the ln k data shows that the variogram for the ln k data falls within the lower confidence interval of the ln k_{air} variogram data. Therefore, the two variograms cannot be separated statistically. Since the two variograms are not statistically different, the presence of the percentage water saturation found at our field site is not geostatistically significant.

Though not geostatistically significant, the presence of the percentage water saturation in the XSF did act to reduce the air permeability, and to increase the range and sill of the ln k_{air} data set as compared to the ln k data set. For situations where a higher percentage of water saturation is present, the effects will be enhanced, possibly to a point

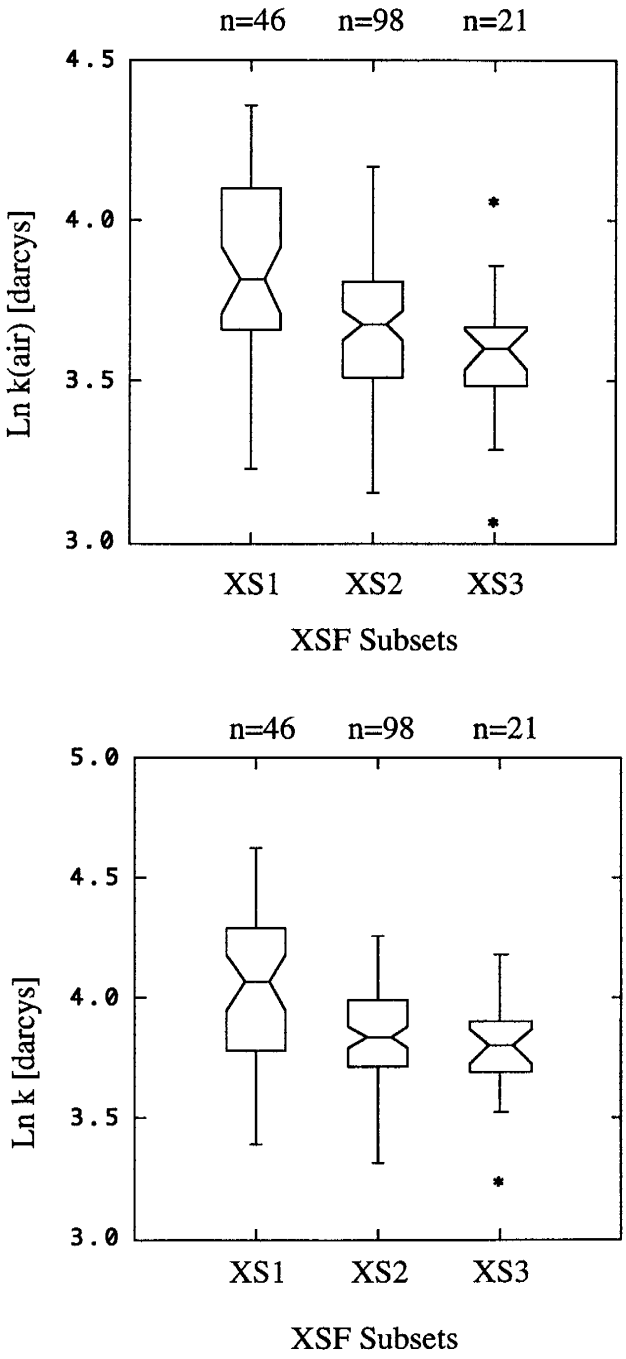

Figure 5.18 - Notched box plots for Cross-Stratified permeability data.
Notches are 95% confidence interval about median value.
Inner fence = 25th (75th) quartile - (+) [1.5*interquartile range]
Asterisks mark values beyond the inner fences.

$\gamma(h) = 0.001 + 0.068*[1-\exp(|h|/50)]$
For Ln k_{air}(effective)

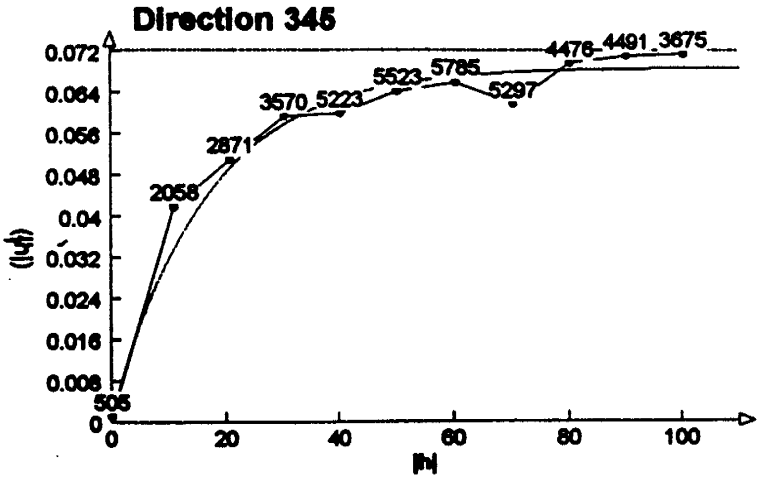

$\gamma(h) = 0.002 + 0.0625*[1-\exp(|h|/40)]$
For Ln k(intrinsic)

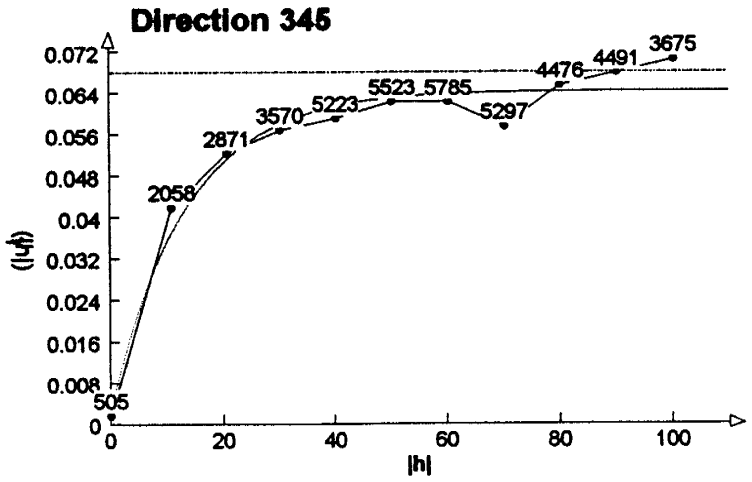

Figure 5.19 - Variograms for Cross-Stratified data set
345° direction; 30° tolerance; 30 cm bandwidth
Numbers represent # of pairs for each lag distance
Lag distance |h| in cm; Horizontal line is sill; Curve is defined by function above the variogram.
Top: Ln k_{air} ; Bottom: Ln k

$\gamma(h) = 0.001 + 0.072*[1-\exp(|h|/17)]$
For Ln k_{air}(effective)

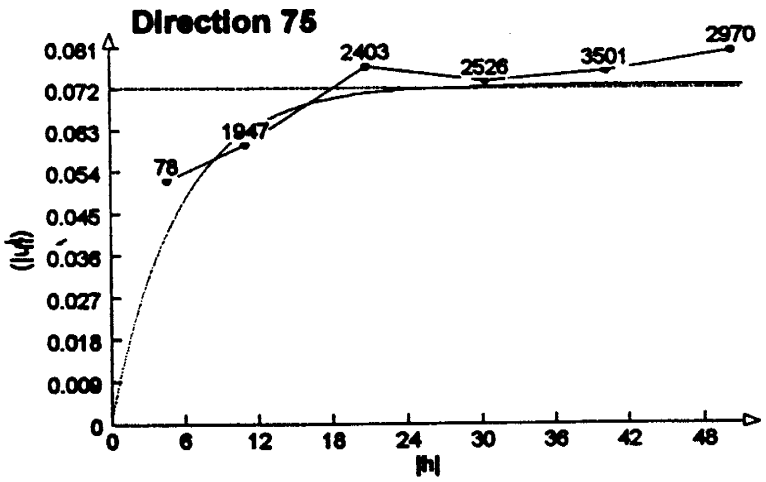

$\gamma(h) = 0.002 + 0.066*[1-\exp(|h|/15)]$
For Ln k(intrinsic)

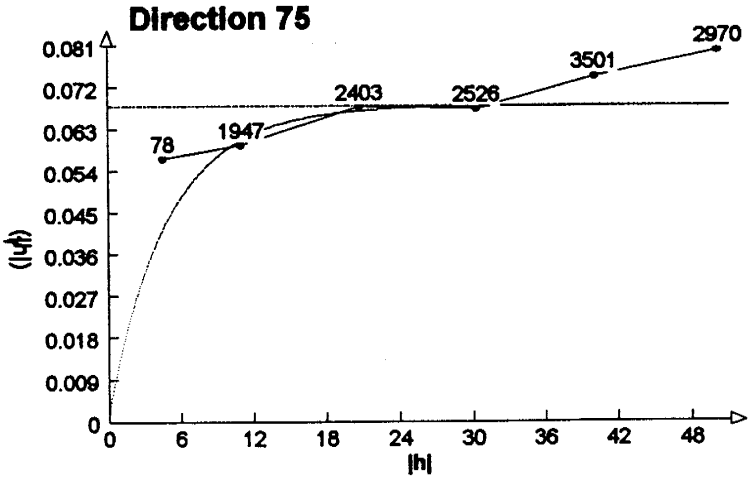

Figure 5.20 - Variograms for Cross-Stratified data set
75° direction; 30° tolerance; 30 cm bandwidth
Numbers represent # of pairs for each lag distance
Lag distance |h| in cm; Horizontal line is sill; Curve is defined by function above the variogram.
Top: Ln k_{air} ; Bottom: Ln k

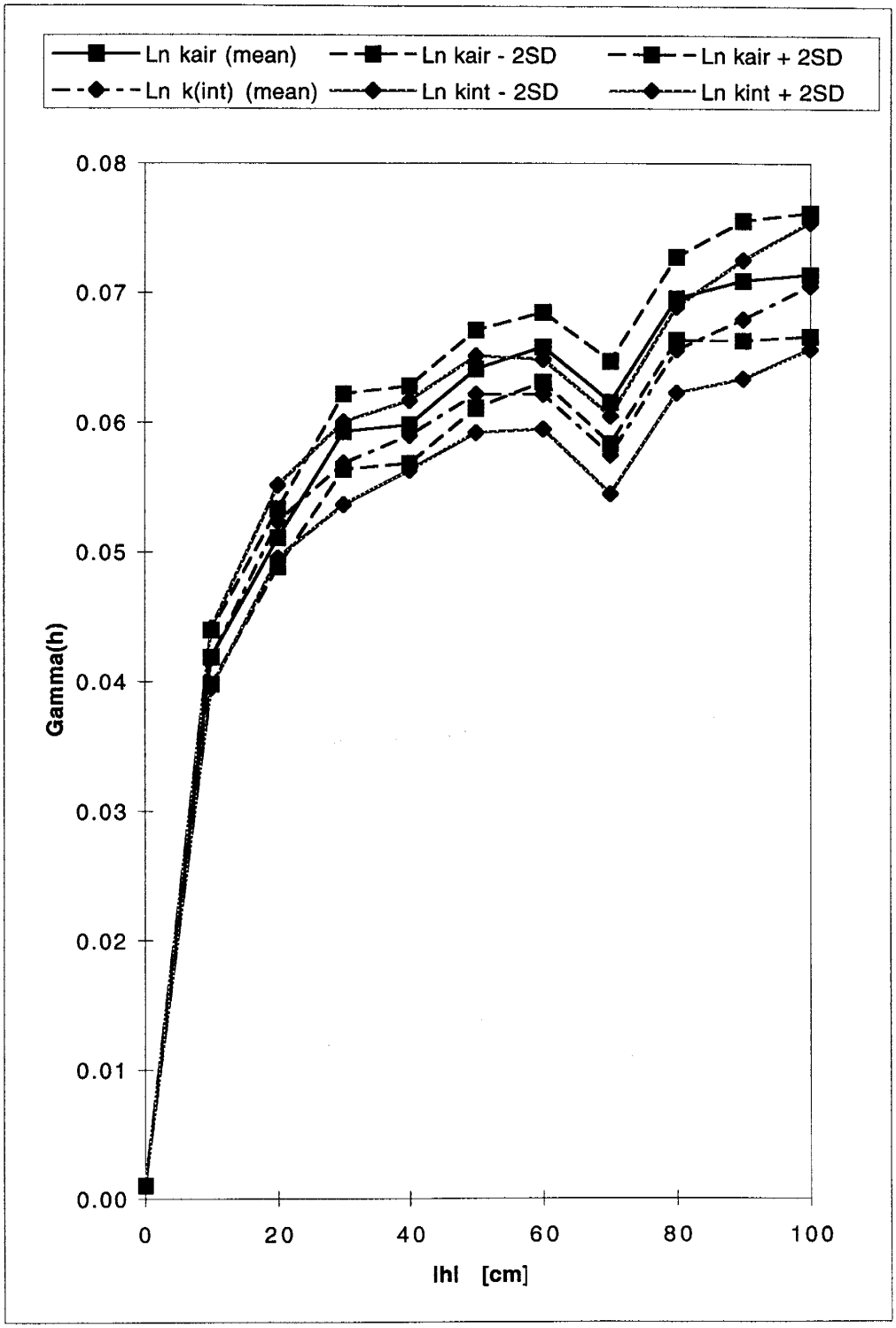

Figure 5.21 - "Jackknife" variograms for Cross-Stratified data set.
345 deg. direction; 30 deg. tolerance; 30 cm bandwidth
Dashed lines represent 95% confidence intervals about the means.

where there is a geostatistical significance. Due to capillarity, the water saturation in the outcrop would have been contained in the smallest pore sizes. With water in those pores, the LSAMP II would have not been able to force air through them. Therefore, we were giving more weight to the larger dry pores, which biased our measured values to lower than actual intrinsic permeability. The presence of the water in the outcrop removed the smallest pore sizes from the measurements, which, in effect, reduced the range of open pore sizes being measured by the LSAMP II. When we corrected our ln k_{air} values to ln k values, we were accounting for the smaller sized pores into our ln k values. Samples with a larger amount of water were corrected upward more than samples with less water. This variable shift acted to reduce the variance in the ln k data set compared to the ln k_{air} data set. Our non-wetting phase relative permeability curves (correction factors) were different due to the differences in the grain size distribution, and therefore sorting, of the samples.

The effects of grain size distribution and mean grain size on the non-wetting phase relative permeability curves (correction factors) can be explained by looking at two end member cases. First is the case where samples have the same grain size distribution, but with different mean grain sizes. As stated previously, capillary tension holds water in the pores against the force of gravity, with water held more tightly in the smallest pores compared to the larger pores. As suction is applied to the samples, the largest pores drain first leaving the smaller pores still filled with water. In our experiments, as was similarly found in Wyckoff and Botset (1936), we found that complete air flow pathways were not established until about 50% water saturation was reached. We also found that the effective permeabilities at 50% water saturation were similar for the various samples. Below 50% water saturation, however, the grain size distribution has an effect on the effective permeability of the samples. The sample with the largest pore sizes will have the highest permeability because it will have the widest pathways for air to travel through. The sample with the largest mean grain size will drain the fastest because the sample will

have the largest pores and require the least amount of suction to overcome the capillary forces holding the water in the pores. For a given water saturation, each of the samples will have the same portion of their pore size distribution occupied by air and have the same pore connectivity. With similar connectivity, the different samples should have similar non-wetting phase relative permeability curves (correction factors).

The second end member case would be a number of samples with similar mean grain or pore sizes, but with different grain size distributions, and therefore sorting, of various samples. Once again, complete air pathways would not be established until 50% of the water has drained from the samples. As samples become less well sorted, the porosity gets smaller, the air entry pressure gets smaller, the residual saturation gets larger, and the intrinsic permeability gets smaller. For samples having a wider grain size distribution, more pores of different sizes need to drain to reach a given water saturation compared to samples having narrower grain size distributions. Draining more pores will cause more complete air pathways which will cause the effective air permeability to be greater. Therefore, a wider grain size distribution, (more poorly sorted sample) will have a wider pore size distribution and will increase in effective air permeability more than a sample with a narrower grain size distribution. This implies that a wider grain size distribution will lead to a larger correction factor, or bigger change in relative air permeability, compared to samples with narrower grain size distribution.

Our Cross-Stratified facies subsets fall between these two end members. **Figure 5.6** contains the grain size distributions for the three subsets. The XS1 subset has the widest grain size distribution and the largest mean grain size. XS2 and XS3 have narrower grain size distributions and higher mean grain sizes, with XS3 having the highest mean grain size. Since the XS1 subset has both the widest grain size distribution and the largest mean grain size, the aforementioned effects cause the largest change in the non-wetting phase relative permeability curve (largest correction factor) to apply. The reduced grain size distributions of the XS2 and XS3 subsets combined with the lower

mean grain sizes reduces the correction factors for these two subsets. To check the validity of the data, the Brooks and Corey (1964) model and the Luckner et al. (1989) model were applied to the data (Appendix D). The Brooks and Corey (1964) model is not sensitive to the differences in sorting, so the modeling results did not match our data well. The Luckner et al. (1979) model, however, has a parameter that assesses the grain size distribution of the sample. Applying this model, we found that samples with larger grain size distributions and larger grain sizes would have larger changes in non-wetting phase relative permeability curves (larger correction factors) compared to samples having reduced grain sizes and narrower grain size distributions.

Though the presence of water caused significant changes along the direction of principal bedding, little change in correlation length was seen normal to the direction of the principal bedding, possibly because we did not sample at a small enough scale. Each depositional coset is composed of thin laminae a few centimeters thick (Muller et al., 1996). Our sampling scheme measured every 10 cm. At this separation distance, the major heterogeneity is defined by the thickness of the coset, not the small scale heterogeneity of the laminae. Though effects of water saturation would have masked the finest heterogeneities within the layers, the thickness of the coset would have remained unchanged. When we corrected for the percentage of water saturation and effectively restored the finest pores, the amount of heterogeneity in the layers increased, but there was no significant difference in the thickness of the coset. Therefore, the resulting correlation length between ln k_{air} and ln k data was similar. Though these effects were not geostatistically significant, it is possible that they would cause an ln k_{air} data set with a higher relative water saturation to be significantly different than its associated ln k data set.

Though the majority of the measurements were separated by 10 cm, one vertical transect with measurements every 5 cm was conducted. Variogram analysis shows a smaller scale heterogeneity (Figure 5.22) for the vertical transect through the Cross-

Stratified sand facies as compared to the variograms for the vertical (90°) direction of all the Cross-Stratified data (Figure 5.23). The layering within the Cross-Stratified facies transect data is implied by the lag distance of 10 cm being more correlated than the lag distance of 5 cm. When all the Cross-Stratified data is examined, this layering is not observed. Though little difference is seen in the correlation of measurements beyond 15 cm in the ln k_{air} data, the ln k data continues to show the layering effect for the transect data. All four variograms show the a similar total range of 20 cm which coincides with the thickness of the individual cosets within the Cross-Stratified facies.

5.6.3 Geostatistical Comparison of the Horizontally Stratified Sand Facies

Unlike the Cross-Stratified sand facies which contained different subsets with differing grain size distributions and heterogeneous sorting, the Horizontally Stratified sand facies was much more homogeneous and well sorted. The homogeneity was observed in the field and quantified in the laboratory using the *in-situ* core we brought back from the field (R26). The homogeneous nature of the sand led to the tight grain size distribution (Figure 5.7), the small correction factor (Figure 5.10d), and the small range of effective permeabilities measured in the field (Figure 5.4). Since the moisture content in the HSF was low (from about 12 to 25%), the water saturation correction was low. It is not surprising, therefore, to find that there was little change when comparing the measured effective permeability, k_{air} , to the approximated intrinsic permeability, k.

Table 5.10 contains the basic statistics for ln k_{air} and ln k. Since a small correction factor was applied to the k_{air} values, the k values are slightly higher giving a slightly higher mean. The variance, skewness, and kurtosis of the distribution do not change significantly. Neither the ln k_{air} nor the ln k distributions show normality when applying the Kolmogorov-Smirnov test as is shown in the histograms of the data (Figure 5.24).

$\gamma(h) = 0.001 + 0.086*[1-\exp(|h|/22)]$
For Ln k_{air}(effective); Central transect data

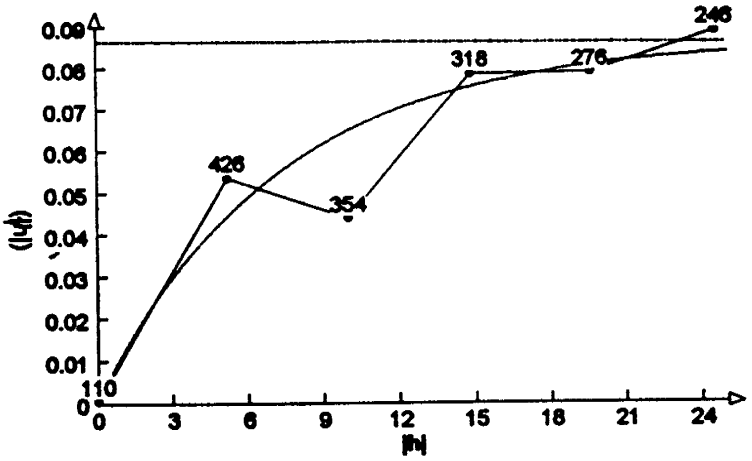

$\gamma(h) = 0.001 + 0.08*[1-\exp(|h|/20)]$
For Ln k(intrinsic); Central transect data

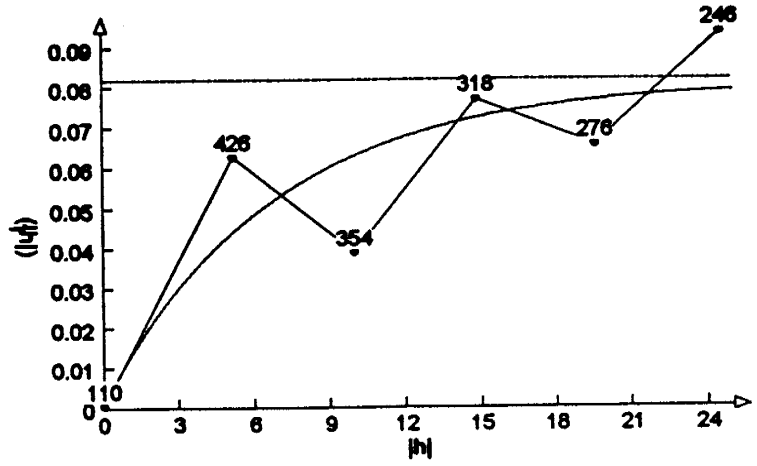

Figure 5.22 - Variograms for vertical transect of Cross-Stratified data set
90° direction; 90° tolerance; 10 cm bandwidth
Numbers represent # of pairs for each lag distance
Lag distance |h| in cm; Horizontal line is sill; Curve is
defined by function above the variogram.
Top: Ln k_{air} ; Bottom: Ln k

$\gamma(h) = 0.001 + 0.07*[1-\exp(|h|/22)]$
For Ln k_{air}(effective); All XS data

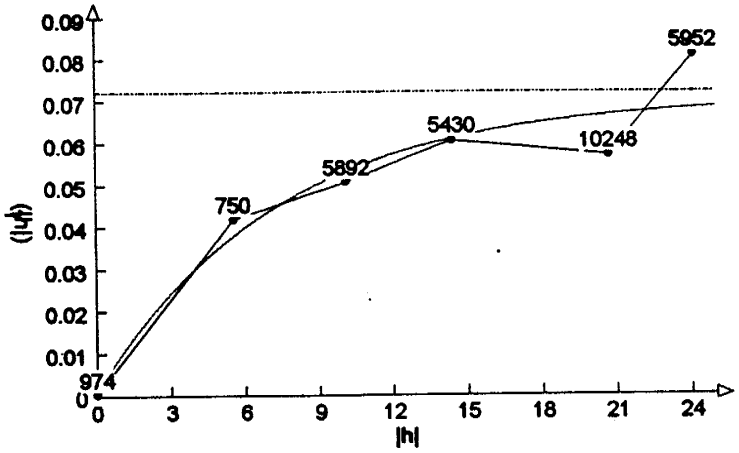

$\gamma(h) = 0.001 + 0.065*[1-\exp(|h|/20)]$
For Ln k(intrinsic); All XS data

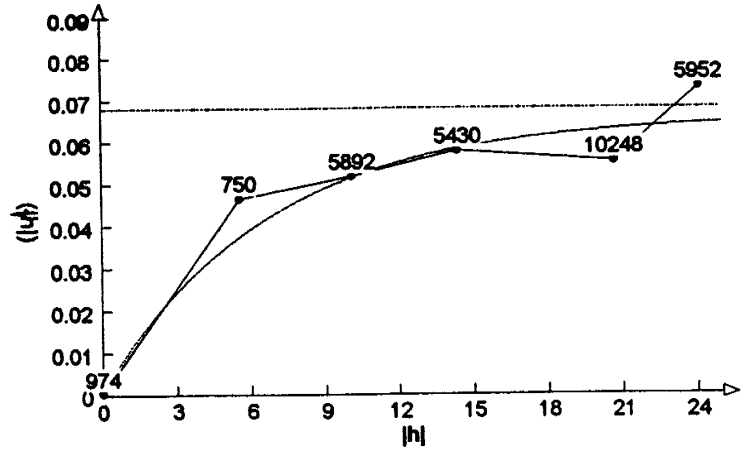

Figure 5.23 - Variograms for Cross-Stratified data set
90° direction; 90° tolerance; 40 cm bandwidth
Numbers represent # of pairs for each lag distance
Lag distance |h| in cm; Horizontal line is sill; Curve is defined by function above the variogram.
Top: Ln k_{air} ; Bottom: Ln k

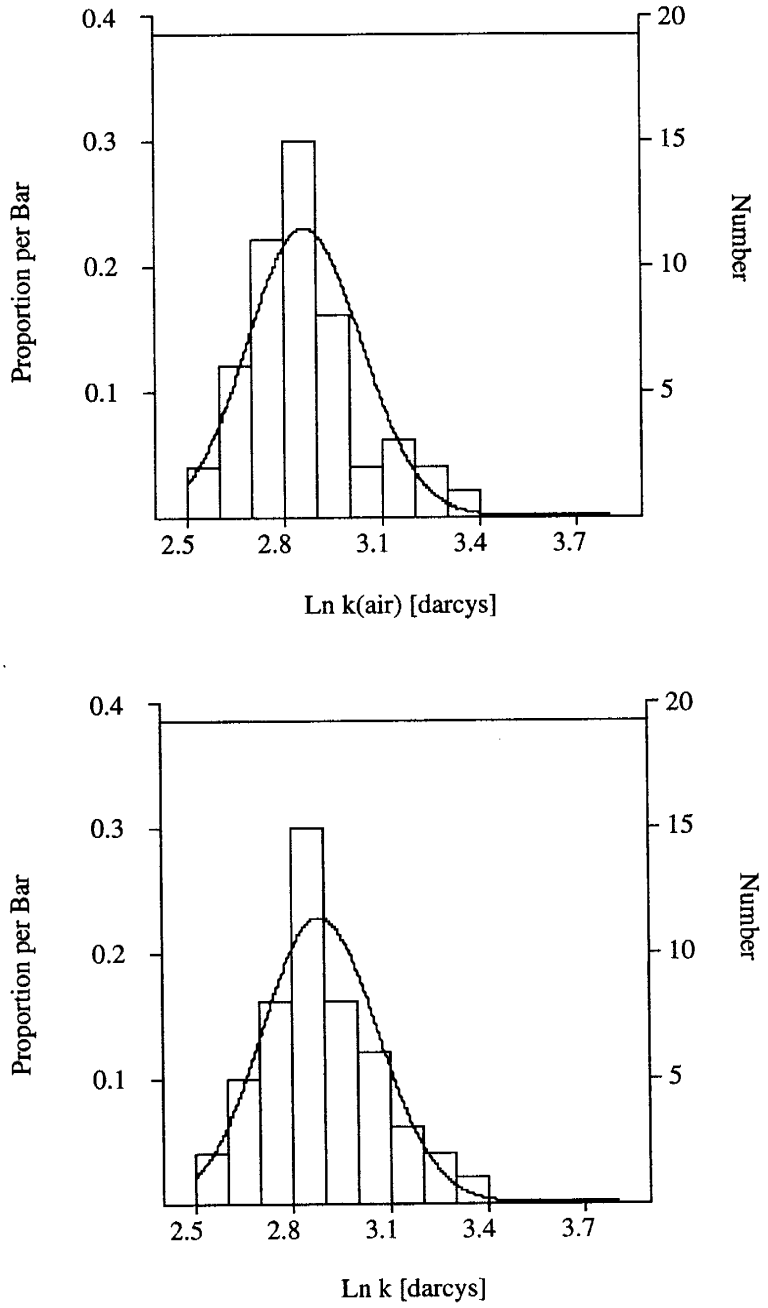

Figure 5.23 - Histograms for Horizontally Stratified data.
The normal distribution is shown for comparison.

Statistic	Ln kair(eff)	Ln k(intrinsic)
N of cases	50	50
Mean	2.862	2.883
Variance	0.030	0.031
Skewness	0.553	0.571
Kurtosis	0.174	0.233

Table 5.10 - Summary statistics for the Horizontally Stratified facies permeability data

As we only had 50 data points over a small vertical extent (from 10 to 30 cm), we only looked at the spatial variability parallel to the bedding plane. Unlike the XSF which showed a significant dip in the primary bedding plane, the HSF did not. Therefore, we used an angle of 0° in our variography tests. Due to the nearly homogeneous correction for all of the samples, the spatial variability of permeability did not change significantly when we tested the ln k_{air} data set or the ln k data set. In both cases the correlation length was about 25 cm (Figure 5.25).

Whereas the non-wetting phase relative permeability curve (correction factor) for the XSF caused a significant change in the spatial variability of permeability because of its poor sorting characteristics, the non-wetting phase relative permeability curve (correction factor) for the HSF caused little change in the spatial variability of permeability because of its well sorted nature. The HSF was very homogeneous and well sorted which would mean that there was not a wide range of pore sizes within the sand. Though any water would be held in the smallest pore sizes, the air-filled pores would have been nearly the same size. The LSAMP II measured the effective permeability in the air-filled pores. When we accounted for the small amount of water that was in the sand, the intrinsic permeability values went up slightly. Since the sand was so homogeneous, the correction was nearly the same for all of the samples, so the variability in permeability between the samples did not change from ln k_{air} to ln k.

$\gamma(h) = 0 + 0.026*[1-\exp(|h|/25)]$
For Ln k_{air}(effective)

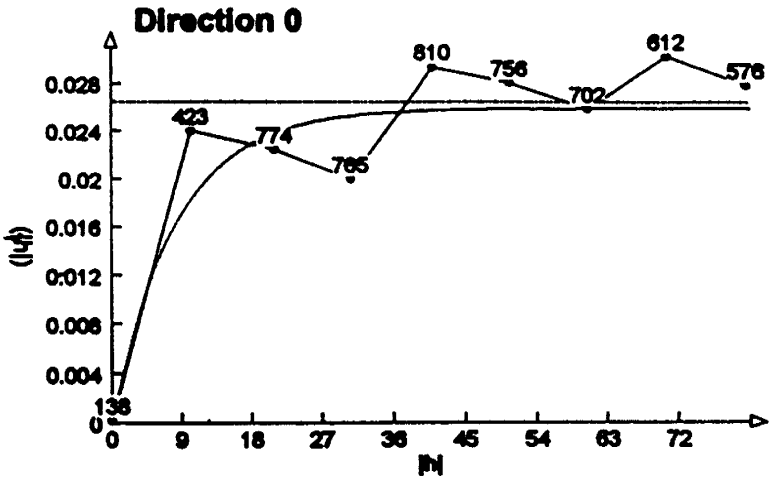

$\gamma(h) = 0 + 0.027*[1-\exp(|h|/23]$
For Ln k(intrinsic)

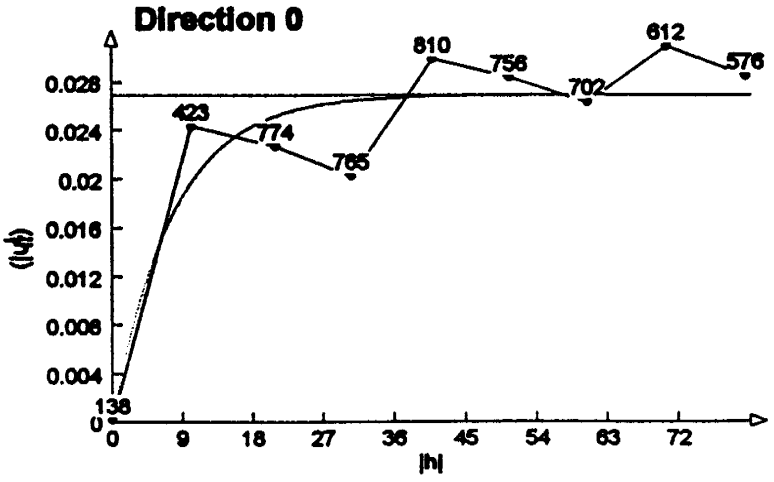

Figure 5.25 - Variograms for Horizontally Stratified data set
0° direction; 30° tolerance; 30 cm bandwidth
Numbers represent # of pairs for each lag distance
Lag distance |h| in cm; Horizontal line is sill; Curve is defined by function above the variogram.
Top: Ln k_{air} ; Bottom: Ln k

5.7 Recommendation for Future Field Outcrop Programs

Our results have shown that there may be a need to account for the water content present in field outcrop studies. There are different methods used to measure the water content in the field (Appendix E). We identified some important issues concerning which method would be most appropriate in similar field sites. The first issue is the volume of sand sampled. Our water content measurements were performed on cores that were 5 cm and 10 cm long, and that sampled 100 cc and 50 cc of sand, respectively. We know that our device (LSAMP II) sampled only the 1 to 2 cc directly below the tip seal. We concluded that our corrections may have been conservative since the core water content values may have been higher than the saturations found at the surface. Ideally, a measurement of the water content in the volume sampled by the air permeability device would be best. A second issue that is important is the time that the water content measurements are taken. Due to the multiple characterization efforts taking place at our field sight, the cores for the water content measurements were taken after the LSAMP II measurements and usually late in the afternoon. With the processes of evaporation from the surface of the outcrop changing with time of day and redistribution of water from further into the outcrop changing with time of day, our water content measurements may have been different from the conditions when we took LSAMP II measurements. A continuous monitoring of the water content in the same size volume sampled by the air minipermeameter, and in the approximate location that air minipermeameter measurements are being recorded, would be the best way to account for these changing conditions through time.

Besides accounting for water content, other secondary measurements are important in getting an accurate result of air permeability in the field. We found that it was important to measure the temperature of the air as well as the temperature of the sand. Though the temperature difference between the ambient air and the upper 1 to 2 cm of sand was small and did not affect our estimates of viscosity, a permeameter that

measured a deeper volume might encounter a significantly different temperature which would affect the viscosity value used in the determination of air permeability. Likewise, we found that an accurate measurement of the barometric pressure was important to our readings. Though our field study was conducted in relatively good weather, there were changes in the barometric pressure as weather fronts passed through. It might also be important to measure the humidity of the air, both for viscosity purposes and to determine if any water is being added to the outcrop during the measurement process.

An accurate measurement of the geology of the field site is important when considering the effect of water saturation on measured air permeability. Our results showed that a measurement of grain size distribution and sorting of the samples was important in determining the magnitude of the non-wetting phase relative permeability curves (correction factors). If the studied outcrop contains a well-sorted, homogeneous facies type, then the effect of water content on air permeability will be reduced. If, however, the studied outcrop is composed of a heterogeneous mixture of sand that is less well sorted, then a more thorough characterization of the geology will be required and the water content present will have to be more carefully assessed since there will be a greater effect on the measured effective air permeability.

CHAPTER 6 - CONCLUSIONS AND RECOMMENDATIONS

6.1 Introduction

We posed a number of questions regarding the effects of percentage of water saturation on air permeability measurements on the unconsolidated sands of Oyster, Virginia. For each of the three facies types encountered in the aquifer and the outcrop we asked: (1) for water saturations found in the field, is it possible to define a non-wetting phase relative permeability curve (correction factor) that will remove the bias from the effective air permeability and yield an estimate for the intrinsic permeability?; (2) is there a water saturation below which the measured effective air permeability approximates the intrinsic permeability?; (3) is the bias introduced by uncorrected data significant in the geostatistical sense?; and (4) what lessons can we learn about conducting outcrop experiments in humid environments?

Our field site had three distinct facies types, the Gravelly Shelly facies, the Horizontally Stratified facies, and the Cross-Stratified facies. We did not conduct any laboratory experiments on the Gravelly Shelly facies so cannot answer the above questions relating to the Gravelly Shelly facies. We have preliminary results for the Horizontally Stratified facies based on a single experimental sample. Our results for the Cross-Stratified facies are the most complete since we have numerous samples from that facies type.

6.2 Answers to Questions Posed

As most of our data comes from the Cross-Stratified facies type, it will be addressed first. We found that it was possible to define a non-wetting phase relative permeability curve (correction factor) based on the grain size distribution and sorting of the sample for a range of about 50% water saturation down to the residual water saturation of the sands. The Cross-Stratified facies was split into three subsets with

different grain size distribution and sorting characteristics. The first, XS1, was found to have the widest grain size distribution and the worst sorting, so it had the largest correction factor for a given water saturation and contained the least percentage of water saturation in our field experiments. The XS2 and XS3 subsets were finer grained and better sorted than XS1 and thus had lower correction values but contained a larger percentage of water in the field outcrop study. From about 10% water saturation to about 50% water saturation, we were able to use these correction factors to produce an estimate of intrinsic permeability from our measured effective permeability values. We found that below the residual water saturation, about 10% for our sands, the measured effective air permeability gave a good estimate of the intrinsic permeability.

The geostatistical analysis on the measured effective air permeability and the estimated intrinsic permeability showed that there was not a geostatistical difference in the results when the Cross-Stratified facies was studied. We found that the presence of the water saturation in the outcrop lowered the mean value of permeability, lowered the variance, and didn't significantly change the skewness or kurtosis of the permeability distribution. We discovered that after we corrected for the presence of the water saturation, we could not statistically differentiate the XS2 and XS3 subsets, though the XS1 subset was significantly different from the other two subsets. These results raised questions regarding the validity of our original choice of splitting the data into three subsets, though we had only a limited number of samples from the XS3 subset. Our variography study showed that after we corrected for the percentage of water saturation in the outcrop, the correlation length in the plane parallel to the dip in the beds was reduced from about 50 cm to 40 cm. Our "jackknife" variography test showed that the ln k variogram was not statistically different from the ln k_{air} data set. We found that the correlation length normal to the primary plane of deposition and along the vertical transect remained unchanged after we corrected for the presence of water saturation in the outcrop. These results suggest that for the percentage of water saturation values we found

in the field (10% to 25%), it is not statistically important to measure the percentage of water saturation values. For larger water saturation percentages or for sands with a greater range of water saturation percentage, it could be important to measure the water saturation percentages during outcrop studies of heterogeneous sands.

We also studied the Horizontally Stratified facies, but in a more limited sense. We were able to determine a non-wetting phase relative permeability curve (correction factor) that would remove the bias presented by the presence of water saturation found in the field. Our non-wetting phase relative permeability curve (correction factor) was based on a single laboratory experiment, but the results were similar to that of the Cross-Stratified facies. As the Horizontally Stratified facies had a tighter grain size distribution and better sorting than the Cross-Stratified facies, it was not surprising to see that the Horizontally Stratified facies had a smaller correction factor. Similar to the Cross-Stratified facies, we found that below about 10% water saturation, the LSAMP II could not distinguish between the measured effective air permeability and the estimated intrinsic permeability.

With such a small correction factor, the homogeneity of the sands, and the fact that the water saturations we found in the field were all very similar, we saw little statistical change in the Horizontally Stratified data set when we compared the measured effective air permeability to the estimated intrinsic permeability. Though the presence of water saturation caused the measured effective air permeability to be lower than the estimated intrinsic permeability, the correction did not significantly change the variance, skewness, or kurtosis of the distribution. Likewise, our variography tests showed that there was no geostatistical difference in the correlation length (about 20 cm) between the measured effective air permeability data set and the estimated intrinsic permeability data set. Unlike the Cross-Stratified facies, the Horizontally Stratified facies is more homogeneous and well sorted, reducing the need to determine the percentage of water saturation present in the outcrop.

6.3 Recommendations for Future Activities

6.3.1 Future Laboratory Questions

In conducting our experiments, we discovered two important issues that we did not attempt to answer. The first issue relates to the type of air pumped into the outcrop when making an air permeability measurement. The LSAMP II pumped ambient air into the outcrop when making measurements. At our field site in Virginia the humidity of the air approached 100% relative humidity, so we were pumping wet air into the outcrop. The question was raised as to whether the use of wet air was influencing the water content already contained in the outcrop. We questioned whether we should use desiccated air, but we felt that we might tend to dry out the outcrop with such air. We did not have measurements of the humidity of the air in the face of the outcrop or measurements of the ambient air humidity, so we did not know how the two types of air were related to each other. We felt that it would be interesting to resolve whether using air of different humidity would have a significant effect on our results.

Another issue that we questioned was whether our results were applicable to a geometry different from the LSAMP II. It would be interesting to assess whether our finding that percentage of water saturation makes a geostatistical difference in air permeability measurements would also be applicable if we used a flow-through device. As the sample volume would probably be much larger than the 1 to 2 cc that the LSAMP II measures, issues of heterogeneity and sorting would be of great importance. Also, the percentage of water saturation in the sample would have to be equivalent throughout the sample at each increment. Answers to these questions would further quantify the implications of our results for other studies being conducted in unconsolidated sand outcrops in humid environments.

REFERENCES

Bloomsburg, G. L. and A. T. Corey. (1964). "Diffusion of Entrapped Air from Porous Media." Hydrology Papers, Colorado State University. August(5): 5-24.

Boggs, S. (1987). Sedimentary Textures. In Principles of Sedimentology and Stratigraphy. Columbus, Merrill Publishing Company: 105-134.

Brooks, R. H. and A. T. Corey. (1964). Hydraulic Properties of Porous Media. Colorado State University Hydrology Paper No. 3, Fort Collins, 27 p.

Brooks, R. H. and A. T. Corey. (1966). "Properties of Porous Media Affecting Fluid Flow." Proc. Amer. Soc. of Civil Eng., J. Irrigation Drainage Div. IR 2(4855): 61-88.

Carsel, S. and R. Parrish. (1988). "Developing Joint Probability Distribution of Soil Water Retention Characteristics." Water Resources Research 24(5): 755-769.

Chandler, M. A., D. J. Goggin, and L.W. Lake. (1989). "A Mechanical Field Permeameter for Making Rapid, Non-destructive, Permeability Measurements." Journal of Sedimentary Petrology. 59(4): 613-635.

Childs, E. C. (1969). An Introduction to the Physical Basis of Soil Water Phenomena. New York, John Wiley & Sons Ltd.

Corey, A. T. (1957). "Measurement of Water and Air Permeability in Unsaturated Soils." Soil Science Society Proceedings: 7-10.

Davis, J. M., J. L. Wilson, and F.M. Phillips (1994). "A Portable Air-Mimipermeameter for Rapid In Situ Field Measurements." Ground Water 32(2): 258-266.

Demond, A. H. and R. P.V. (1987). "An Examination of Relative Permeability Relations for Two-Phase Flow in Porous Media." Water Resources Bulletin 23(4): 617-628.

Deutsch, C.V. and A.G. Journel. (1992). GSLIB: Geostatistical Software Library and User's Guide. Oxford, Oxford University Press.

DeVries, D. A. (1963). Thermal Properties of Soils. In Physics of Plant Environment. W. R. Van Wijk. New York, John Wiley & Sons, Inc.: 210-231.

Dreyer, T., A. Scheie, and O. Walderhaug. (1990). "Minipermeameter-Based Study of Permeability Trends in Channel Sand Bodies." Amer. Assoc. Petrol. Geol. Bull. 74(4): 359-374.

Dullien, F.A.L. (1992). Chapter 2: Capillarity in Porous Media. In Porous Media: Fluid Transport and Pore Structure. 2nd edition, New York, Academic Press, Inc. 117-236.

Eagleson, P. S. (1970). Chapter 14: Infiltration and Groundwater Flow. In Dynamic Hydrology. New York, McGraw-Hill Book Company: 276-323.

Eijpe, R. and K. J. Weber. (1971). "Mini-Permeameters for Consolidated Rock and Unconsolidated Sand." Amer. Assoc. Petrol. Geol. Bull. 55(2): 307-309.

Gardner, W. R. (1956). "Calculation of Capillary Conductivity from Pressure Plate Outflow Data." Soil Science Society of America Proceedings: 317-320.

Goggin, D. J., R. L. Thrasher, and L.W. Lake (1988). "A Theoretical and Experimental Analysis of Minipermeameter Response Including Gas Slippage and High Velocity Flow Effects." In Situ 12(1&2): 79-116.

Goggin, D. J. (1993). "Probe permeametry: is it worth the effort?" Marine and Petroleum Geology 10(4): 299-308.

Golder Federal Services. (1995). Field Operations Summary Report: Oyster, Virginia Bacterial Transport Site; July 21-30, 1995. Oak Ridge, Golder Associates.

Halvorsen, C. and A. Hurst. (1990). Principles, Practice, and Applications of Laboratory Minipermeametry. In Advances in Core Evaluation, Accuracy and Precision in Reserves Estimation. London, Gordon & Breach Science Publisgers: 521-549.

Hanks, R.J. and G.L. Ashcroft. (1980). Applied Soil Physics: Soil Water and Temperature Applications. New York, Springer-Verlag.

Hartkamp, C. A., J. Arribas, and A. Tortosa. (1993). "Grain size, composition, porosity and permeability contrasts within cross-bedded sandstones in Tertiary fluvial deposits, central Spain." Sedimentology 40(4): 787-799.

Heller, J. P. (1991). "Dynamic Analysis of Syringe (Mini) Permeameter." New Mexico Petroleum Recovery Research Center 91-27: 1-9.

Hillel, D., Ed. (1971). Soil and Water: Physical Principles and Processes. Edited by T.T. Kozlowski. Physiological Ecology. Madison, Academic Press.

Hillel, D. (1980). Chapter 7: Soil Water: Content and Potential. In Fundamentals of Soil Physics. New York, Academic Press.

Hillel, D. (1980). Chapter 12: Soil Temperature and Heat Flow. In Fundamentals of Soil Physics. New York, Academic Press: 287-313.

Isaaks, E. H. and R. M. Srivastava. (1989). An Introduction to Applied Geostatistics. New York, Oxford University Press.

Johnson, N. M. (1995). "Characterization of alluvial hydrostratigraphy with indicator semivariograms." Water Resources Research 31(12): 3217-3227.

Juca, J.F.T. (1994). Flow Properties of Unsaturated Soils Under Controlled Suction. In Unsaturated Soils. New York, Academic Press: 151-174.

Kelly, S.F., J.S. Selker, and J.L. Green. (1995). "Using Short Soil Moisture Probes with High-Bandwidth Time Domain Reflectometry Instruments." Soil Science America Journal. 59: 97-102.

Klute, A. (1986). Chapter 26: Water Retention: Laboratory Methods. In Methods of Soil Analysis, Part I, Physical and Mineralogical Methods. A. S. o. Agronomy. Madison, Soil Science Society of America. 9: 635-662.

Koltermann, C. E. and S. M. Gorelick. (1995). "Fractional packing model for hydraulic conductivity derived from sediment mixtures." Water Resources Research 31(12): 3283-3297.

Kolyasev, F. E. and A. I. Gupalo. (1958). On the Correlation of Heat and Moisture Properties of Soils. In Water and Its Conduction in Soils. Highway Research Board, Special Report 40, Washington, D.C., pp 106-112.

Laliberte, G. E., A. T. Corey, and R.H. Brooks (1966). Properties of Unsaturated Porous Media. Colorado State University Hydrology Paper No. 17, Fort Collins, 40 p.

Luckner, L., M. T. van Genuchten, and D.R. Nielsen (1989). "A Consistent Set of Parametric Models for the Two-Phase Flow of Immiscible Fluids in the Subsurface." Water Resources Research 25(10): 2187-2193.

Mixon, R. B. (1985). "Stratigraphic and geomorphic framework of uppermost Cenozoic deposits in the southern Delmarva Peninsula, Virginia and Maryland." U.S. Geol. Surv. Prof. Paper 1067-C: p. 53.

Mualem, Y. (1976). "A New Model for Predicting the Hydraulic Conductivity of Unsaturated Porous Media." Water Resources Research. 12(3): 513-522.

Muller, A. C., B.S. Parsons, and D.J.P. Swift. (1996). Comparison Between Petrographic, Photomosaic, and Core "Facies," Oyster Site: Preliminary Report to the Bacterial Transport Program. Department of Oceanography, Old Dominion University, Norfolk, Va., 23508.

Pannatier, Y. (1994). VARIOWIN 2.1. Institute of Minerology, University of Lausanne, Switzerland.

Parsons, B. S. and D. J. P. Swift. (1995). Stratigraphy of the Oyster, Virginia, Site; a Preliminary Report. Department of Oceanography, Old Dominion University, Norfolk, Va., 23508.

Parsons, B. S., D. J. P. Swift, and A. Muller (1996). "Systems versus Sequence Architecture in Shallow Marine Sediments: Scales of Physical Heterogeneity in an Atlantic Coastal Plain Aquifer." Geology Submitted.

Quenouille, M.H. (1956). "Notes on Bias in Estimation." Biometrika. 43: 353-360.

Ritzi Jr., R. W., D. F. Dominic, N.R. Brown, K.W. Kausch, P.J. McAlenney, and M.J. Basial. (1995). "Hydrofacies distribution and correlation in the Miami Valley aquifer system." Water Resources Research. 31(12): 3271-3281.

Robertson, G. M. and C. A. McPhee. (1990). High Resolution Probe Permeability: An Aid to Reservoir Description. In Advances in Core Evaluation, Accuracy and Precision in Reserves Estimation. London, Gordon & Breach Science Publishers: 495-520.

Scheibe, T. D., T. R. Ginn, A. Chilakapati. (1996). Integration of diverse information into a heterogeneous aquifer model at multiple stages of a microbial transport field experiment. Geological Society of America 1996 Annual Meeting. Denver, Co., October 28-31.

Selker, J.S., L. Graff, and T. Steenhuis. (1993). "Noninvasive Time Domain Reflectometry Moisture Measurement Probe." Soil Science Soc. Am. J. 57: 934-936.

Shafer, J.M. and M.D. Varljen. (1990). "Approximation of Confidence Limits on Sample Semivariograms From Single Realizations of Spatially Correlated Random Fields." Water Resources Research. 26(8): 1787-1802.

Suboor, M. A. and J. P. Heller. (1995). "Minipermeameter Characteristics Critical to Its Use." In Situ 19(3): 225-248.

Swift, D. and B. Parsons. (1994). Geologic Characterization of the Oyster, Virginia site: A Preliminary Report. Contribution no. 5 of the Sediment Dynamics Laboratory, Old Dominion University, Norfolk, Va., 23529-0276.

Swift, D. J. P., B. Parsons, A. Muller, J.L. Wilson, R.G. Taylor, R. Holt, R. Smith, A. Schafer, and T. McLing. (1996). Sedimentary Facies as a Guide to Hydrologic Properties in an Experimental Aquifer of Shallow Marine Origin: Virginia's Eastern Shore Peninsula. San Francisco, American Geophysical Union Spring Meeting.

Symon, K.R. (1971). Mechanics. Addison-Wesley, Menlo Park, 639 pp.

Tidwell, V.C. and J.L. Wilson. (1997). "Laboratory Method for Investigating Permeability Upscaling." Water Resources Research in press.

Wilkinson, L. (1992). SYSTAT. Evanston, SYSTAT, Inc.

Wyckoff, R. D. and H. G. Botset (1936). "The Flow of Gas-Liquid Mixtures through Unconsolidated Sands." Physics 7(September): 325-345.

APPENDIX A - DETAILED LABORATORY METHODS

A.1 - Determination of LSAMP Frictional Coefficients

As discussed in Chapter 4 of this volume, we calibrated each of the LSAMP devices to account for the frictional losses of the system. Following Davis et al. (1994) we modeled the mechanical friction of the syringe as lubricated friction, which is proportional to some fixed power of the velocity (Symon, 1971). Using $F_f = \beta v^n$, where F_f is the frictional force [N] and v is the velocity [m/sec], we measured the time and pressure readings for multiple standards to get a range of velocities and frictional force readings (Tables A.1 through A.3). We plotted the frictional force versus the velocity and fit a quadratic (n=2) to our data. The β value was obtained from the absolute value of the coefficient of the quadratic term (Figure A.1a, c, & e).

Recalling **Figure 4.1**, we measured the pressure of our system with the manometer attached to Ports 1 and 2 for the same standards. By subtracting the pressure obtained at Port 1 from that obtained at Port 2 for the same standard, we acquired a measurement of the pressure losses for the tubing between Ports 1 and 2 (ΔP [Pa]). We obtained the flow rate by multiplying the velocity by the area of the piston. We plotted the change in pressure versus the flow rate and fit a regression line (Figures A.1b, d, & f). We used this linear model, $\Delta P = \alpha q - b$, to account for the tubing pressure losses.

Time (s)	P(mm H2O)	Vel.[m/s]	Fric.Force	del Ff	q=v*A	ΔP (Pa)
0.60	68	0.112	0.64	0.132	1.1E-04	137
0.82	112	0.082	1.05	-0.038	7.9E-05	-39
1.17	120	0.057	1.13	0.038	5.5E-05	39
3.10	138	0.022	1.30	0.000	2.1E-05	0
1320	139	0.000	1.32	0.021	4.9E-08	22
0.39	0	0.172	0.00	0.092	1.7E-04	96

Table A.1 - LSAMP II Calibration Data

Time (s)	P(mm H2O)	Vel.[m/s]	Fric.Force	del Ff	q=v*A	ΔP (Pa)
0.74	68	0.074	0.67	0.394	7.4E-05	390
1.0	124	0.054	1.22	0.337	5.5E-05	333
1.13	144	0.048	1.42	0.208	4.9E-05	206
185	180	0.000	1.78	-0.020	3.0E-07	-20

Table A.2 - LSAMP I New Set-Up Calibration Data

Time (s)	P(mm H2O)	Vel.[m/s]	Fric.Force	del Ff	q=v*A	ΔP (Pa)
0.45	37	0.121	0.36	0.364	1.2E-04	361
579	179	0.000	1.77	-0.020	9.5E-08	-20
1.1	158	0.050	1.56	0.178	5.0E-05	177
0.82	140	0.066	1.39	0.218	6.7E-05	216
0.64	110	0.085	1.09	0.337	8.6E-05	333
2.45	178	0.022	1.76	0.099	2.2E-05	98

Table A.3 - LSAMP I Old Set-Up Calibration Data

A.2 - Hanging Column Experiments

Though the general method was discussed in Section 4.3, we will detail the hanging column method by discussing sample R16 in great detail (data contained in Appendix C). We repacked sand from Oyster, Va. in standard 100 cc soil rings. We measured the length and diameter of the soil ring to get the exact volume. We used glue to attach a piece of filter paper to the bottom to prevent sand loss and to create a good seal with the porous plate in the Buchner funnel. We weighed the empty ring. We vibrated the sample ring while slowly pouring the sand into the ring. The vibration caused the sand to settle and prevented the formation of layers or gaps in the sand. The vibration also caused the finest grained sands to migrate to the bottom of the sample. Once the sample ring was completely filled, we weighed it full. Using the weight of sand, the volume of the ring, and a particle density of 2.66 g/cc (Travis Mcling, personnel communication, 1996), we determined the porosity of the sample.

We placed our sample ring on the prewetted porous plate inside the Buchner funnel and covered the top of the funnel with a rubber stopper. We raised the burrette

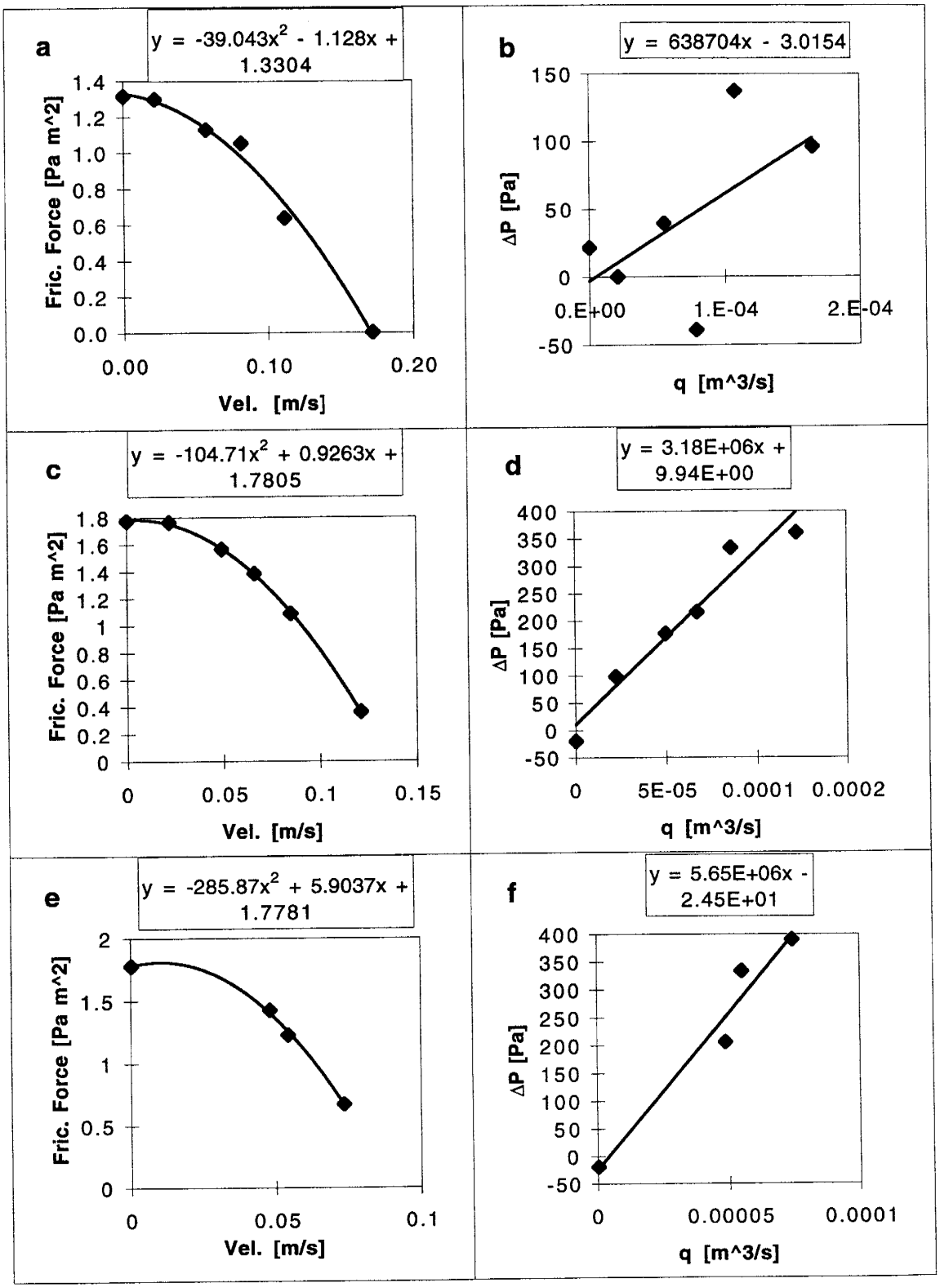

Figure A.1 - Calibration curves for determining Beta (left) and Alpha (right)
Top Level: LSAMP II; Middle Level: LSAMP I New Set-Up;
Bottom Level: LSAMP I Old Set-Up

(Figure 4.2) above the level of the porous plate to wet the sample from below. Our samples were not set up to reach complete saturation, but we were not as concerned about the water saturated end of the curve. Though the majority of the water entered the sample quickly, stable equilibrium did not occur until 4 days of wetting. This was probably due to the internal air of the system having to each 100% relative humidity. For R16, we reached an initial saturation of 85.1%. Once the initial saturation had been reach, we slowly applied suction by lowering the burrette. Before the air-entry value was reached, no water came out of the sample, so our equilibrium condition was recorded after 1 to 2 days. Once water started coming out of the sample, we had to wait a longer period of time to reach an approximate equilibrium state. For each step, we lowered the burrette to the appropriate suction. We returned to the set-up systematically throughout the experiment to readjust the burrette to the appropriate suction. Between each suction step, we recording the height of the porous plate, the height of the water in the burrette, and the volume of the water in the burrette. When the water level in the burrette did not visually change over a period of 12 to 24 hours, we assumed that we had reached an approximate equilibrium state and that we could move to the next suction step.

For R16, we applied 28.5 cm of suction to the sample as the first step after the bubbling pressure was reached. We drained over 15% of the water and that step took 7 days for an approximate euilibrium state to be reached. We found that the more water that was drained from the system, the less time that was required to wait for an equilibrium state to be reached. As we began to approach the residual water saturation value (about 11%) we only had to wait 3 days between suction steps.

APPENDIX B - LABORATORY SAMPLE CHARACTERIZATION AND GRAIN SIZE DISTRIBUTION

B.1 - Laboratory Sample Characterization

For each of the sample rings we used to conduct our hanging column experiments on, we measured the volume of sand studied, the estimated initial water saturation, the estimated porosity, the water density used in the hanging column, the calculated porosity, the grain size distribution, and the facies type that the sand sample was from. A compilation of this data is below (Table B.1). We measured the volume of the sample rings by measuring the length and diameter of each ring. For samples R3 through R10, we packed the sample rings with slightly wet sand and estimated the initial water saturation by conducting gravimetric analysis (Appendix D) on the bulk sands. Using this estimate of water saturation, we approximated the porosity (n) with:

$$n = \frac{\text{Volume} - \frac{\text{Mass of sand}}{\text{Particle density of sand}}}{\text{Volume}}$$

. For each of our experiments we measured the density of the Type I water that we filled the hanging columns with so we could accurately convert mass to volume for water. At the end of our tests, we oven dried the samples and determined the actual mass of sand used and the actual porosity of the sample. This oven dried sand was then sieved to determine the grain size distribution for each of the samples.

Descriptor\Sample	R3	R4	R5	R6	R7	R8	R9
Volume [cc]	104	104	105	104	104	103	99.2
Estimated initial ø [%]	11.5	8.8	3.3	3.2	9.1	5.0	8.9
Estimated n	44	37	41	38	42	41	43
Water density [g/cc]	0.997	0.996	0.995	0.995	0.996	0.995	0.996
Calculated n	41	42	39	37	39	39	43
Mean phi size	1.6	1.63	1.47	1.45	1.88	1.75	1.92
Facies	XS1	XS1	XS1	XS1	XS3	XS2	XS3

Descriptor\Sample	R10	R11	R12	R13	R14	R15	R16
Volume [cc]	98.9	104	104	104	104	104	104
Estimated init. sat. [%]	4.9	0	0	0	0	0	0
Estimated n	41	36	37	37	37	37	36
Water density [g/cc]	0.995	0.997	0.997	0.995	0.995	0.994	0.994
Calculated n	40	36	37	37	37	38	36
Mean phi size	1.77	1.49	1.70	1.74	1.63	1.92	1.81
Facies	XS2	XS1	XS2	XS2	XS1	XS3	XS2

Descriptor\Sample	R17	R18	R19	R20	R24	R25	R26
Volume [cc]	104	103	99.6	100	101	95.2	99.2
Estimated init. sat. [%]	0	0	0.0	0.0	0.0	22.9	23.4
Estimated n	37	37	37	38	37	38	42
Water density [g/cc]	0.995	0.995	0.996	0.995	0.997	0.996	0.997
Calculated n	37	37	37	38	37	41	46
Mean phi size	1.8	1.98	1.91	1.8	1.69	1.88	2.81
Facies	XS2	HS	XS3	XS2	XS2	XS3	HS

Table B.1 - Basic Parameters of Samples R3-R20, R24-R26

B.2 - Grain Size Distribution

We used a standard sieving method to determine the grain size distribution and facies type for each of our samples. We used 8 sieves of U.S. Standard sieve mesh sizes of 10, 18, 35, 40, 50, 60, 70, and 200. These sieves gave us a range of 75 microns to 2000 microns (-1 phi to 3.75 phi). We poured the sand into the sieves, shook the sieves, and weighed the sand in each of the sieves. We checked to see that we recovered > 99% of the sand. We calculated the percentage by mass of each of the classes of sand (Table B.2). Using this information, we determined the mean $\phi = \sum_i \left(\frac{\phi_i + \phi_{i-1}}{2} \right) * (\text{weight } \%)_i$, where ϕ_i is the phi unit of the ith sieve and ϕ_{i-1} is the phi unit of the next larger sieve. For example, the portion of the mean phi size contributed by the sand by the #50 sieve (300 microns and phi = 1.75) that also passed through the #40 sieve (417 microns and phi = 1.25) is calculated by $\left(\frac{1.75 + 1.25}{2} \right) * (\text{weight } \%)_{1.75}$.

Once we had calculated the mean phi size for each of our samples, we determined the facies type by examing the grain size distribution. Recalling the facies classifications presented in **Chapter 1**, the Gravelly Shelly facies was characterized by samples that had

greater than 10% by weight of sand larger than 2000 microns. None of our samples were in this category. For sands outside this category, a mean phi size of less than 2.00 meant the sample was from the Cross-Stratified facies and samples with a mean phi size greater than 2.00 were from the Horizontally Stratified facies. Though **Table B.2** contains the data needed to reconstruct the individual histograms, we provide the individual histograms for each of our samples below plotted as weight % per sieve versus range [microns] per sieve (Figures R3-R20, R24-R26).

Descriptor\Sample	R3		R4		R5		R6		R7	
Size (microns)	mass (g)	%	mass (g)	%	mass (g)	%	mass (g)	%	mass (g)	%
>2000	0.90	0.55	0.49	0.31	10.34	6.10	9.42	5.43	1.53	0.91
1000-2000	3.56	2.19	2.99	1.87	10.48	6.19	13.94	8.03	5.76	3.43
500-1000	12.56	7.70	11.51	7.19	14.61	8.62	18.53	10.68	15.40	9.16
417-500	11.14	6.83	9.44	5.90	7.47	4.41	6.57	3.79	5.82	3.46
300-417	82.71	50.74	80.97	50.59	49.93	29.47	43.50	25.08	38.05	22.65
250-300	23.42	14.37	27.24	17.02	27.24	16.07	31.29	18.04	28.67	17.07
212-250	12.50	7.67	10.84	6.78	22.89	13.51	21.80	12.57	25.48	15.17
75-212	14.81	9.09	15.14	9.46	26.33	15.54	28.23	16.28	47.16	28.07
<75	1.41	0.87	1.43	0.89	0.17	0.10	0.18	0.10	0.16	0.09

Descriptor\Sample	R8		R9		R10		R11		R12	
Size (microns)	mass (g)	%	mass (g)	%	mass (g)	%	mass (g)	%	mass (g)	%
>2000	0.40	0.24	1.29	0.82	0.25	0.16	0.51	0.29	0.91	0.52
1000-2000	1.66	1.01	4.90	3.12	1.06	0.67	4.55	2.59	4.98	2.87
500-1000	8.83	5.35	13.12	8.37	8.61	5.46	15.68	8.94	14.87	8.57
417-500	9.10	5.51	5.71	3.64	10.33	6.55	17.87	10.19	10.26	5.91
300-417	68.28	41.35	35.44	22.60	65.41	41.48	89.24	50.87	58.19	33.53
250-300	34.59	20.95	25.42	16.21	30.08	19.07	26.30	14.99	34.05	19.62
212-250	21.44	12.99	25.07	15.99	19.62	12.44	11.43	6.52	24.43	14.08
75-212	20.74	12.56	45.68	29.13	22.17	14.06	9.65	5.50	25.76	14.84
<75	0.09	0.05	0.18	0.11	0.18	0.12	0.20	0.11	0.09	0.06

Descriptor\Sample	R13		R14		R15		R16		R17	
Size (microns)	mass (g)	%	mass (g)	%	mass (g)	%	mass (g)	%	mass (g)	%
>2000	0.69	0.39	0.77	0.44	0.28	0.16	0.00	0.00	0.00	0.00
1000-2000	5.46	3.12	4.55	2.60	2.29	1.33	0.29	0.17	0.13	0.07
500-1000	17.75	10.16	14.88	8.52	14.63	8.47	20.53	11.70	10.45	6.02
417-500	10.26	5.87	11.01	6.30	7.92	4.58	9.31	5.30	9.25	5.33
300-417	50.17	28.71	72.57	41.54	44.54	25.78	51.12	29.12	71.16	41.02
250-300	34.79	19.91	32.45	18.58	33.14	19.18	36.52	20.81	34.82	20.07
212-250	23.29	13.33	18.57	10.63	25.13	14.55	25.29	14.41	22.29	12.85
75-212	32.21	18.43	19.65	11.25	44.51	25.77	32.03	18.25	24.97	14.39
<75	0.15	0.08	0.24	0.14	0.31	0.18	0.44	0.24	0.41	0.25

Descriptor\Sample	R18		R19		R20		R24		R25	
Size (microns)	mass (g)	%	mass (g)	%	mass (g)	%	mass (g)	%	mass (g)	%
>2000	0.00	0.00	0.00	0.00	0.00	0.00	0.98	0.58	0.31	0.21
1000-2000	0.15	0.09	0.19	0.12	0.26	0.16	3.39	2.02	0.97	0.65
500-1000	14.59	8.57	16.43	10.09	12.33	7.50	20.12	11.98	6.93	4.64
417-500	60.60	3.88	5.55	3.41	9.02	5.48	6.65	3.96	3.86	2.59
300-417	42.20	24.80	41.27	25.34	59.93	36.44	61.40	36.55	52.25	35.01
250-300	33.11	19.46	36.30	22.29	35.61	21.65	29.13	17.34	36.89	24.72
212-250	26.88	15.80	26.22	16.10	21.56	13.11	18.93	11.27	21.26	14.25
75-212	46.35	27.24	36.79	22.59	25.35	15.42	27.26	16.23	26.50	17.75
<75	0.30	0.16	0.13	0.06	0.39	0.24	0.15	0.07	0.27	0.18

Descriptor\Sample	R26		R27	
Size (microns)	mass (g)	%	mass (g)	%
>2000	0.01	0.01	0.43	0.28
1000-2000	0.06	0.04	0.46	0.30
500-1000	0.19	0.14	28.33	18.73
417-500	0.07	0.05	16.90	11.17
300-417	0.29	0.21	77.08	50.97
250-300	1.22	0.86	4.41	2.92
212-250	9.47	6.70	1.42	0.94
150-212	98.66	69.84	NR	0.00
110-150	30.14	21.34	NR	0.00
75-110	0.88	0.62	21.98	14.53
<75	0.27	0.19	0.23	0.16

Table B.2 - Grain size distributions for laboratory samples

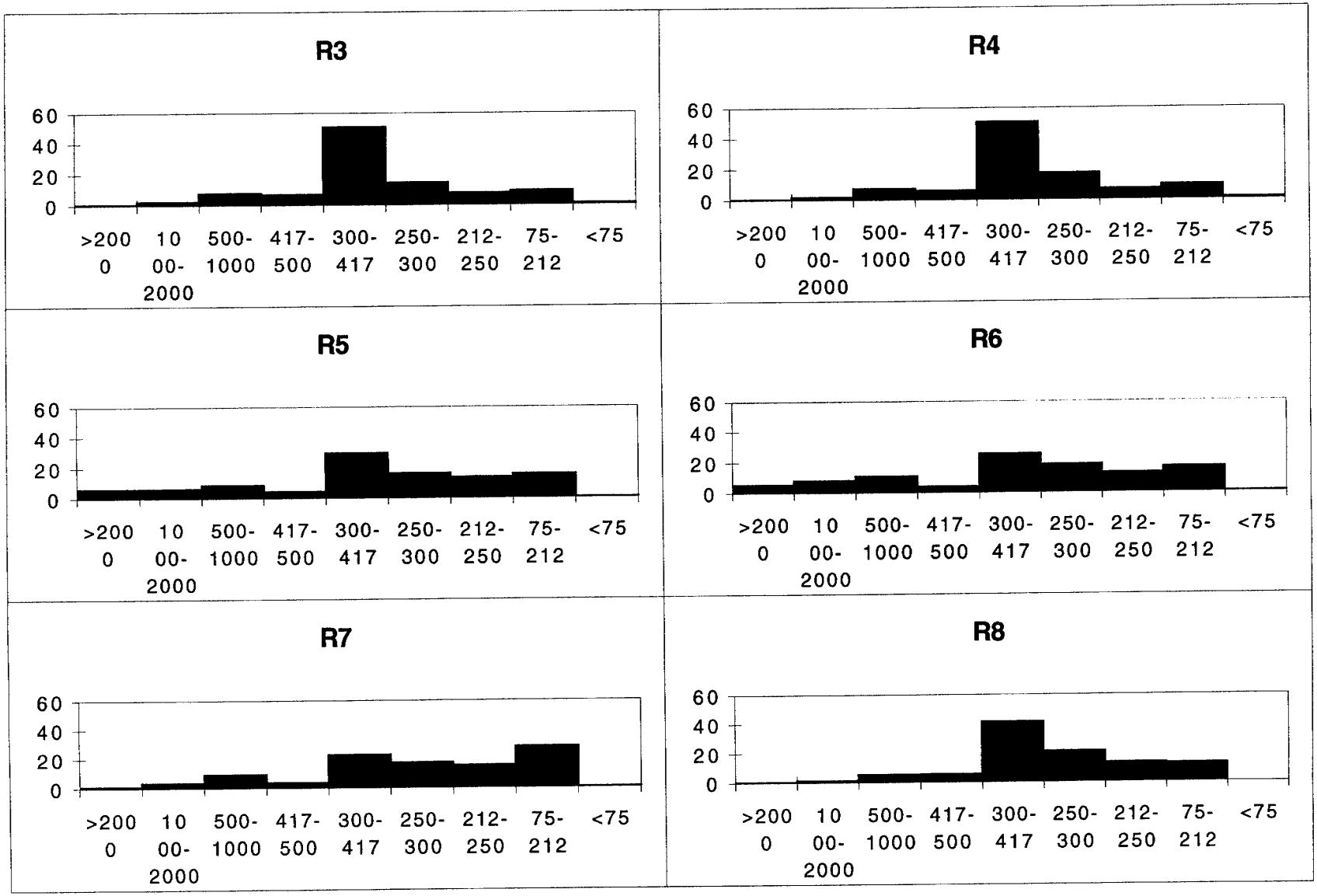
R3
60
40
20
0
>2000
1000-2000
500-1000
417-500
300-417
250-300
212-250
75-212
<75
R4
60
40
20
0
>2000
1000-2000
500-1000
417-500
300-417
250-300
212-250
75-212
<75
R5
60
40
20
0
>2000
1000-2000
500-1000
417-500
300-417
250-300
212-250
75-212
<75
R6
60
40
20
0
>2000
1000-2000
500-1000
417-500
300-417
250-300
212-250
75-212
<75
R7
60
40
20
0
>2000
1000-2000
500-1000
417-500
300-417
250-300
212-250
75-212
<75
R8
60
40
20
0
>2000
1000-2000
500-1000
417-500
300-417
250-300
212-250
75-212
<75

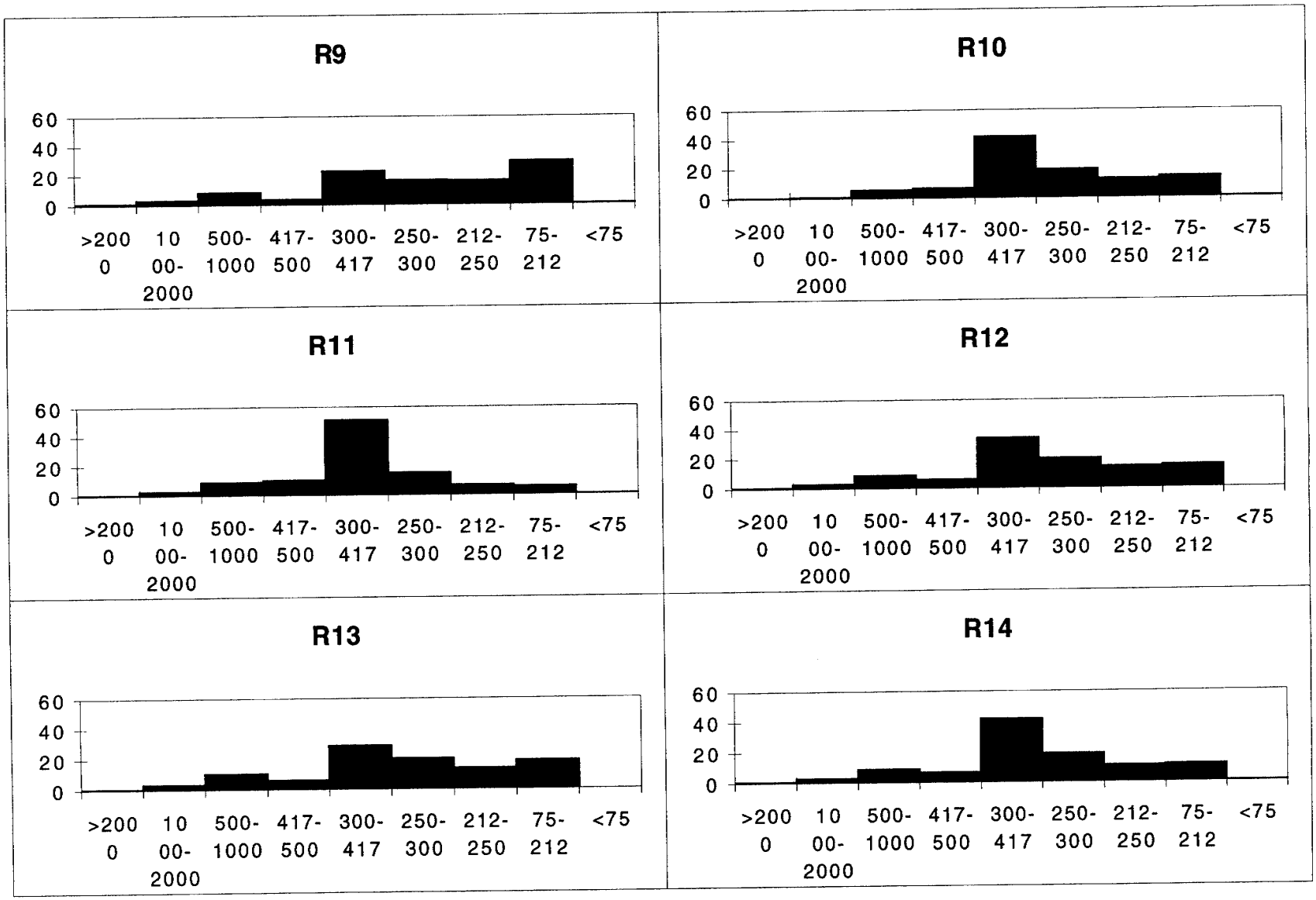
R9
60
40
20
0
>2000
1000-2000
500-1000
417-500
300-417
250-300
212-250
75-212
<75
R10
60
40
20
0
>2000
1000-2000
500-1000
417-500
300-417
250-300
212-250
75-212
<75
R11
60
40
20
0
>2000
1000-2000
500-1000
417-500
300-417
250-300
212-250
75-212
<75
R12
60
40
20
0
>2000
1000-2000
500-1000
417-500
300-417
250-300
212-250
75-212
<75
R13
60
40
20
0
>2000
1000-2000
500-1000
417-500
300-417
250-300
212-250
75-212
<75
R14
60
40
20
0
>2000
1000-2000
500-1000
417-500
300-417
250-300
212-250
75-212
<75

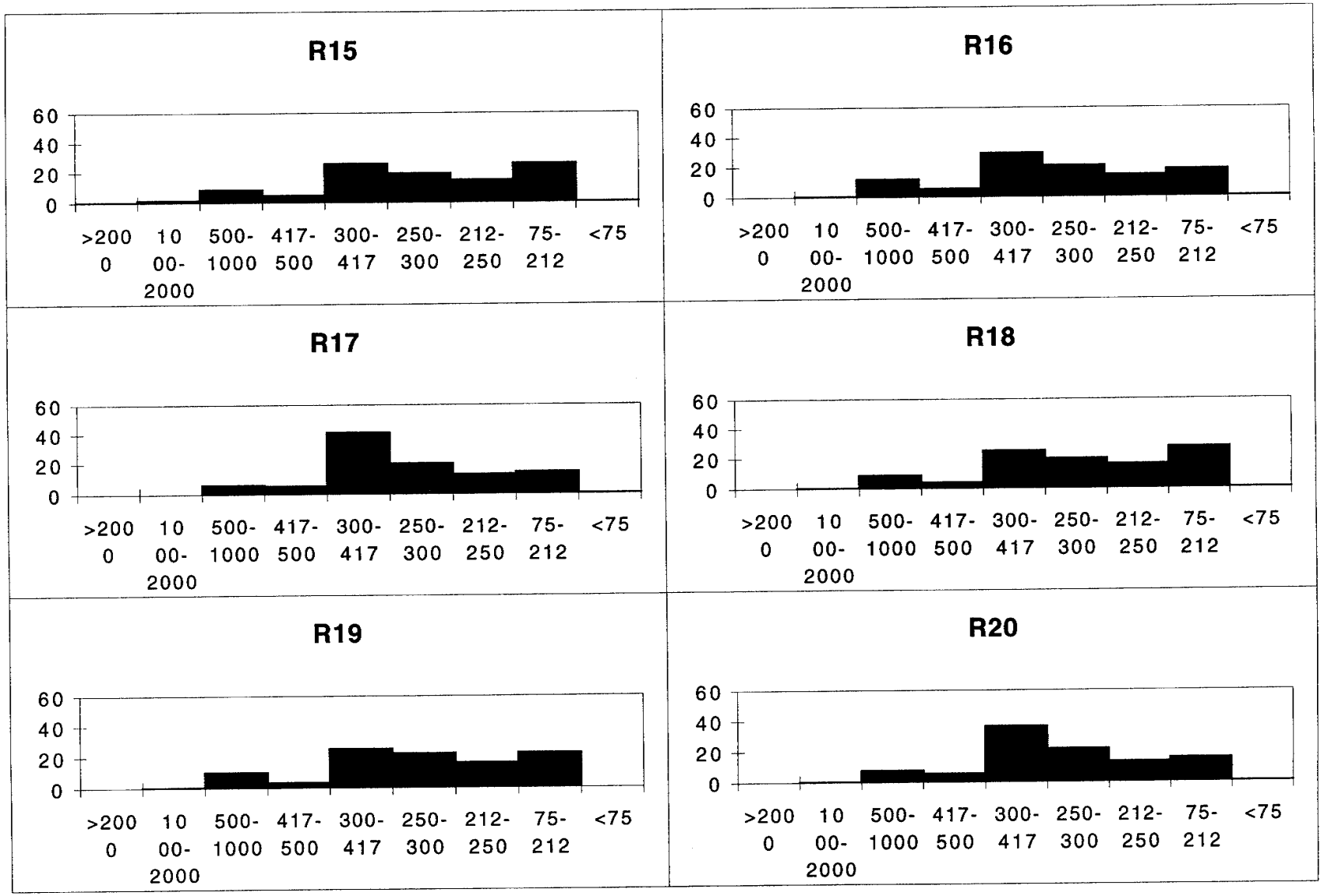
R15
60
40
20
0
>2000
1000-2000
500-1000
417-500
300-417
250-300
212-250
75-212
<75
R16
60
40
20
0
>2000
1000-2000
500-1000
417-500
300-417
250-300
212-250
75-212
<75
R17
60
40
20
0
>2000
1000-2000
500-1000
417-500
300-417
250-300
212-250
75-212
<75
R18
60
40
20
0
>2000
1000-2000
500-1000
417-500
300-417
250-300
212-250
75-212
<75
R19
60
40
20
0
>2000
1000-2000
500-1000
417-500
300-417
250-300
212-250
75-212
<75
R20
60
40
20
0
>2000
1000-2000
500-1000
417-500
300-417
250-300
212-250
75-212
<75

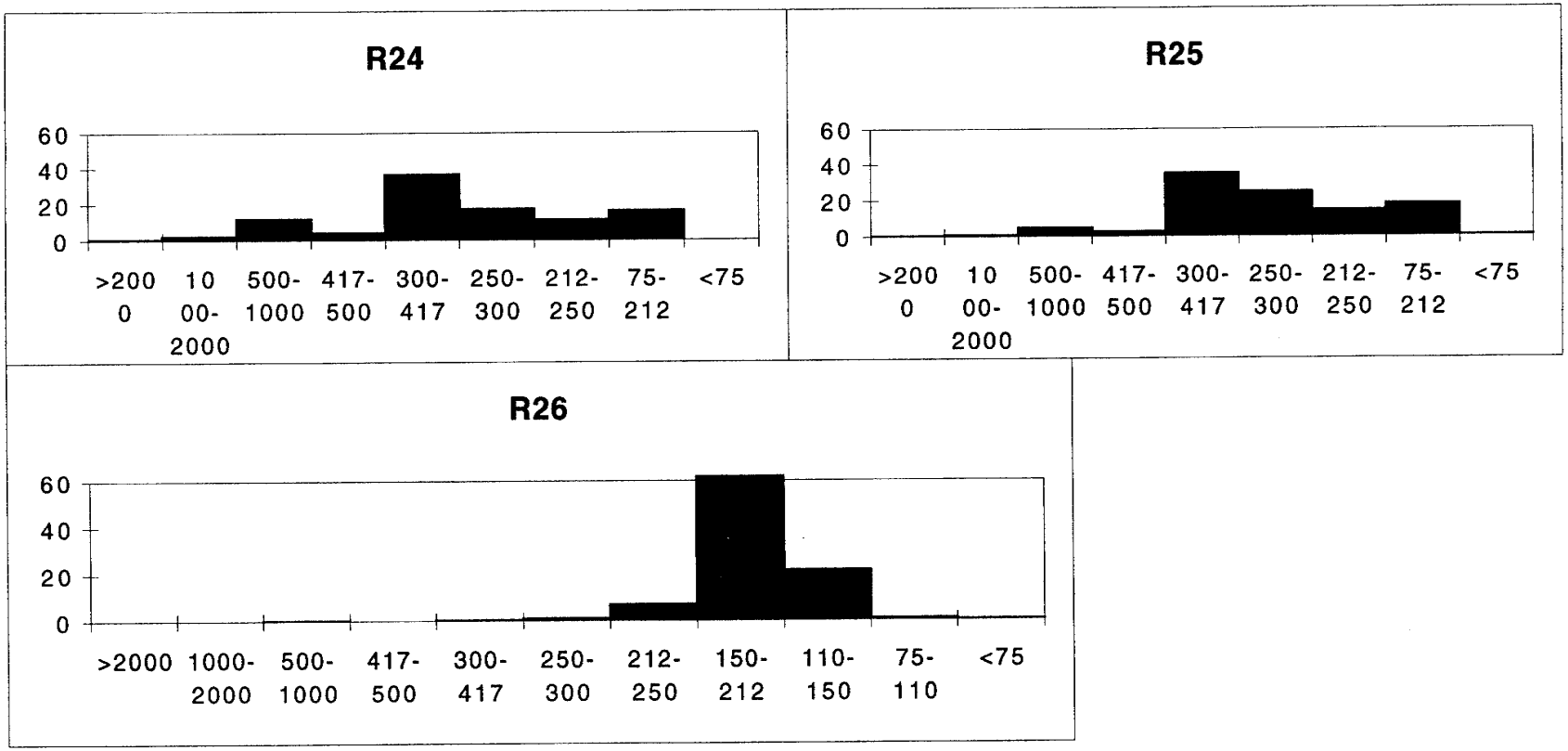

Mean weight percentages for each grain size bin (sieve) for all of the laboratory samples.

APPENDIX C - INDIVIDUAL MOISTURE RETENTION DATA, PERMEABILITY VERSUS PERCENTAGE WATER SATURATION, AND MEASURED PERMEABILITY DATA

C.1 - Individual Moisture Retention Data

Below are presented the measured and calculated data that went into the moisture retention functions compiled in **Figure 5.8** and **Figure 5.11a**. Also contained in the data charts are the measured k_{air}(eff) values [darcys], the natural log of k_{air}, and the natural log of relative permeability to air for each of the samples. This data was used to create **Figures 5.9** through **5.12**. The time [days] records the time that was allowed for an approximate equilibrium condition to be reached for each hanging column step. Theta is the volumetric water content for each step. The suction [cm] value denotes the distance between the water level in the burrette and the center of the sample. Percentage Water Saturation was obtained by dividing theta by the porosity of the sample. For each data set, the corresponding moisture retention function is graphed.

C.2 - Ln Air Permeability versus Percentage Water Saturation

Along with the graphed moisture retention functions are the individual results that make up **Figure 5.10**. These plots of Ln k_{air}(eff) versus percentage water saturation are fitted with a regression line. The points represent the measurements made by the LSAMP II during each of the experiments.

C.3 - Panel 5 Data Compilation

Following the moisture retention tables and graphs is a compilation of the air permeability data from Panel 5 that was used to conduct the geostatistical analyses. The Sample Alias is the name associated with the gridded section of the panel. Local x and Local y are the coordinates of the measurement points taking (0,0) to be the lower left

corner of the panel. k_{air_psat} is the measured effective air permeability before any saturation correction was made. Saturation denotes the measured saturation from the 10 cm deep cores (INEL), and Sat. used is the kridged saturation used in applying the non-wetting phase relative permeability curve (correction factor). Ln kr(air) is the calculated natural log of relative permeability to air found using the correction factors. Phi ave is measured in the 10 cm deep INEL cores, and Facies Desig. is the appropriate facies subset that each point is associated with. Finally, k(intrinsic) is the estimated intrinsic permeability for each data point after we applied our correction factors.

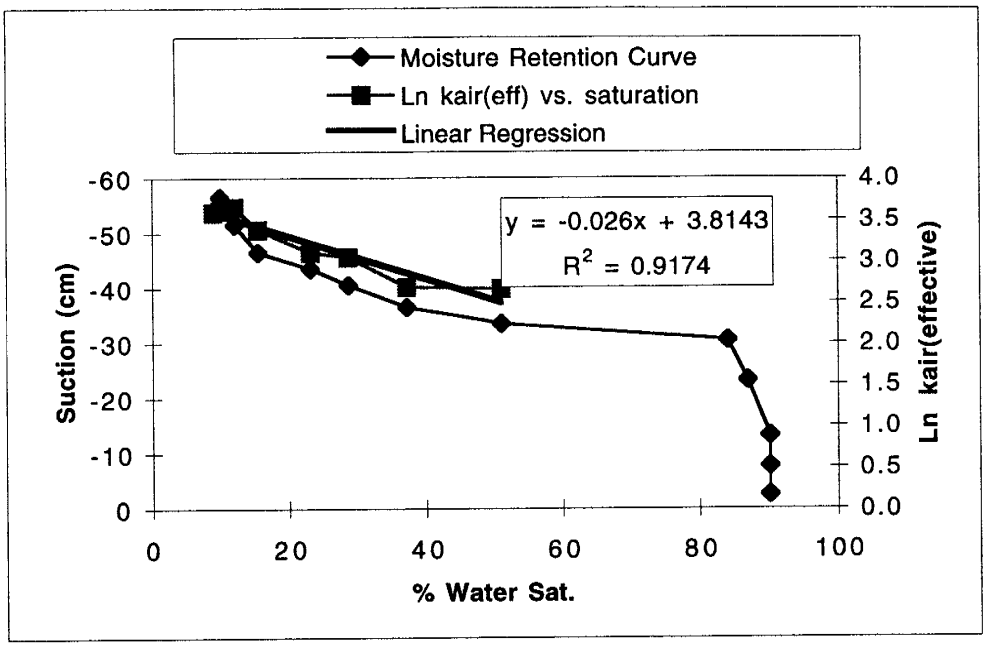

Time	Theta	Suction [cm]	k(air)	% Water Sat.	Ln k(air)	Ln kr(air)
		0				
3.5	32.62	-2.5		90.12		
2.5	32.62	-7.7		90.12		
4.5	32.62	-13.2		90.12		
5	31.49	-23.2		87.00		
4.5	30.45	-30.5		84.11		
7.5	18.45	-33.5	14.20	50.98	2.65	-0.96
5	13.46	-36.5	14.56	37.19	2.68	-0.93
5.5	10.39	-40.5	20.90	28.70	3.04	-0.57
5.5	8.39	-43.5	22.11	23.17	3.10	-0.51
7	5.60	-46.5	29.21	15.48	3.37	-0.24
2	4.36	-51.5	38.32	12.05	3.65	0.04
3	3.59	-56.5	36.80	9.93	3.61	0.00
	3.23		35.94	8.93	3.58	-0.03

Sample R11 Moisture Retention and kair(effective) Data and Graph

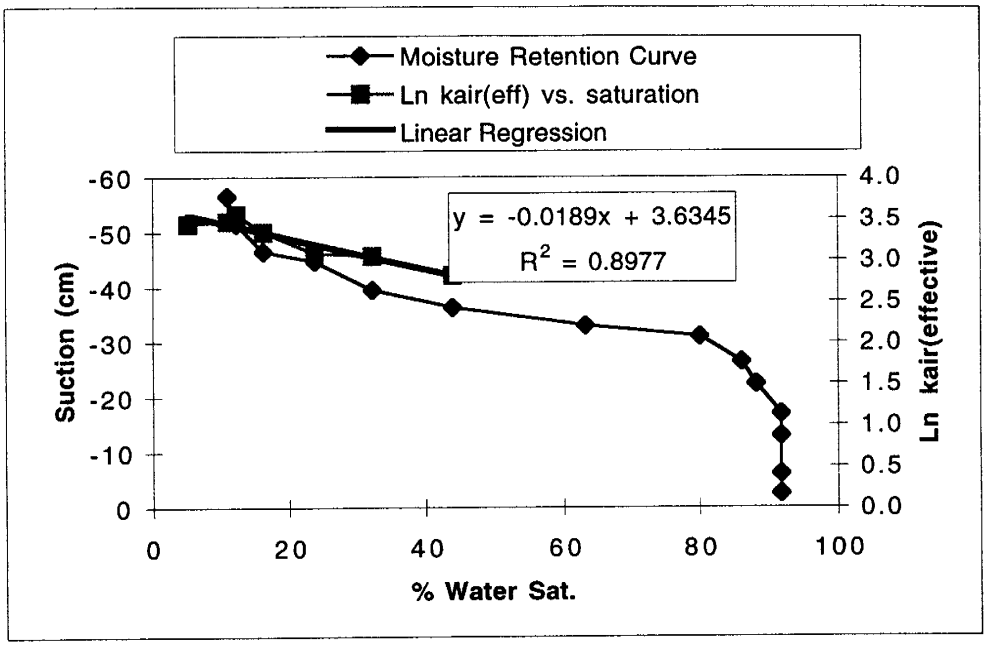

Time	Theta	Suction [cm]	k(air)	% Water Sat.	Ln k(air)	Ln kr(air)
		0				
3.5	33.53	-2.5		91.85		
7	33.53	-6.1		91.85		
2	33.53	-13		91.85		
1.5	33.53	-17		91.85		
2	32.22	-22.4		88.27		
1.5	31.45	-26.4		86.16		
3.5	29.23	-31		80.09		
7.5	23.07	-33		63.20		
3	16.03	-36.3	16.60	43.93	2.81	-0.67
7.5	11.80	-39.5	21.03	32.32	3.05	-0.43
4	8.71	-44.7	21.66	23.87	3.08	-0.40
5	5.92	-46.5	28.11	16.22	3.34	-0.14
4	4.47	-51.5	34.69	12.25	3.55	0.07
3	3.99	-56.5	32.00	10.93	3.47	-0.01
	1.89		30.94	5.19	3.43	-0.05

Sample R12 Moisture Retention and kair(effective) Data

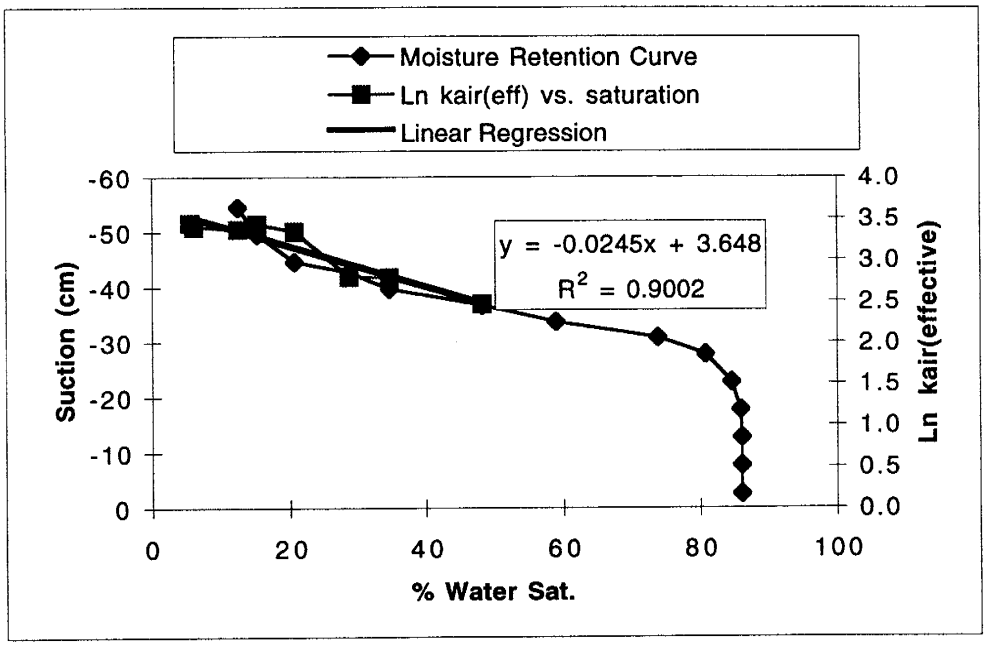

Time	Theta	Suction [cm]	k(air)	% Water Sat.	Ln k(air)	Ln kr(air)
		0				
2	31.89	-2.5		86.18		
2	31.89	-7.7		86.18		
1.25	31.89	-12.7		86.18		
2.75	31.81	-17.7		85.97		
1.25	31.33	-22.7		84.67		
2.5	29.89	-27.7		80.79		
2	27.30	-30.7		73.78		
6.5	21.81	-33.6		58.94		
4	17.86	-36.6	11.65	48.27	2.46	-0.97
5	12.85	-39.6	16.09	34.73	2.78	-0.65
5	10.63	-42.6	16.20	28.74	2.79	-0.64
6	7.65	-44.5	28.11	20.67	3.34	-0.09
4	5.62	-49.5	30.80	15.20	3.43	0.00
4	4.57	-54.5	28.85	12.34	3.36	-0.07
	2.23		29.64	6.04	3.39	-0.04
	2.04		31.21	5.52	3.44	0.01

Sample R13 Moisture Retention and kair(effective) Data

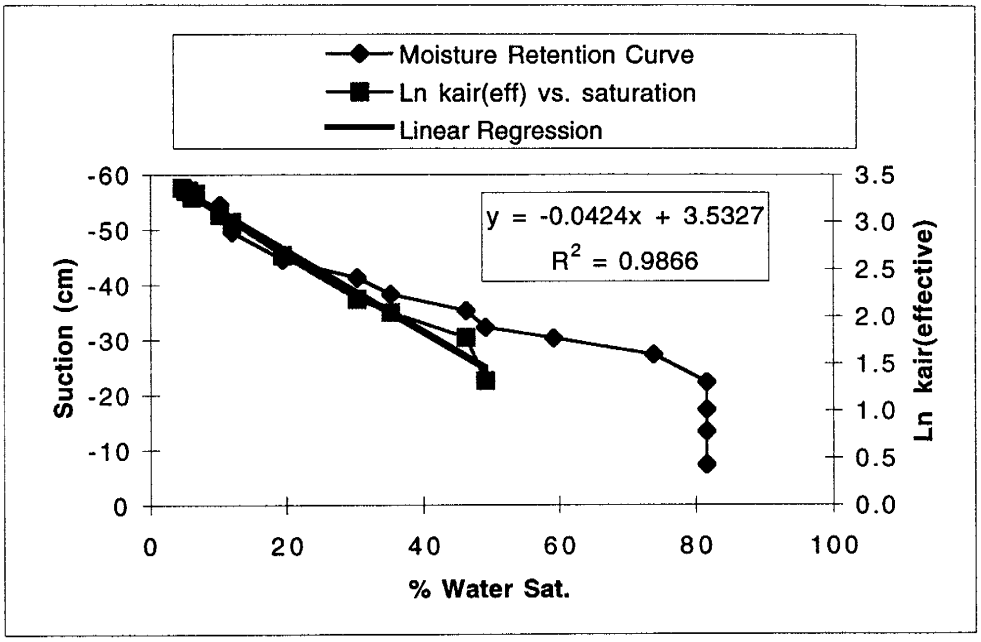

Time	Theta	Suction [cm]	k(air)	% Water Sat.	Ln k(air)	Ln kr(air)
		0				
2	30.37	-7.3		81.63		
1.5	30.37	-13.3		81.63		
3	30.37	-17.3		81.63		
1.5	30.37	-22.3		81.63		
1.5	27.49	-27.3		73.90		
2.5	22.02	-30.3		59.19		
5	18.28	-32.3	3.73	49.13	1.32	-2.02
3	17.22	-35.3	5.91	46.29	1.78	-1.56
5	13.09	-38.3	7.73	35.20	2.05	-1.29
2	11.27	-41.3	8.86	30.29	2.18	-1.16
6	7.24	-44.5	14.09	19.45	2.65	-0.69
3	4.45	-49.5	20.05	11.97	3.00	-0.34
2	3.78	-54.5	21.62	10.16	3.07	-0.27
	3.20			8.61		
	2.45		27.14	6.58	3.30	-0.04
	2.25		25.99	6.04	3.26	-0.08
	2.07		28.05	5.57	3.33	-0.01
	1.93		27.88	5.18	3.33	-0.01
	1.71		28.83	4.59	3.36	0.02

Sample R14 Moisture Retention and kair(effective) Data

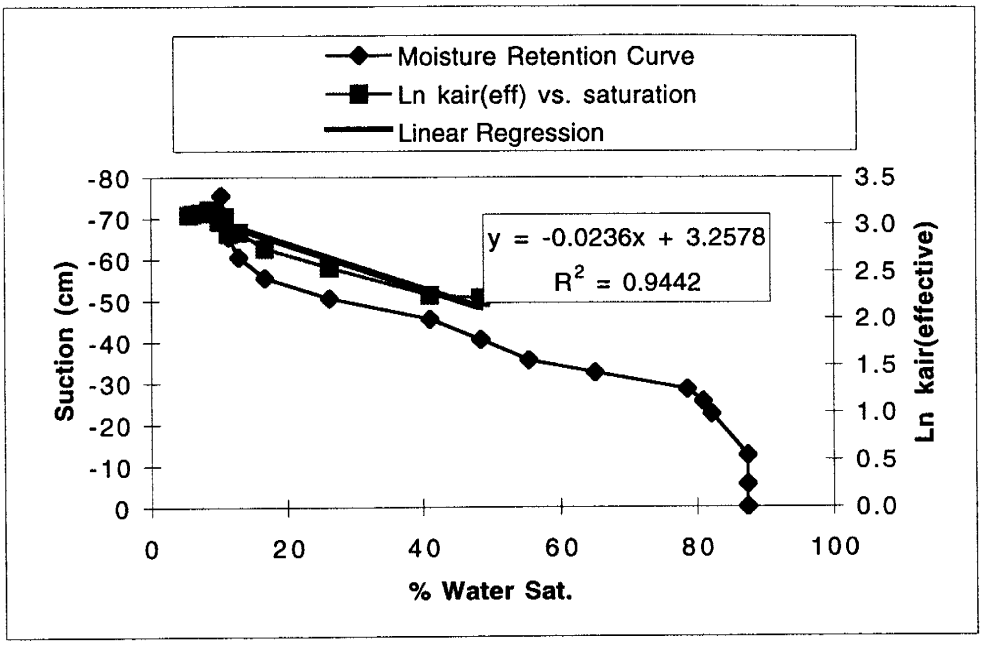

Time	Theta	Suction [cm]	k(air)	% Water Sat.	Ln k(air)	Ln kr(air)
	32.82	0		87.52		
1	32.82	-5.5		87.52		
1	32.82	-12.5		87.52		
4	30.82	-22.5		82.19		
3	30.35	-25.5		80.94		
3	29.49	-28.5		78.64		
7	24.39	-32.5		65.03		
10	20.79	-35.5		55.45		
5	18.19	-40.5	9.19	48.50	2.22	-0.90
6	15.40	-45.5	9.43	41.07	2.24	-0.88
4	9.83	-50.5	12.67	26.20	2.54	-0.58
4	6.26	-55.5	15.47	16.68	2.74	-0.38
4	4.81	-60.5	18.42	12.82	2.91	-0.21
4	4.23	-65.5	18.15	11.29	2.90	-0.22
4	4.04	-70.5	21.78	10.77	3.08	-0.04
3	3.85	-75.5	20.65	10.27	3.03	-0.09
	3.72		20.77	9.93	3.03	-0.09
	3.47		22.97	9.26	3.13	0.01
	3.18		23.46	8.49	3.16	0.04
	2.73		22.68	7.28	3.12	0.00
	2.28		22.40	6.07	3.11	-0.01
	2.09		22.09	5.58	3.10	-0.02

Sample R15 Moisture Retention and kair(effective) Data

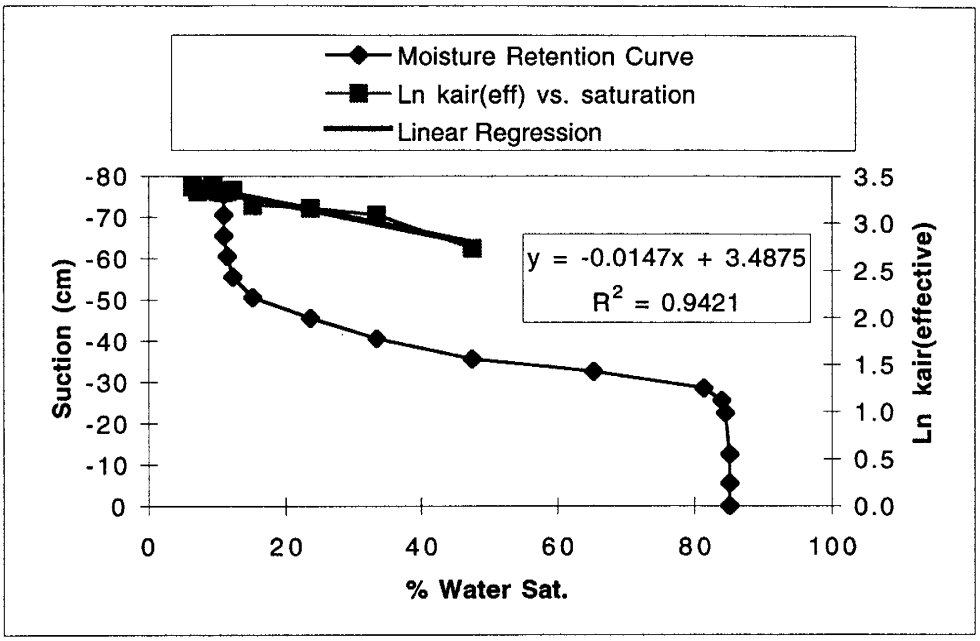

Time	Theta	Suction [cm]	k(air)	% Water Sat.	Ln k(air)	Ln kr(air)
4	30.98	0		85.11		
1	30.98	-5.5		85.11		
2	30.98	-12.5		85.11		
4	30.77	-22.5		84.53		
3	30.58	-25.5		84.01		
3	29.62	-28.5		81.37		
7	23.77	-32.5		65.30		
10	17.29	-35.5	15.33	47.50	2.73	-0.63
7	12.15	-40.5	21.85	33.38	3.08	-0.28
6	8.60	-45.5	23.50	23.63	3.16	-0.20
4	5.53	-50.5	24.26	15.19	3.19	-0.17
4	4.48	-55.5	28.44	12.31	3.35	-0.01
3	4.19	-60.5	28.11	11.51	3.34	-0.02
3	4.00	-65.5	27.83	10.99	3.33	-0.03
3	4.00	-70.5	27.99	10.99	3.33	-0.03
3	4.00	-75.5	27.77	10.99	3.32	-0.04
	3.87		28.16	10.15	3.34	-0.02
	3.70		29.83	9.41	3.40	0.04
	3.43		28.79	8.54	3.36	0.00
	3.11		28.56	7.69	3.35	-0.01
	2.80		28.05	7.19	3.33	-0.03
	1.39		29.51	6.42	3.38	0.02

Sample R16 Moisture Retention and kair(effective) Data

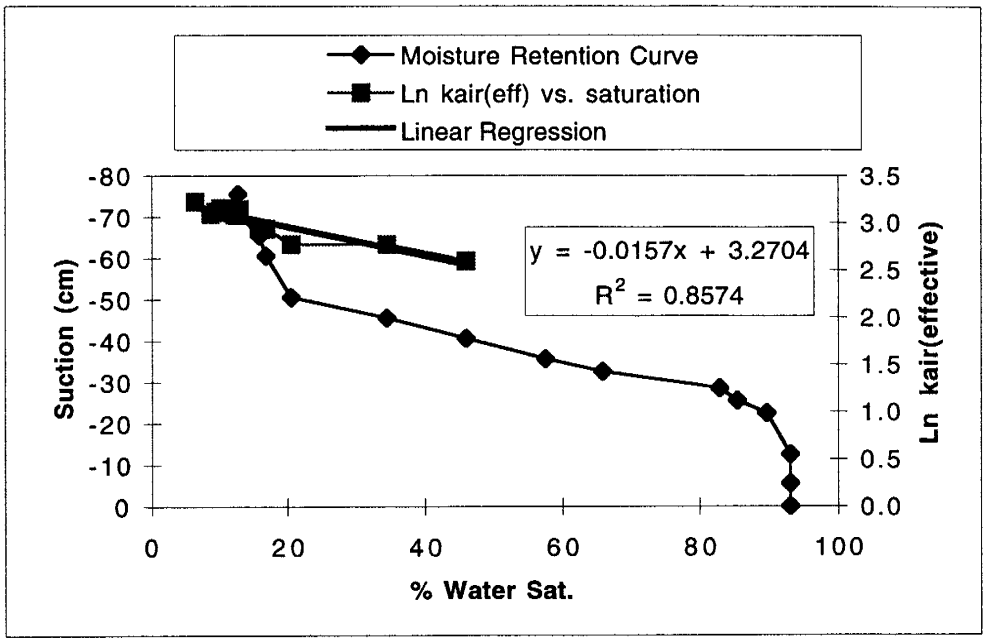

Time	Theta	Suction [cm]	k(air)	% Water Sat.	Ln k(air)	Ln kr(air)
4	34.43	0		93.05		
1	34.43	-5.5		93.05		
4	34.43	-12.5		93.05		
2	33.17	-22.5		89.65		
3	31.63	-25.5		85.49		
3	30.67	-28.5		82.89		
7	24.39	-32.5		65.92		
11	21.30	-35.5		57.57		
6	17.01	-40.5	13.34	45.97	2.59	-0.61
6	12.76	-45.5	15.92	34.49	2.77	-0.43
4	7.60	-50.5	15.95	20.54	2.77	-0.43
4	6.24	-60.5	18.84	16.86	2.94	-0.26
3	5.86	-65.5	18.96	15.84	2.94	-0.26
4	4.80	-70.5	23.16	12.97	3.14	-0.06
3	4.70	-75.5	22.33	12.70	3.11	-0.09
	4.70		21.92	12.70	3.09	-0.11
	4.52		21.98	12.22	3.09	-0.11
	4.17		23.31	11.27	3.15	-0.05
	3.75		23.50	10.14	3.16	-0.04
	3.50		22.54	9.46	3.12	-0.08
	3.19		22.02	8.62	3.09	-0.11
	2.35		25.16	6.35	3.23	0.03

Sample R17 Moisture Retention and kair(effective) Data

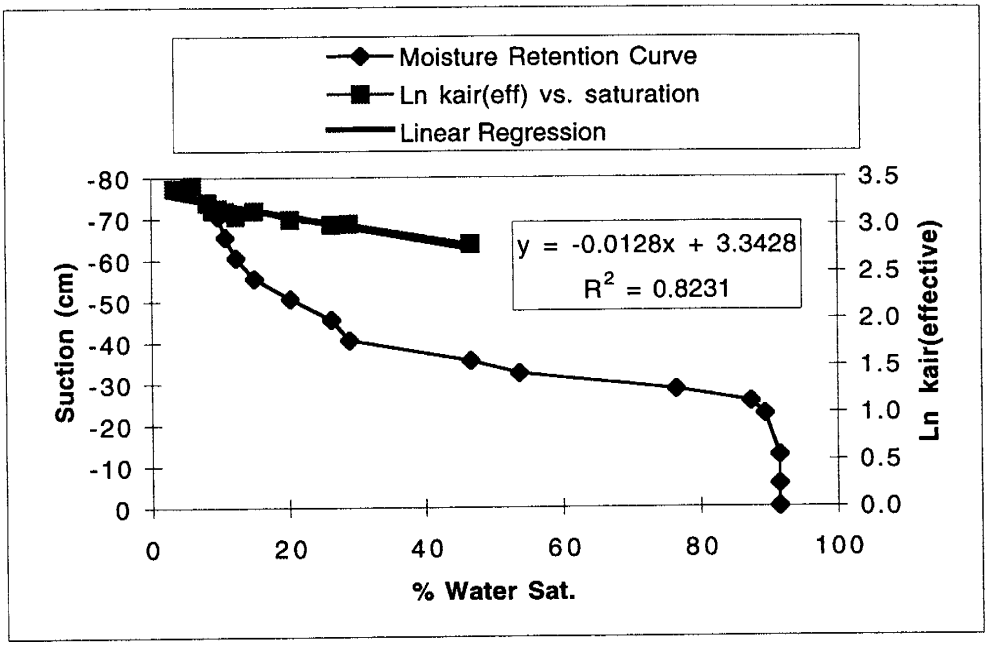

Time	Theta	Suction [cm]	k(air)	% Water Sat.	Ln k(air)	Ln kr(air)
4	34.05	0		91.53		
1	34.05	-5.5		91.53		
3	34.05	-12.5		91.53		
2	33.27	-22.5		89.44		
2	32.52	-25.5		87.42		
2	28.44	-28.5		76.45		
7	19.97	-32.5		53.68		
10	17.35	-35.5	16.33	46.64	2.79	-0.59
5	10.73	-40.5	20.24	28.84	3.01	-0.37
3	9.76	-45.5	20.02	26.24	3.00	-0.38
6	7.52	-50.5	21.14	20.22	3.05	-0.33
4	5.58	-55.5	23.16	15.00	3.14	-0.24
3	4.60	-60.5	21.95	12.37	3.09	-0.29
3	4.02	-65.5	23.09	10.81	3.14	-0.24
4	3.63	-70.5	23.78	9.76	3.17	-0.21
3	3.63	-71.5	23.82	9.76	3.17	-0.21
	3.32		23.46	8.93	3.16	-0.22
	3.03		25.30	8.15	3.23	-0.15
	2.21		30.27	5.94	3.41	0.03
	2.01		28.91	5.39	3.36	-0.02
	1.24		29.45	3.34	3.38	0.00

Sample R18 Moisture Retention and kair(effective) Data

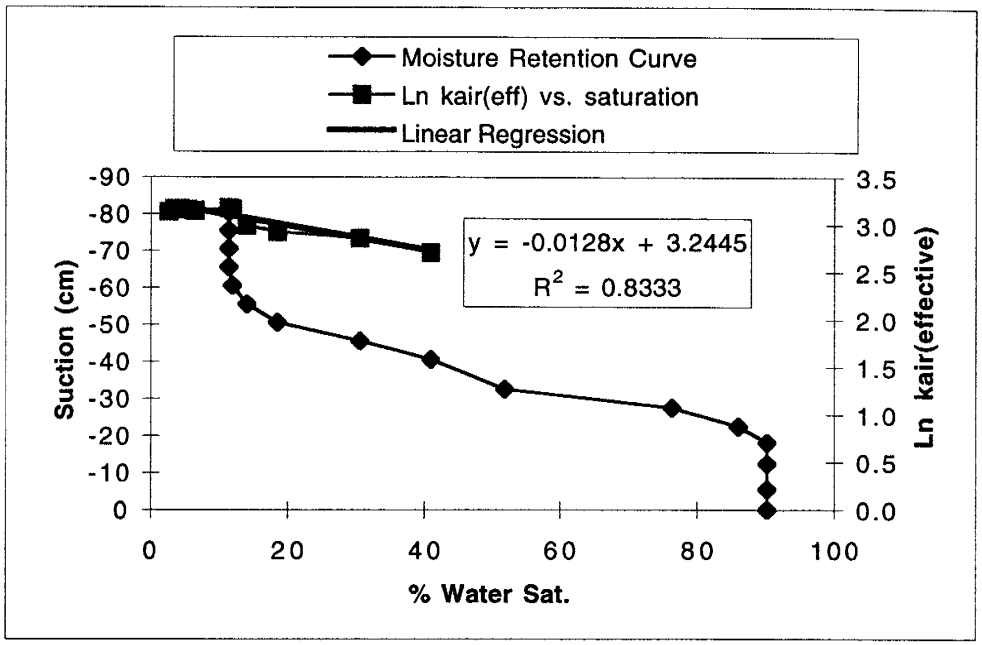

Time	Theta	Suction [cm]	k(air)	% Water Sat.	Ln k(air)	Ln kr(air)
4	33.65	0		90.10		
0.5	33.65	-5.5		90.10		
3	33.65	-12.5		90.10		
3	33.65	-18.2		90.10		
1	32.12	-22.5		86.00		
4	28.52	-27.5		76.36		
7	19.37	-32.5		51.86		
8	15.29	-40.5	14.90	40.94	2.70	-0.46
7	11.40	-45.5	17.34	30.52	2.85	-0.31
6	6.92	-50.5	18.57	18.53	2.92	-0.24
4	5.27	-55.5	19.80	14.11	2.99	-0.17
3	4.49	-60.5	23.62	12.02	3.16	0.00
3	4.30	-65.5	23.74	11.51	3.17	0.01
4	4.30	-70.5	23.90	11.51	3.17	0.01
3	4.30	-75.5	23.90	11.51	3.17	0.01
4	4.30	-80.5	23.70	11.51	3.17	0.01
	2.43		23.20	6.51	3.14	-0.02
	2.05		23.39	5.48	3.15	-0.01
	1.65		23.66	4.43	3.16	0.00
	1.29		23.66	3.46	3.16	0.00
	0.99		22.94	2.65	3.13	-0.03

Sample R19 Moisture Retention and kair(effective) Data

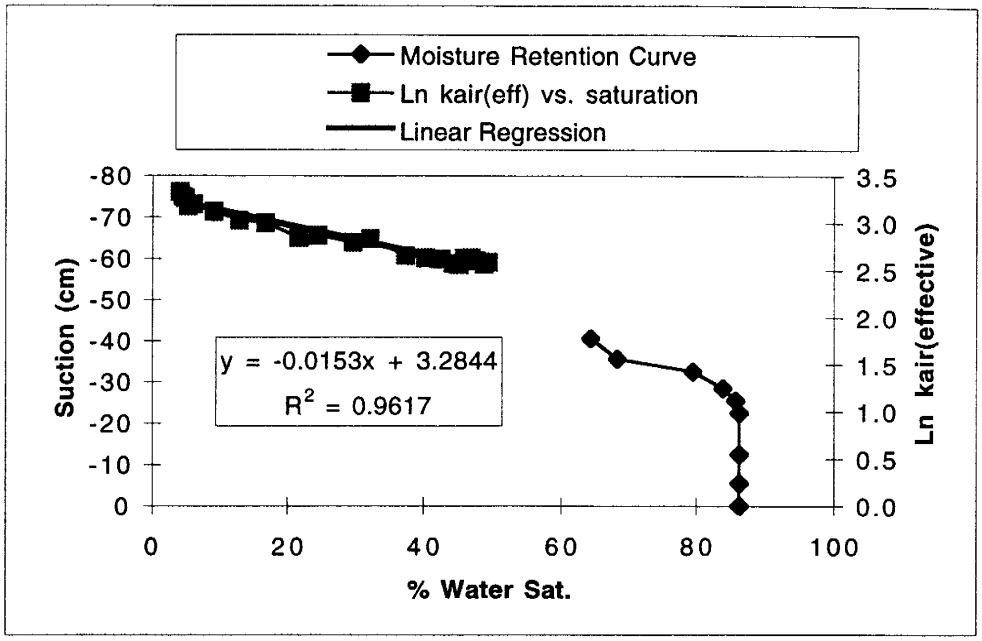

Time	Theta	Suction [cm]	k(air)	% Water Sat.	Ln k(air)	Ln kr(air)
4	32.97	0		86.30		
1	32.97	-5.5		86.30		
3	32.97	-12.5		86.30		
3	32.97	-22.5		86.30		
1	32.77	-25.5		85.79		
5	32.07	-28.5		83.95		
7	30.37	-32.5		79.50		
10	26.07	-35.5		68.25		
5	24.57	-40.5		64.32		
	21.68			56.75		
	18.85		13.27	49.35	2.59	-0.74
	18.64		12.98	48.80	2.56	-0.77
	18.21		13.48	47.67	2.60	-0.73
	17.93		13.88	46.94	2.63	-0.70
	17.55		13.82	45.94	2.63	-0.70
	17.24		12.95	45.13	2.56	-0.77
	16.92		13.06	44.29	2.57	-0.76
	16.24		13.69	42.51	2.62	-0.71
	15.38		13.87	40.26	2.63	-0.70
	14.29		14.20	37.41	2.65	-0.68
	12.31		17.01	32.23	2.83	-0.50
	11.34		16.37	29.69	2.80	-0.53
	9.35		17.63	24.48	2.87	-0.46
	8.28		17.19	21.68	2.84	-0.49
	6.37		20.10	16.68	3.00	-0.33
	4.89		20.68	12.80	3.03	-0.30
	3.45		22.68	9.03	3.12	-0.21

	2.31		24.47	6.05	3.20	-0.13
	2.00		24.02	5.24	3.18	-0.15
	1.82		26.18	4.76	3.26	-0.07
	1.68		26.58	4.40	3.28	-0.05
	1.52		27.94	3.98	3.33	0.00

Sample R20 Moisture Retention and kair(effective) Data

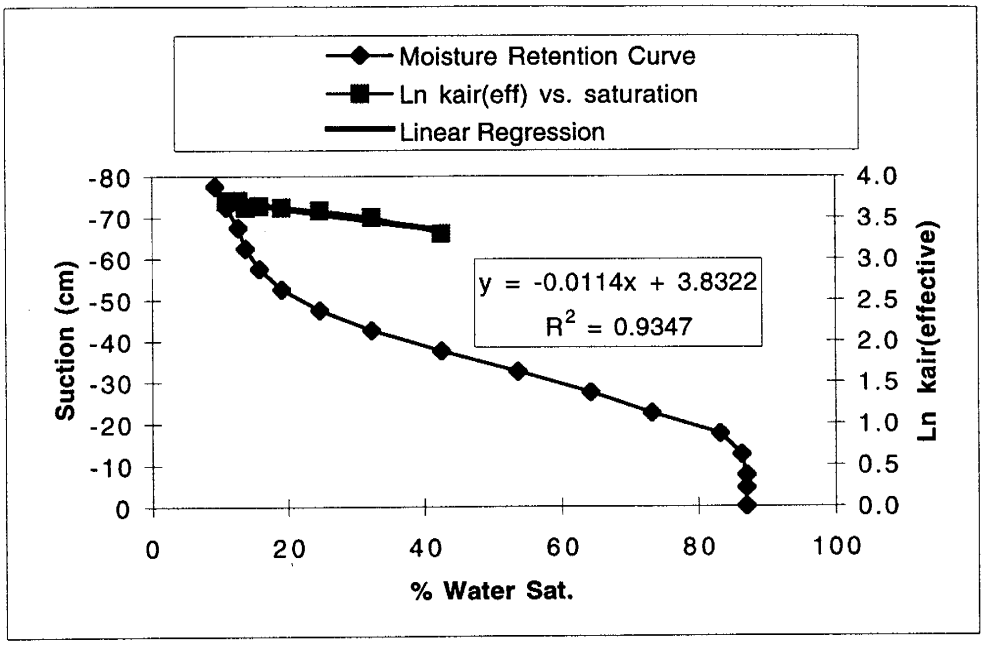

Time	Theta	Suction [cm]	k(air)	% Water Sat.	Ln k(air)	Ln kr(air)
3	35.18	0		87.07		
1	35.18	-4.5		87.07		
1	33.59	-7.5		87.07		
2	33.39	-12.5		86.36		
2	32.29	-17.5		83.24		
5	28.71	-22.5		73.17		
4	25.13	-27.5		64.26		
6	21.15	-32.5		53.66		
4	16.87	-37.5	27.24	42.52	3.30	-0.41
3	12.59	-42.5	33.21	32.27	3.50	-0.21
3	9.41	-47.5	36.13	24.69	3.59	-0.12
3	7.12	-52.5	37.49	19.09	3.62	-0.09
3	5.53	-57.5	38.21	15.80	3.64	-0.07
3	4.43	-62.5	37.49	13.76	3.62	-0.09
2	3.54	-67.5	40.69	12.72	3.71	0.00
3	3.14	-72.5	40.45	10.95	3.70	-0.01
3	2.64	-77.5	38.32	9.29	3.65	-0.06

Sample R24 Moisture Retention and kair(effective) Data

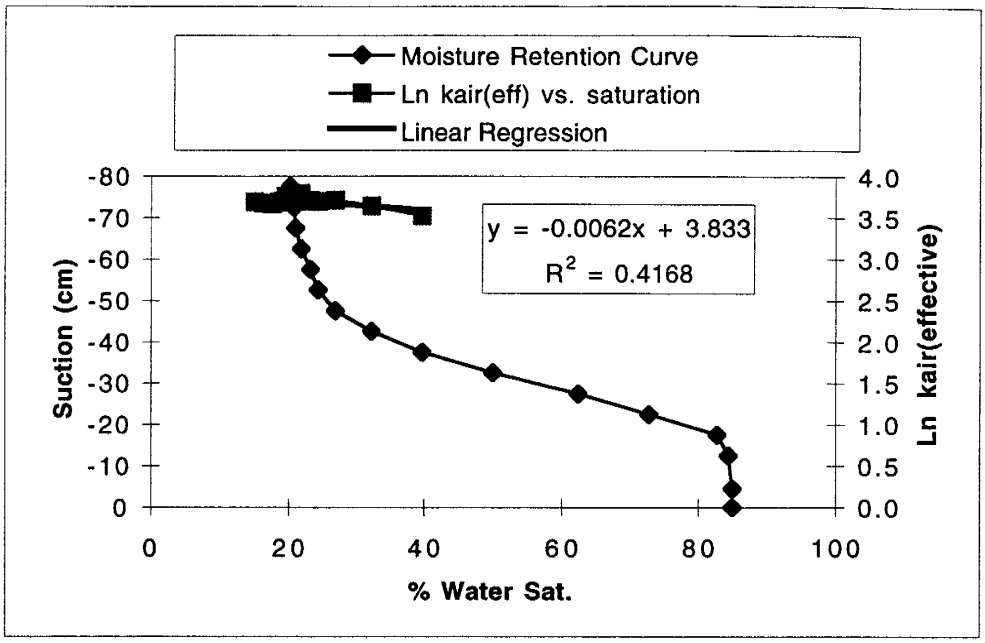

Time	Theta	Suction [cm]	k(air)	% Water Sat.	Ln k(air)	Ln kr(air)
1	31.95	0		84.97		
1	31.95	-4.5		84.97		
2	31.74	-12.5		84.41		
2	31.11	-17.5		82.74		
7	27.33	-22.5		72.69		
4	23.44	-27.5		62.35		
5	18.82	-32.5		50.06		
4	14.94	-37.5	33.77	39.73	3.52	-0.17
3	12.10	-42.5	38.11	32.19	3.64	-0.05
3	10.11	-47.5	40.81	26.88	3.71	0.02
2.5	9.16	-52.5	40.22	24.37	3.69	0.00
4	8.74	-57.5	40.45	23.25	3.70	0.01
2.5	8.22	-62.5	44.23	21.86	3.79	0.10
1	7.90	-67.5	41.68	21.02	3.73	0.04
2	7.80	-72.5	42.32	20.74	3.75	0.06
3	7.59	-77.5	42.19	20.18	3.74	0.05
	7.59		39.87	20.18	3.69	0.00
	7.35		42.71	19.54	3.75	0.06
	7.15		40.22	19.00	3.69	0.00
	6.98		40.10	18.56	3.69	0.00
	6.59		39.08	17.52	3.67	-0.02
	6.10		39.41	16.23	3.67	-0.02
	5.63		40.10	14.97	3.69	0.00

Sample R25 Moisture Retention and kair(effective) Data

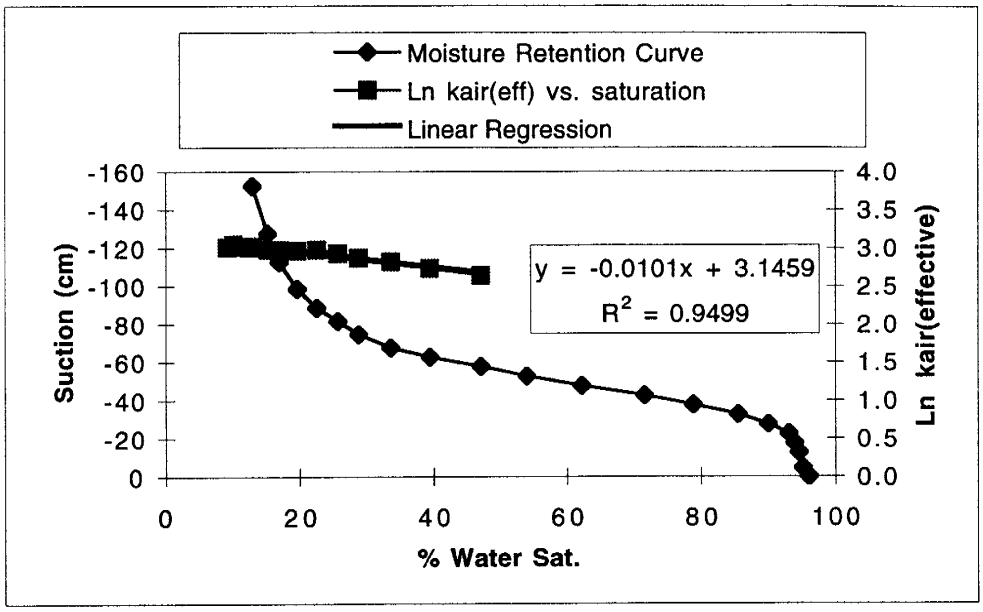

Time	Theta	Suction [cm]	k(air)	% Water Sat.	Ln k(air)	Ln kr(air)
1	44.63	0		96.11		
1	44.21	-4.5		95.20		
2	43.93	-12.5		94.59		
2	43.65	-17.5		93.98		
2	43.22	-22.5		93.07		
5	41.81	-27.5		90.03		
4	39.73	-32.5		85.56		
5	36.61	-37.5		78.83		
4	33.22	-42.5		71.53		
5	28.88	-47.5		62.19		
4	25.09	-52.5		54.03		
3	21.88	-57.5	13.97	47.12	2.64	-0.38
5	18.31	-62.5	15.29	39.44	2.73	-0.29
4	15.59	-67.5	16.74	33.57	2.82	-0.20
3	13.35	-74.5	17.57	28.75	2.87	-0.15
3	11.92	-81.5	18.69	25.67	2.93	-0.09
3	10.46	-88.5	19.63	22.52	2.98	-0.04
4	9.10	-98.5	19.34	19.59	2.96	-0.06
3	7.87	-112.5	19.53	16.94	2.97	-0.05
2	7.07	-127.5	19.63	15.22	2.98	-0.04
4	6.01	-152.5	20.19	12.94	3.01	-0.01
	6.01		20.56	12.94	3.02	0.00
	5.78		20.27	12.44	3.01	-0.01
	5.44		20.50	11.70	3.02	0.00
	4.71		21.11	10.14	3.05	0.03
	4.28		20.19	9.21	3.01	-0.01

Sample R26 Moisture Retention and kair(effective) Data

Sample Alias	Local x	Local y	k(air)	Ln k(air)	% Sat.	Sat. used	Ln kr(air)	phi ave	Facies	k(int)	Ln k(int)
05A014	7.54	91.60	81.1	4.40					SG	81.1	4.40
05A024	7.80	82.01	42.7	3.75		10	0.0000		XS1	42.7	3.75
05A034	8.04	71.57	40	3.69	13.3	13.3	-0.0666	1.6732	XS2	42.8	3.76
05A044	6.95	61.54	64.7	4.17		14	-0.0812		XS2	70.2	4.25
05A054	7.29	52.02	59.4	4.08		15	-0.1020		XS2	65.8	4.19
05A064	8.99	42.06	69	4.23	15.4	15.4	-0.2021	1.4245	XS1	84.5	4.44
05A074	8.42	32.76	62.1	4.13		8	0.0000		SG	62.1	4.13
05A084	8.29	20.89	15.5	2.74		13.6	-0.0238		HS	15.9	2.76
05A094	8.28	10.89	14.4	2.67		13.6	-0.0238		HS	14.7	2.69
05A104	8.06	1.76	22.9	3.13		13.6	-0.0238		HS	23.5	3.15
05B014	19.38	91.27	78.5	4.36					SG	78.5	4.36
05B024	17.72	82.00	43.9	3.78		10	0.0000		XS1	43.9	3.78
05B034	16.76	71.68	37	3.61		14	-0.0812		XS2	40.1	3.69
05B042	18.88	67.69	42	3.74		14	-0.0812		XS2	45.6	3.82
05B044	16.96	61.42	36.8	3.61		15	-0.1020		XS2	40.8	3.71
05B054	16.78	51.68	61.5	4.12		15	-0.1020		XS2	68.1	4.22
05B064	18.47	39.61	78	4.36		14	-0.1474		XS1	90.4	4.50
05B074	18.04	31.45	140.9	4.95		8	0.0000		SG	140.9	4.95
05B084	18.33	21.30	16.3	2.79		13.6	-0.0238		HS	16.7	2.81
05B094	17.94	11.39	17.7	2.87		13.6	-0.0238		HS	18.1	2.90
05B104	17.25	2.79	16.2	2.79		13.6	-0.0238		HS	16.6	2.81
05C014	27.77	90.85	68.7	4.23					SG	68.7	4.23
05C024	27.58	81.42	72.7	4.29		10	0.0000		XS1	72.7	4.29
05C034	27.28	70.88	35.6	3.57	17.8	17.8	-0.1602	1.7765	XS2	41.8	3.73
05C044	28.05	62.65	29.7	3.39		17	-0.1436		XS2	34.3	3.53
05C054	27.15	51.82	42.2	3.74		15	-0.1020		XS2	46.7	3.84
05C064	27.79	41.37	58.5	4.07	11.8	11.8	-0.0614	1.3827	XS1	62.2	4.13
05C074	28.18	32.28	34.5	3.54		13	-0.1083		XS1	38.4	3.65
05C084	27.69	21.28	14.8	2.69		13.6	-0.0238		HS	15.2	2.72

Sample Alias	Local x	Local y	k(air)	Ln k(air)	% Sat.	Sat. used	Ln kr(air)	phi ave	Facies	k(int)	Ln k(int)
05C094	28.17	11.53	17	2.83		13.6	-0.0238		HS	17.4	2.86
05C104	28.04	3.23	19.9	2.99		13.6	-0.0238		HS	20.4	3.01
05D014	37.43	90.47	70.5	4.26					SG	70.5	4.26
05D024	38.40	81.81	42.2	3.74		10	0.0000		XS1	42.2	3.74
05D034	37.52	70.26	38.2	3.64		17	-0.1436		XS2	44.1	3.79
05D044	39.46	61.30	34.4	3.54		17	-0.1436		XS2	39.7	3.68
05D054	37.62	51.91	35.7	3.58		14	-0.0812		XS2	38.7	3.66
05D064	38.09	40.35	61.2	4.11		12	-0.0692		XS1	65.6	4.18
05D074	37.86	33.04	57.2	4.05		12	-0.0692		XS1	61.3	4.12
05D084	38.13	21.89	17.4	2.86		13.6	-0.0238		HS	17.8	2.88
05D094	38.04	11.83	16.7	2.82		13.6	-0.0238		HS	17.1	2.84
05D104	38.11	2.81	18.5	2.92		13.6	-0.0238		HS	18.9	2.94
05E014	48.31	90.67	82.8	4.42					SG	82.8	4.42
05E024	48.15	80.98	38.8	3.66		10	0.0090		XS1	38.5	3.65
05E034	47.58	70.86	45	3.81	17.2	17.2	-0.1478	1.8264	XS2	52.2	3.95
05E044	47.24	60.55	30.2	3.41		17	-0.1436		XS2	34.9	3.55
05E052	49.57	58.26	40.2	3.69		15	-0.1020		XS2	44.5	3.80
05E054	47.45	51.42	30.6	3.42		16	-0.1228		XS2	34.6	3.54
05E064	47.73	41.26	43.7	3.78	14.3	14.3	-0.1591	1.3771	XS1	51.2	3.94
05E074	47.70	32.50	60.5	4.10		13	-0.1083		XS1	67.4	4.21
05E084	47.54	21.73	19.2	2.95		13.6	-0.0238		HS	19.7	2.98
05E094	47.81	11.66	18.1	2.90		13.6	-0.0238		HS	18.5	2.92
05E104	47.56	2.59	18.2	2.90		13.6	-0.0238		HS	18.6	2.93
05F014	57.72	91.17	73.9	4.30					SG	73.9	4.30
05F024	57.34	81.07	41.1	3.72		12	-0.0692		XS1	44.0	3.79
05F034	57.51	71.38	41.3	3.72		18	-0.1644		XS2	48.7	3.89
05F044	57.56	60.65	40.2	3.69		20	-0.2060		XS2	49.4	3.90
05F054	58.43	53.05	35.7	3.58		16	-0.1228		XS2	40.4	3.70
05F064	58.29	39.55	44.3	3.79		15	-0.1020		XS2	49.1	3.89

Sample Alias	Local x	Local y	k(air)	Ln k(air)	% Sat.	Sat. used	Ln kr(air)	phi ave	Facies	k(int)	Ln k(int)
05F074	57.21	31.56	25.6	3.24		14	-0.1474		XS1	29.7	3.39
05F084	57.52	21.40	15	2.71		13.6	-0.0238		HS	15.4	2.73
05F094	57.42	12.84	15.6	2.75		13.6	-0.0238		HS	16.0	2.77
05F104	57.59	3.40	19.8	2.99		13.6	-0.0238		HS	20.3	3.01
05G014	68.68	90.91	98.9	4.59					SG	98.9	4.59
05G024	67.64	81.63	30.7	3.42		13	-0.1083		XS1	34.2	3.53
05G034	66.97	70.89	33.2	3.50	23.7	23.7	-0.2830	1.7045	XS2	44.1	3.79
05G044	67.94	60.54	45.3	3.81		20	-0.2060		XS2	55.7	4.02
05G054	69.00	51.80	50.9	3.93		20	-0.2060		XS2	62.5	4.14
05G064	67.77	41.62	32.5	3.48	18.3	18.3	-0.1706	1.7593	XS2	38.5	3.65
05G074	67.20	31.65	41.7	3.73		15	-0.1865		XS1	50.2	3.92
05G084	67.46	23.45	25.4	3.23		13.6	-0.0238		HS	26.0	3.26
05G094	67.39	12.71	17.1	2.84		13.6	-0.0238		HS	17.5	2.86
05G104	66.27	4.32	20.3	3.01		13.6	-0.0238		HS	20.8	3.03
05H014	77.63	91.37	69.5	4.24		14	-0.1474		XS1	80.5	4.39
05H024	77.62	82.24	45.6	3.82		14	-0.1474		XS1	52.8	3.97
05H034	77.87	71.41	27.8	3.33		26	-0.3308		XS2	38.7	3.66
05H044	77.59	60.99	37.8	3.63		24	-0.2892		XS2	50.5	3.92
05H054	78.36	51.60	54.2	3.99		22	-0.2476		XS2	69.4	4.24
05H064	78.07	39.58	36.8	3.61		19	-0.1852		XS2	44.3	3.79
05H074	77.45	32.68	45.1	3.81		15.5	-0.2061		XS1	55.4	4.01
05H084	77.23	23.03	71.1	4.26		11	0.0000		SG	71.1	4.26
05H094	77.27	12.35	17.4	2.86		13.6	-0.0238		HS	17.8	2.88
05H104	76.84	3.57	19.8	2.99		13.6	-0.0238		HS	20.3	3.01
05I014	88.03	90.74	69.2	4.24		14	-0.1474		XS1	80.2	4.38
05I024	88.22	81.20	34.2	3.53		15	-0.1865		XS1	41.2	3.72
05I034	87.51	71.02	24.3	3.19	28.4	28.4	-0.3807	-999	XS2	35.6	3.57
05I044	87.71	60.72	30.8	3.43		26	-0.3308		XS2	42.9	3.76
05I054	88.21	52.47	35.8	3.58		22	-0.2476		XS2	45.9	3.83

Sample Alias	Local x	Local y	k(air)	Ln k(air)	% Sat.	Sat. used	Ln kr(air)	phi ave	Facies	k(int)	Ln k(int)
05I064	87.24	41.60	37	3.61	21.3	21.3	-0.2330	1.6996	XS2	46.7	3.84
05I074	87.34	32.61	29	3.37		16	-0.2256		XS1	36.3	3.59
05I084	87.52	22.86	32.6	3.48		16	-0.2256		XS1	40.9	3.71
05I094	87.39	10.95	14.1	2.65		13.6	-0.0238		HS	14.4	2.67
05I104	87.49	2.74	17	2.83		13.6	-0.0238		HS	17.4	2.86
05J014	97.17	90.89	65.6	4.18		14	-0.1474		XS1	76.0	4.33
05J024	97.94	81.08	35.1	3.56		15	-0.1865		XS1	42.3	3.74
05J034	97.75	71.49	39	3.66		26	-0.3926		XS3	57.8	4.06
05J044	97.61	60.87	31	3.43		26	-0.3308		XS2	43.2	3.76
05J054	96.71	51.26	32.9	3.49		24	-0.2892		XS2	43.9	3.78
05J064	97.65	40.37	44.2	3.79		20	-0.2060		XS2	54.3	3.99
05J074	97.49	32.97	39.8	3.68		16.5	-0.2452		XS1	50.9	3.93
05J084	96.84	22.49	128.2	4.85		11	0.0000		SG	128.2	4.85
05J094	96.91	11.30	18.4	2.91		13.6	-0.0238		HS	18.8	2.94
05J104	96.84	4.09	20.4	3.02		13.6	-0.0238		HS	20.9	3.04
05K012	108.08	95.32	77.8	4.35	7.6	7.6	0.1028	1.1509	XS1	70.2	4.25
05K013	104.19	89.43	57.7	4.06	16.3	16.3	-0.2373	1.5579	XS1	73.2	4.29
05K014	109.16	90.73	59.5	4.09	15.5	15.5	-0.2061	1.3784	XS1	73.1	4.29
05K022	107.74	85.71	44.9	3.80	24	24	-0.2892	1.7218	XS2	60.0	4.09
05K023	103.32	79.94	41.5	3.73	15.8	15.8	-0.1186	1.5701	XS2	46.7	3.84
05K024	107.66	80.57	40.6	3.70	19.7	19.7	-0.3703	1.5756	XS1	58.8	4.07
05K032	107.65	75.85	41.7	3.73	20	20	-0.2060	1.555	XS2	51.2	3.94
05K034	107.42	70.73	38.2	3.64	20.5	20.5	-0.2546	1.971	XS3	49.3	3.90
05K042	108.30	66.57	36.7	3.60	20.2	20.2	-0.2470	1.8533	XS3	47.0	3.85
05K044	108.15	61.61	27.4	3.31	25.5	25.5	-0.3801	1.9352	XS3	40.1	3.69
05K052	108.23	55.86	28.4	3.35	17.8	17.8	-0.1868	1.9017	XS3	34.2	3.53
05K054	107.21	51.23	32.3	3.48	22.7	22.7	-0.3098	1.9013	XS3	44.0	3.78
05K062	107.42	45.51	24.6	3.20	15.7	15.7	-0.1166	1.8127	XS2	27.6	3.32
05K063	103.80	42.16	56.7	4.04		20	-0.2060		XS2	69.7	4.24

Sample Alias	Local x	Local y	k(air)	Ln k(air)	% Sat.	Sat. used	Ln kr(air)	phi ave	Facies	k(int)	Ln k(int)
05K064	107.45	41.12	42.9	3.76	18.3	18.3	-0.1706	1.8349	XS2	50.9	3.93
05K072	107.80	36.30	27.6	3.32	18.3	18.3	-0.1706	1.7914	XS2	32.7	3.49
05K074	107.30	31.44	40.2	3.69	19.6	19.6	-0.1977	1.7094	XS2	49.0	3.89
05K082	108.07	26.29	36.7	3.60	17.9	17.9	-0.2999	1.3112	XS1	49.5	3.90
05K084	107.66	22.65	51.7	3.95	20.3	20.3	-0.3937	1.3173	XS1	76.6	4.34
05K092	108.02	16.89	25.4	3.23	16.7	13.6	-0.0238	2.5946	HS	26.0	3.26
05K094	107.64	11.10	14.2	2.65	19.8	13.6	-0.0238	2.7182	HS	14.5	2.68
05K102	108.21	6.85	15.7	2.75	19.2	13.6	-0.0238	2.7283	HS	16.1	2.78
05K104	108.00	2.64	16.2	2.79	17.7	13.6	-0.0238	2.7609	HS	16.6	2.81
05K112	108.67	-3.18	17.2	2.84	25.9	13.6	-0.0238	2.7954	HS	17.6	2.87
05K114	109.10	-7.00	20	3.00	18.2	13.6	-0.0238	2.7756	HS	20.5	3.02
05K122	109.25	-11.96	27.7	3.32	18.8	13.6	-0.0238	2.7723	HS	28.4	3.35
05L014	117.85	91.24	55	4.01		13	-0.1083		XS1	61.3	4.12
05L024	117.29	81.62	36.7	3.60		24	-0.2892		XS2	49.0	3.89
05L034	116.91	71.64	35	3.56		20	-0.2420		XS3	44.6	3.80
05L044	117.82	61.16	26.9	3.29		20	-0.2420		XS3	34.3	3.53
05L054	118.05	52.53	31.3	3.44		18	-0.1644		XS2	36.9	3.61
05L064	116.50	41.50	47.6	3.86		18	-0.1644		XS2	56.1	4.03
05L071	113.05	38.68	41.3	3.72		18	-0.1644		XS2	48.7	3.89
05L072	117.82	37.12	47.9	3.87		18	-0.1644		XS2	56.5	4.03
05L074	117.58	31.58	35	3.56		18	-0.1644		XS2	41.3	3.72
05L084	118.77	21.59	47.2	3.85		18	-0.3038		XS1	64.0	4.16
05L094	118.07	11.76	14.1	2.65		12.8	-0.0165		HS	14.3	2.66
05L104	118.42	2.41	16.6	2.81		12.8	-0.0165		HS	16.9	2.83
05M014	127.39	92.44	70	4.25		13	-0.1083		XS1	78.0	4.36
05M024	126.71	82.42	33.3	3.51		24	-0.2892		XS2	44.5	3.79
05M034	127.01	71.36	21.4	3.06	17.5	17.5	-0.1793	1.9041	XS3	25.6	3.24
05M044	127.38	62.26	32.8	3.49		21	-0.2671		XS3	42.8	3.76
05M054	127.70	51.88	29.5	3.38		18	-0.1644		XS2	34.8	3.55

Sample Alias	Local x	Local y	k(air)	Ln k(air)	% Sat.	Sat. used	Ln kr(air)	phi ave	Facies	k(int)	Ln k(int)
05M064	126.92	41.91	35	3.56	18.9	18.9	-0.1831	1.8093	XS2	42.0	3.74
05M074	127.48	31.69	36.2	3.59		19	-0.1852		XS2	43.6	3.77
05M084	127.88	21.75	25.2	3.23		18	-0.3038		XS1	34.1	3.53
05M094	127.54	11.80	18	2.89		12.8	-0.0165		HS	18.3	2.91
05M104	128.26	2.18	23.6	3.16		12.8	-0.0165		HS	24.0	3.18
05N014	137.39	91.05	52	3.95		13	-0.1083		XS1	57.9	4.06
05N024	137.73	81.95	27.2	3.30		24	-0.2892		XS2	36.3	3.59
05N034	138.42	71.68	47.4	3.86		20	-0.2420		XS3	60.4	4.10
05N044	137.87	61.00	38.8	3.66		18	-0.1918		XS3	47.0	3.85
05N054	138.58	51.74	46.6	3.84		20	-0.2060		XS2	57.3	4.05
05N064	137.00	41.00	48.6	3.88		19	-0.1852		XS2	58.5	4.07
05N073	132.43	33.21	48.3	3.88		19	-0.1852		XS2	58.1	4.06
05N074	137.90	31.85	37.7	3.63		19	-0.1852		XS2	45.4	3.81
05N084	137.74	21.40	69.3	4.24		19	-0.3429		XS1	97.6	4.58
05N094	137.44	11.26	15.7	2.75		12.8	-0.0165		HS	16.0	2.77
05N104	137.67	1.63	15.1	2.71		12.8	-0.0165		HS	15.4	2.73
05O014	147.94	91.57	55.6	4.02		13	-0.1083		XS1	62.0	4.13
05O024	148.26	81.62	30.3	3.41		24	-0.2892		XS2	40.5	3.70
05O034	147.82	71.50	39.1	3.67	38.7	38.7	-0.5950	1.7256	XS2	70.9	4.26
05O044	147.96	61.57	37.4	3.62		15	-0.1165		XS3	42.0	3.74
05O054	147.68	51.47	33.9	3.52		15	-0.1020		XS2	37.5	3.63
05O064	147.35	41.64	39.3	3.67	19.1	19.1	-0.2194	1.8499	XS3	48.9	3.89
05O074	147.99	31.90	37.8	3.63		19	-0.1852		XS2	45.5	3.82
05O084	147.72	22.29	39.5	3.68		20	-0.3820		XS1	57.9	4.06
05O094	147.34	11.86	12.7	2.54		12.8	-0.0165		HS	12.9	2.56
05O104	147.18	2.03	16.7	2.82		12.8	-0.0165		HS	17.0	2.83
05P014	157.65	91.89	49.5	3.90		20	-0.2060		XS2	60.8	4.11
05P024	158.09	81.82	34.8	3.55		24	-0.2892		XS2	46.5	3.84
05P034	157.71	71.01	24.6	3.20		22	-0.2476		XS2	31.5	3.45

Sample Alias	Local x	Local y	k(air)	Ln k(air)	% Sat.	Sat. used	Ln kr(air)	phi ave	Facies	k(int)	Ln k(int)
05P044	157.75	60.93	58.2	4.06		15	-0.1165		XS3	65.4	4.18
05P054	157.72	51.90	30.7	3.42		15	-0.1020		XS2	34.0	3.53
05P064	157.00	41.00	45	3.81		19	-0.1852		XS2	54.2	3.99
05P074	157.84	32.56	40.8	3.71		20	-0.2060		XS2	50.1	3.91
05P081	152.53	28.73	57.7	4.06		20	-0.2060		XS2	70.9	4.26
05P084	157.15	21.71	43.5	3.77		20	-0.3820		XS1	63.7	4.15
05P094	157.51	12.29	18.1	2.90		12.8	-0.0165		HS	18.4	2.91
05P104	157.81	2.38	16.5	2.80		12.8	-0.0165		HS	16.8	2.82
05Q014	168.11	91.41	52.8	3.97	16.2	16.2	-0.1270	1.6482	XS2	59.9	4.09
05Q024	167.84	81.84	33.2	3.50	25.9	25.9	-0.3287	1.7827	XS2	46.1	3.83
05Q034	167.79	71.27	35.1	3.56	20.6	20.6	-0.2185	1.4181	XS2	43.7	3.78
05Q044	168.00	61.72	44.1	3.79	14	14	-0.0914	1.8636	XS3	48.3	3.88
05Q054	167.87	51.68	34.7	3.55	16.8	16.8	-0.1617	1.9743	XS3	40.8	3.71
05Q064	167.97	42.14	40.1	3.69	-999	20	-0.2060	1.8315	XS2	49.3	3.90
05Q074	167.58	31.59	43.1	3.76	3	20	-0.2060	1.7275	XS2	53.0	3.97
05Q081	162.88	27.40	45.9	3.83		20	-0.2060		XS2	56.4	4.03
05Q084	167.79	21.34	35.7	3.58	22.2	22.2	-0.4680	1.5422	XS1	57.0	4.04
05Q094	167.48	11.87	22.8	3.13	33.2	13.6	-0.0238	2.5028	HS	23.3	3.15
05Q104	168.01	2.21	13.7	2.62	25.5	13.6	-0.0238	2.6761	HS	14.0	2.64
05Q114	167.95	-7.86	19.7	2.98	19.3	13.6	-0.0238	2.7477	HS	20.2	3.00
05R014	177.52	91.18	45.1	3.81		18	-0.1644		XS2	53.2	3.97
05R024	177.63	81.07	32.1	3.47		25	-0.3100		XS2	43.8	3.78
05R034	177.68	70.73	41.6	3.73		20	-0.2060		XS2	51.1	3.93
05R044	177.61	60.20	45	3.81		16	-0.1416		XS3	51.8	3.95
05R054	177.94	51.90	38.6	3.65		15	-0.1020		XS2	42.7	3.76
05R064	177.70	41.50	41.2	3.72		21	-0.2268		XS2	51.7	3.95
05R074	177.77	31.35	39.6	3.68		21	-0.2268		XS2	49.7	3.91
05R084	177.82	21.26	34.9	3.55		22	-0.2476		XS2	44.7	3.80
05R094	178.09	12.53	50.5	3.92		22	-0.4602		XS1	80.0	4.38

Sample Alias	Local x	Local y	k(air)	Ln k(air)	% Sat.	Sat. used	Ln kr(air)	phi ave	Facies	k(int)	Ln k(int)
05R104	177.36	1.76	15.7	2.75		12.8	-0.0165		HS	16.0	2.77
05S014	188.31	91.36	47.6	3.86		17	-0.1436		XS2	55.0	4.01
05S024	188.22	81.23	23.7	3.17		20	-0.2060		XS2	29.1	3.37
05S034	187.52	71.74	46.6	3.84	17.7	17.7	-0.1582	1.6366	XS2	54.6	4.00
05S044	188.06	60.93	33.4	3.51		15	-0.1165		XS3	37.5	3.63
05S054	188.19	50.96	42	3.74		15	-0.1020		XS2	46.5	3.84
05S064	187.85	41.67	41.9	3.74	24.6	24.6	-0.3575	1.8925	XS3	59.9	4.09
05S074	188.32	31.77	48.4	3.88		22	-0.2476		XS2	62.0	4.13
05S084	188.23	21.41	28.6	3.35		22	-0.2476		XS2	36.6	3.60
05S094	188.22	11.50	27.1	3.30		23	-0.4993		XS1	44.6	3.80
05S104	187.86	2.19	16.7	2.82		12.8	-0.0165		HS	17.0	2.83
05T014	197.60	92.00	43.8	3.78		17	-0.1436		XS2	50.6	3.92
05T024	197.99	81.46	23.4	3.15		18	-0.1644		XS2	27.6	3.32
05T034	197.90	71.15	48.4	3.88		17	-0.1436		XS2	55.9	4.02
05T044	198.34	60.75	33.3	3.51		15	-0.1165		XS3	37.4	3.62
05T054	197.80	50.85	37.2	3.62		15	-0.1020		XS2	41.2	3.72
05T064	197.00	41.30	52.1	3.95		16	-0.1228		XS2	58.9	4.08
05T074	198.31	31.33	41.6	3.73		22	-0.2476		XS2	53.3	3.98
05T084	197.83	21.12	23.9	3.17		22	-0.2476		XS2	30.6	3.42
05T094	198.17	10.93	61.8	4.12		23	-0.4993		XS1	101.8	4.62
05T102	198.34	4.78	12.6	2.53		12.8	-0.0165		HS	12.8	2.55
05U034	207.47	69.11	62.5	4.14	18.7	11.2	-0.0230	1.6927	XS2	64.0	4.16
05U064	208.23	41.19	49.4	3.90	10.5	10.5	-0.0084	1.8574	XS2	49.8	3.91

Collected and calculated data for Panel 5. "Sample Alias", "Local x", and "Local y" denote location of sample. "k(air)" is measured effective air permeability. "% Sat." is measured INEL water saturation from cores. "Sat. used" is interpolated water saturation value. "Ln kr(air)" was determined using facies type and corrections. "phi ave" is mean phi from ODU core data. "k(int)" is estimated intrinsic permeability for the measurement location.

APPENDIX D - MODEL COMPARISONS OF DATA

D.1 - Introduction

A number of models have been suggested to get at the functional relationships between permeability, saturation, and pressure. We shall look at the Brooks and Corey (1964) model and the Luckner et al. (1989) model which employs the Mualem (1976) model. Both models use the moisture retention function of soils to predict the relative permeability versus percentage water saturation curves. We measured the moisture retention curves as well as the effective air permeability of our samples. In finding our corrections, we produced relative permeability versus percentage water saturation functions. We will use our moisture retention functions to model the relative permeability curves and then compare the modeled functions to our experimentally found functions.

D.2 - Brooks and Corey (1964) model

The Brooks and Corey (1964) model describes the functional relationships between the saturation, the pressure difference between air and water, and the permeabilities of air and water. Their model depends on two soil properties; the "bubbling pressure" (P_b) which is the point on the moisture retention curve when water starts to drain, and the "pore-size distribution index" (λ) which is evaluated using the model. The model for the non-wetting phase (air in our case) uses an effective water saturation, S_e, and the capillary pressure, or suction, P_c, with $S_e = \left(\frac{P_b}{P_c}\right)^{\lambda}$ for $P_c \geq P_b$. The model for the relative permeability to air is, $k_{r(air)} = (1 - S_e)^2\left(1 - S_e^{(2+\lambda/\lambda)}\right)$ for $P_c \geq P_b$. The pore-size distribution index, λ, can be any positive number, though it tends to be small for media with a wide range of pore sizes and large for media with a relatively uniform pore size. The effective saturation, S_e, is also defined as $S_e = \frac{S - S_r}{1 - S_r}$ for $S_r < S \leq 1.0$. The authors suggest that the theory is only valid for isotropic media and

only for drainage. The theory also assumes that $k_{r(air)}$ reaches its maximum value at the residual saturation, S_r.

Application of the model requires a moisture retention curve. We estimated a residual saturation based on our moisture retention functions. We then plotted log S_e versus log (suction). A portion of the data fell along a straight line, where the slope of the line was λ. The estimate of S_r is adjusted for the data. Using this value of S_r we computed the S_e for each point and the $k_{r(air)}$ for each point. We plotted our data versus the Brooks and Corey (1964) modeled data and compared the results (Graphs D.1).

We found that the Brooks and Corey (1964) model consistently showed a greater effect of water saturation than our measured data. The Brooks and Corey (1964) model makes the assumption that the relative permeability to air at the residual saturation is 1.0. The model does not apply to values less than the residual saturation, but we had data for these lower values. The other difficulty in applying the model is that the value λ is obtained from the slope of the log-log plot, which is not exactly linear. Choosing the section of the curve to fit the straight line to changes the value of λ, and thus the ln $k_{r(air)}$ functional relationship on water saturation. The difficulties associated with using this model and the lack of a good fit with the measured data caused us to consider another model.

D.3 - Luckner et al. (1989) model

Like the Brooks and Corey (1964) model, the Luckner et al. (1989) model was developed to obtain accurate estimates of the unsaturated hydraulic properties of sediments. These properties, if well described, could be used to help describe multiphase flow in porous media. Luckner et al.'s (1989) model however, accounts for the air trapped in the porous medium from the wetting process. This assumption fits our results better than the Brooks and Corey (1964) model which assumes 100% water saturation on the moisture retention curve. We use the model to help accurately predict the relative

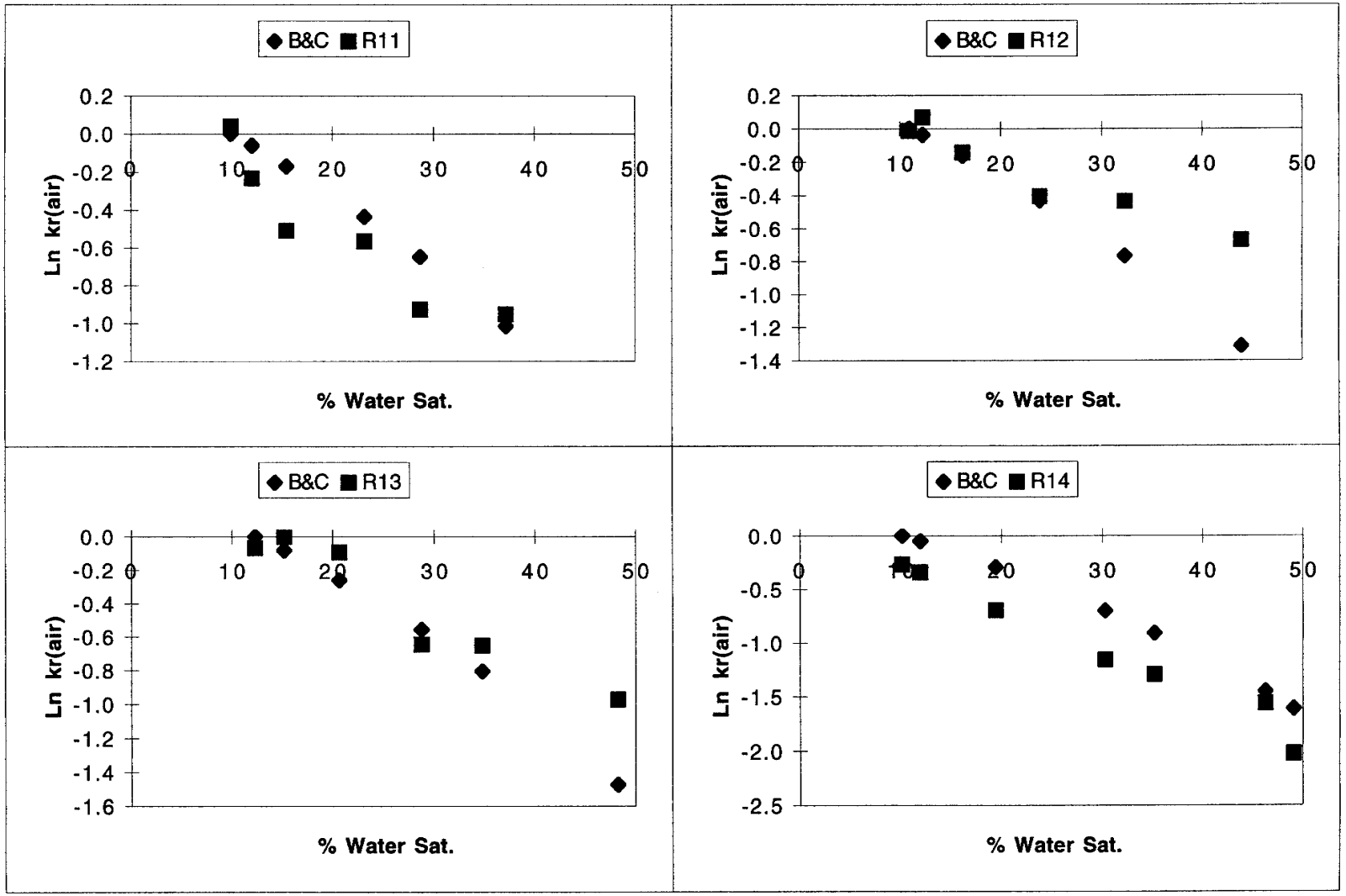
B&C
R11
Ln kr(air)
% Water Sat.
B&C
R12
Ln kr(air)
% Water Sat.
B&C
R13
Ln kr(air)
% Water Sat.
B&C
R14
Ln kr(air)
% Water Sat.

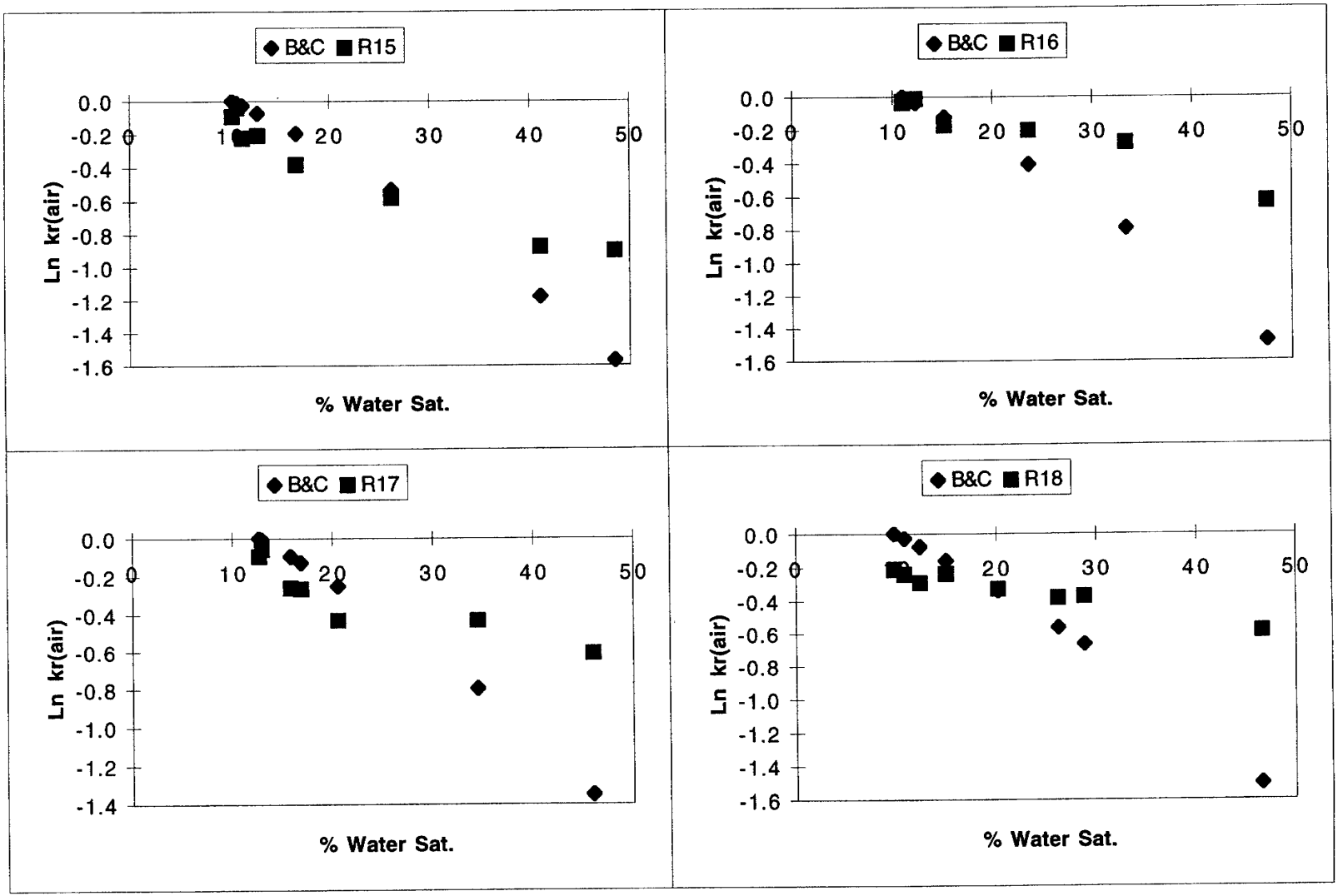
◆B&C ■R15
Ln kr(air)
% Water Sat.
◆B&C ■R16
Ln kr(air)
% Water Sat.
◆B&C ■R17
Ln kr(air)
% Water Sat.
◆B&C ■R18
Ln kr(air)
% Water Sat.

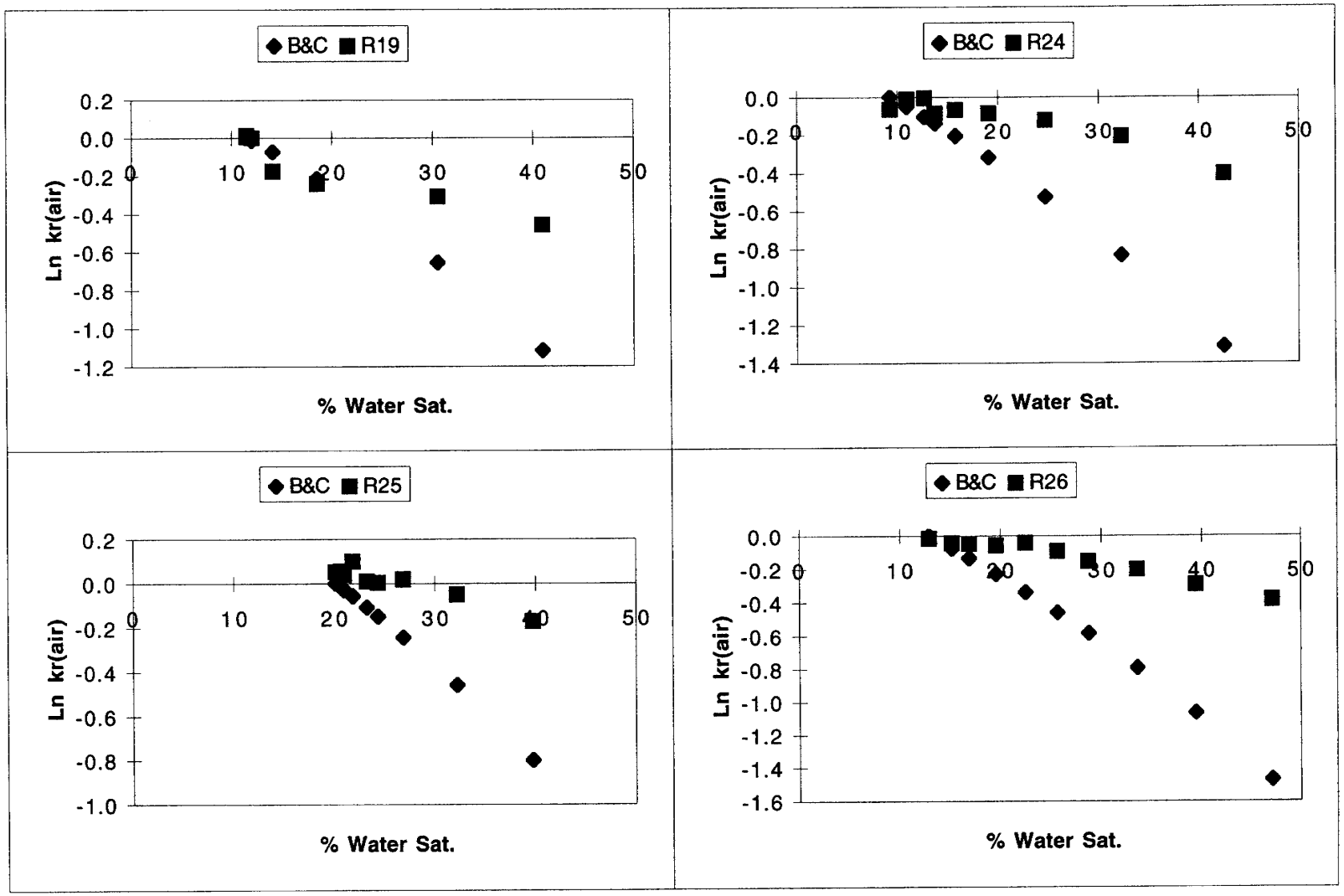

Graphs D.1 - Comparisons of calculated laboratory data and Brooks and Corey (1964) model data.

permeability as a function of air for our different sands. Similar to the Brook and Corey (1964) model, Luckner et al. (1989) uses a scaled, or effective, non-wetting saturation of $\bar{S}^* = \frac{1 - S_{nw,r} - S_w}{1 - S_{nw,r}}$, where $S_{nw,r}$ is non-wetting phase residual saturation, and S_w is the wetting phase saturation. The model then uses the residual water saturation, S_{w0}, and Mualem's (1976) model to obtain a formulation for the non-wetting phase relative permeability: $k_{r(air)} = \left[\bar{S}^* / \bar{S}_0^*\right]^{\gamma} \left\{ \frac{\left[1 - (1 - \bar{S}^*)^{1/m}\right]^m}{\left[1 - (1 - \bar{S}_0^*)^{1/m}\right]^m} \right\}^2$, where $\bar{S}_0^*$ is the $\bar{S}^*$ value evaluated at the residual water saturation, γ is the pore connectivity parameter for the non-wetting fluid, and m = 1-1/n where n is a constant affecting the shape of the retention curve. Carsel and Parrish (1988) found that n ranged from 1.5 to 4.0 in sands with finer grained sands having lower values of n compared to samples with larger grained sands.

To apply the model to our data, we determined the $\bar{S}^*$ for each measurement point using a non-wetting phase (air) residual saturation value of 12% that was an average of our experiments. Mualem (1976) found that γ ranged from -0.4 to 1.0 for sands with an average value of 0.5, which we applied. From our different subsets within the Cross-Stratified facies, we applied different values of m, associated with the different grain-size distribution, or sorting, of the samples. The m values were 0.75, 0.60, and 0.50, for XS1, XS2, and XS3, respectively. This model was easier to apply than the Brooks and Corey (1964) model because we picked the residual air saturation off our moisture retention curves, and applied the γ and m values we found in Carsel and Parrish (1988). We produced $k_{r(air)}$ versus $\bar{S}^*$ curves and plotted them with our data in the range below 50% water saturation. We then compared the data sets (Graphs D.2).

We found that for the Cross-Stratified samples, the Luckner et al. (1989) model either predicted similar results (R11-R12, R16-R20, R24, R26) or predicted less of a change for a given water saturation (R13-R15). The data from our two samples taken from the field (R25 and R26), from the Cross-Stratified facies and the Horizontally

Stratified facies respectively, showed the smallest change in relative air permeability for a given water saturation and the model slightly over-predicted the results in R25. Compared to the Brooks and Corey (1964) model that consistently over-predicted the measured results, Luckner et al.'s (1989) model, with parameters of $\gamma = 1/2$ and m values ranging from 0.5 to 0.75, fairly accurately predicted the results we saw in the laboratory. We suggest that the Luckner et al. (1989) model, with $\gamma = 1/2$, varying m, $S_{nw,r} = 12\%$, and $\bar{S}_0^* =$ to the residual water saturation of about 10%, be applied as the model of the estimate of the unsaturated hydraulic properties for the XSF sands. The Luckner et al. (1989) model, with $\gamma = 1/2$, m = 0.3, $S_{nw,r} = 12\%$, and $\bar{S}_0^* =$ about 15%, be applied as the model of the estimate of the unsaturated hydraulic properties for the HSF sands.

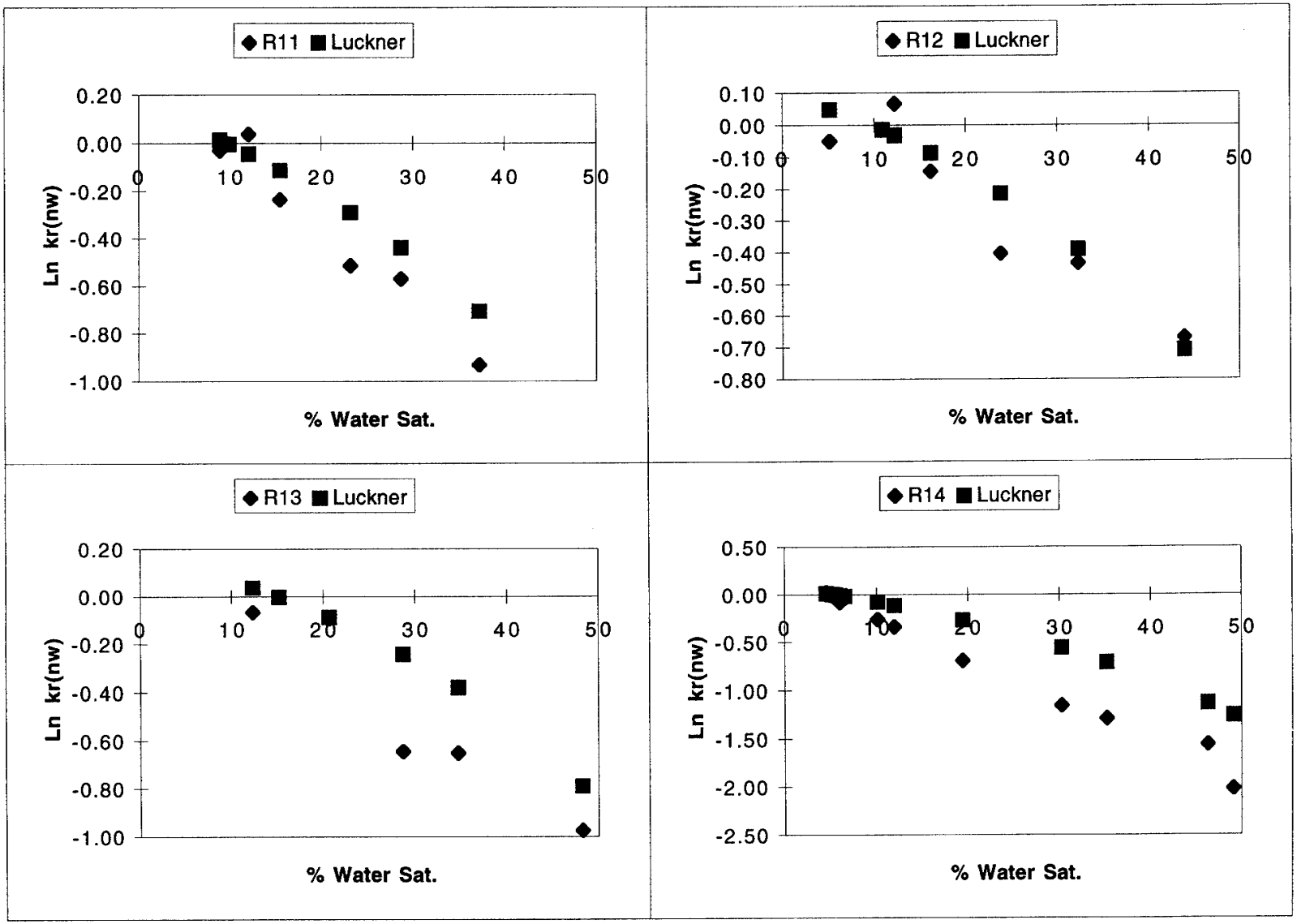
R11 Luckner
0.20
0.00
-0.20
-0.40
-0.60
-0.80
-1.00
0
10
20
30
40
50
Ln kr(nw)
% Water Sat.
R12 Luckner
0.10
0.00
-0.10
-0.20
-0.30
-0.40
-0.50
-0.60
-0.70
-0.80
0
10
20
30
40
50
Ln kr(nw)
% Water Sat.
R13 Luckner
0.20
0.00
-0.20
-0.40
-0.60
-0.80
-1.00
0
10
20
30
40
50
Ln kr(nw)
% Water Sat.
R14 Luckner
0.50
0.00
-0.50
-1.00
-1.50
-2.00
-2.50
0
10
20
30
40
50
Ln kr(nw)
% Water Sat.

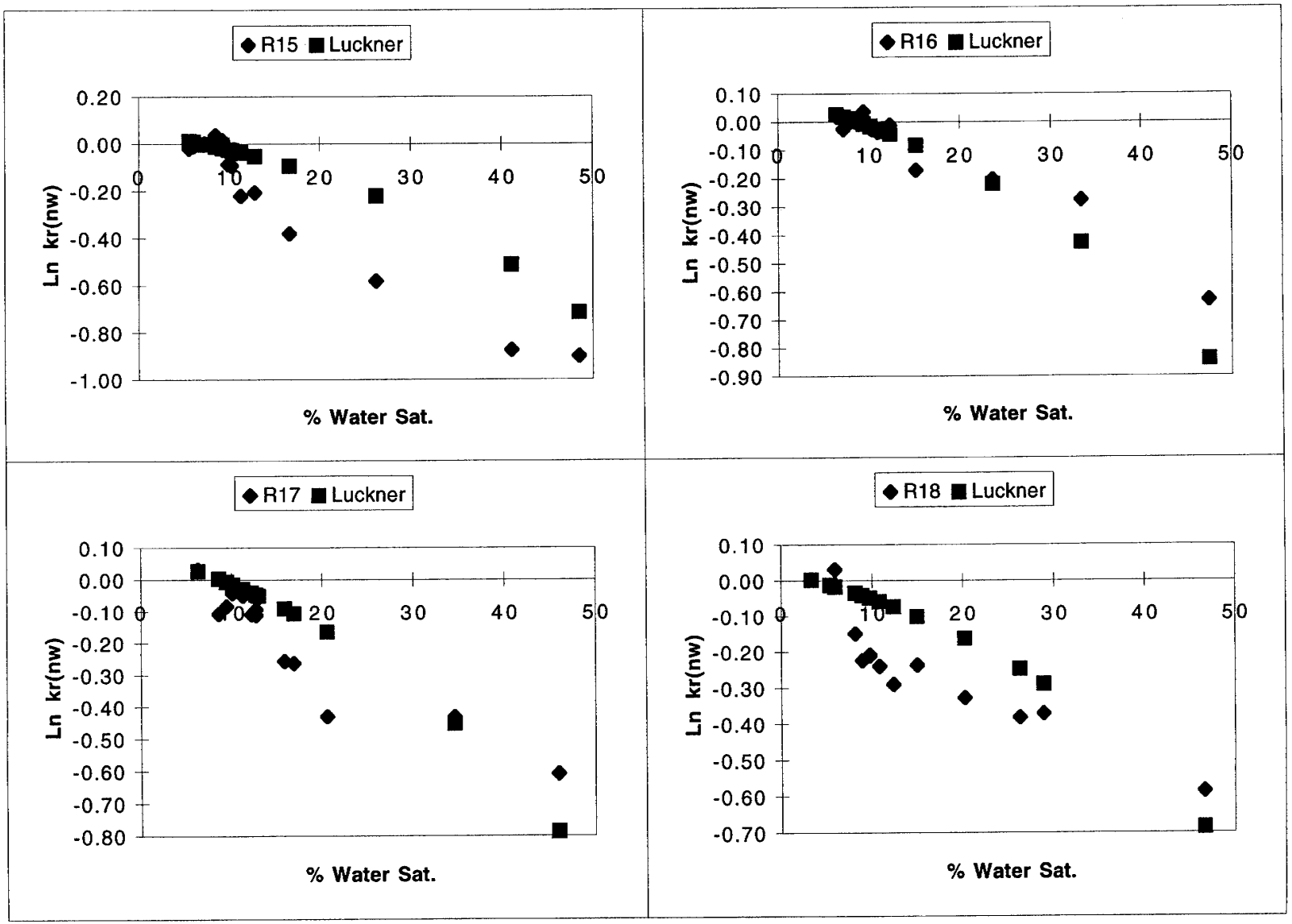
R15 Luckner
0.20
0.00
-0.20
-0.40
-0.60
-0.80
-1.00
0
10
20
30
40
50
Ln kr(nw)
% Water Sat.
R16 Luckner
0.10
0.00
-0.10
-0.20
-0.30
-0.40
-0.50
-0.60
-0.70
-0.80
-0.90
0
10
20
30
40
50
Ln kr(nw)
% Water Sat.
R17 Luckner
0.10
0.00
-0.10
-0.20
-0.30
-0.40
-0.50
-0.60
-0.70
-0.80
0
10
20
30
40
50
Ln kr(nw)
% Water Sat.
R18 Luckner
0.10
0.00
-0.10
-0.20
-0.30
-0.40
-0.50
-0.60
-0.70
0
10
20
30
40
50
Ln kr(nw)
% Water Sat.

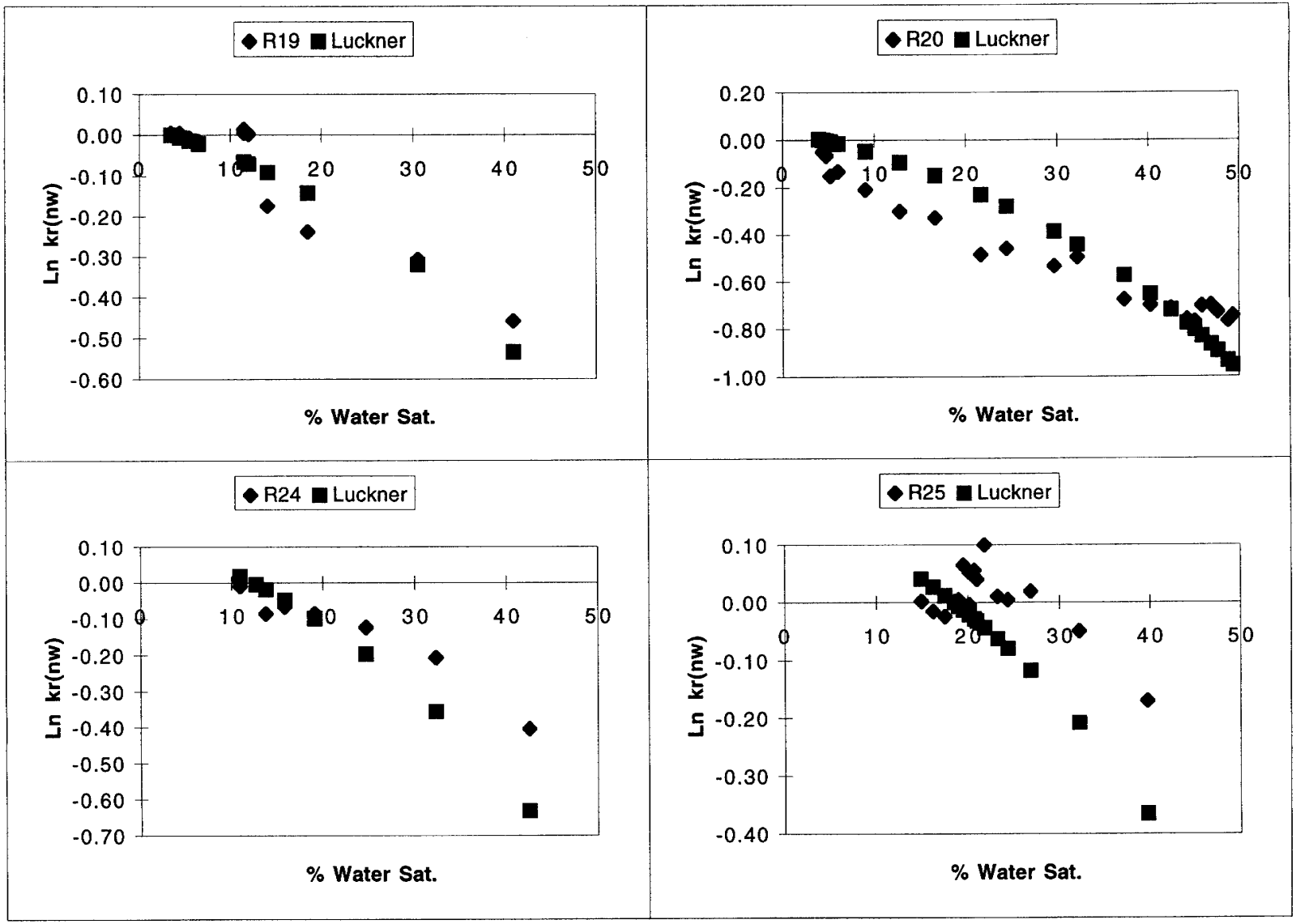
R19 Luckner
0.10
0.00
-0.10
-0.20
-0.30
-0.40
-0.50
-0.60
0
10
20
30
40
50
Ln kr(nw)
% Water Sat.
R20 Luckner
0.20
0.00
-0.20
-0.40
-0.60
-0.80
-1.00
0
10
20
30
40
50
Ln kr(nw)
% Water Sat.
R24 Luckner
0.10
0.00
-0.10
-0.20
-0.30
-0.40
-0.50
-0.60
-0.70
0
10
20
30
40
50
Ln kr(nw)
% Water Sat.
R25 Luckner
0.10
0.00
-0.10
-0.20
-0.30
-0.40
0
10
20
30
40
50
Ln kr(nw)
% Water Sat.

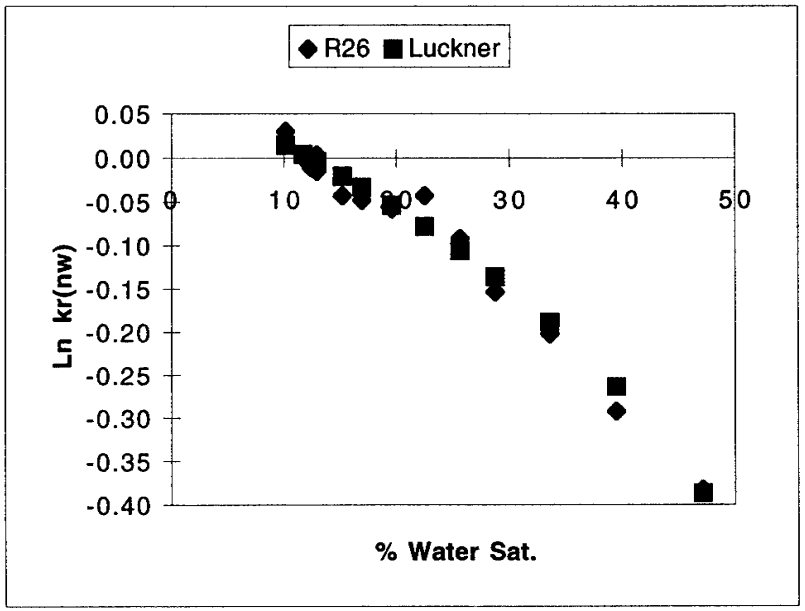

Graphs D.2 - Comparison of calculated laboratory data and Luckner et al. (1989) model data.
Important model parameters: gamma = 0.5, m_XS1 = 0.75, m_XS2 = 0.6, m_XS3 = 0.5, m_HS = 0.3

APPENDIX E - WATER SATURATION MEASUREMENT DEVICES

E.1 - Gravimetric Analysis

We collected 100 cc cores in the field in order to help characterize the water saturation present in the outcrop. We used gravimetric analysis to determine the water saturation of these samples. We had a known volume of sand. We weighed the sand wet, oven dried the sand at 80° C for 3 days, and then weighed the oven dry sand. We determined the weight of the sand and the weight of the water present in our samples. Using a measured bulk density of 2.66 g/cc (Travis Mcling, personnel communication, 1996), we determined the volume of sand, and therefore the porosity in our samples. Assuming a water density of 1.0 g/cc, we determined the volume of water contained in each of our samples. By dividing the volume of water by the porosity of the sample, we determined the water saturation contained in each of our 100 cc field samples.

Gravimetric determination of water saturation is the easiest field method, but there are some issues associated with its use. Gravimetric analysis is a destructive technique. A known or measured volume of sand must be removed from the field and brought back to the lab. The act of drying the sand will cause it to lose its structure, so the sand can not be reused in its original field condition. To use this method, the bulk density of the sample must be known to get volumetric measurements of the sand. Errors can be introduced through the taking of the sample from the field, transporting the sample from the field, and the repeated weighings conducted in the laboratory. On the positive side, the volume of sand to be tested can be controlled and as stated previously, the technique is easy and costs little.

E.2 - Electrical Resistance Method

Use of the electrical resistance method depends on the water content, composition, texture, and soluble salt concentration of the tested soil. The technique

involves the emplacement of porous bodies into the soil. Generally, the porous bodies contain a pair of electrodes. The porous bodies are allowed to equilibrate with the soil moisture suction. This is an indirect method in which the electrical condictivity of the porous block is a function of the water absorbed from the soil by the block. The porous bodies are then monitored by a data-logger to get a continuous reading of the soil moisture content.

Though this technique gives a continuous reading of the soil moisture content, is nondestructive, fairly simple, and inexpensive, there are some problems associated with the technique. These devices must be calibrated for each soil. However, the calibration changes with time as the porous bodies degrade changing the internal porosity and pore size distribution of the soil. This limits the accuracy of the technique. It has also been found that the elctrical resistance method is not very accurate in wet soils (Hillel, 1980; Hanks and Ashcroft, 1980).

E.3 - Neutron Scattering Method

The neutron scattering method works by emitting fast neutrons from a radioactive source placed down hole. The neutrons are slowed down by the hydrogen atoms in the soil. The density of the slow neutrons formed around the probe is, therefore, nearly proportional to the concentration of hydrogen in the soil, and therefore more or less proportional to the volume fraction of water in the soil. The slow neutrons are counted and simple calibration curves that exist for most soils are used to convert the density of slow neutrons into a measurement of the volume fraction of water.

There are many advantages and disadvantages associated with this technique. The advantages include: (1) the method is independent of the temperature and pressure; and (2) the method allows less laborious, more rapid, non-destructive, and repeatable measurements of volumetric water content in the same locations and depths. The disadvantages to this device are: (1) the intial high cost of the instrument; (2) the health

hazard due to radiation; (3) the low degree of spatial resolution; and (4) the difficulty of measuring moisture near the surface. The sphere of influence that the device averages over radiuses from about 10 cm in wet soils to up to 25 cm or more in dry soils. This sphere limits how close to the surface the device can be used since the neutrons will escape from the surface if the device is used to close to the surface. (Hillel, 1980; Hanks and Ashcroft, 1980). This lack of fine spatial resolution and the lack of ability to measure close to the surface were the main reasons we did not use this device for our experiment.

E.4 - Gamma-Ray Absorption Method

The gamma-ray absorption method consists of a radioactive source and a scintillating counter. When there is nothing contained between the two devices, then the fraction of radiation emitted that is received is dependent only on the distance of separation. When used in a soil of constant bulk density, the intensity of the transmitted radiation vary with changes in the water content. The device is best used in the laboratory where the bulk density of the soil as well as the temperature can be better controlled. Laboratory tests have shown a high degree of spatial resolution down to 2 mm or so. The device can be used in the field if the access tubes are strictly parallel and have shown a depth resolution of about 1 cm (Hillel, 1980). We did not use this device in our experiments becuase we did not have this device or the expertise of its use.

E.5 - Time Domain Reflectometry

Time Domain Reflectometry (TDR) relies on the slowing of electrical signal propagation with increased dielectric in the volume surrounding a set of parallel conductors. A measurement of the travel time of a short electrical pulse between the conductors determines the volume of the soil taken up by water. Most common probes are greater than 15 cm long, though Selker et al. (1993) were developing a 1 cm long prototype and Kelly et al. (1995) were testing probes of lengths 2.5, 5.0, and 7.5 cm.

Once measurements are made, the dielectric constant is determined for each point and the moisture content of the volume between the probes is determined by using a polynomial fit.

As with all high technology instruments, the TDR has certain disadvantages to it. Most TDR units cost upwards of $6,000 and require expert signal interpretation to obtain reliable water content readings. TDR units show a decreased sensitivity in low moisture content soil compared to higher moisture content soil. The unit needs to be calibrated for each probe length and type of soil that the probes are placed into. Recent studies have shown that shorter probes encounter problems with air gaps that are formed from slight movements in the probes. These air gaps disturb the measured sample volume and introduce an unquatifiable error. (Kelly et al., 1995). If the difficulties in developement can be solved, this technology could be useful in measuring the moisture content in near surface outcrop studies.